



## ATLAS Note

ATL-COM-PHYS-2019-962

30th May 2021



1

# 2 WZ + Heavy Flavor Production in pp collisions 3 at $\sqrt{s} = 13$ TeV

4

The ATLAS Collaboration<sup>1</sup>, Aaron Webb<sup>a</sup>, Peter Onyisi<sup>a</sup>

5

<sup>a</sup>*Univ. of Texas at Austin*

6

A measurement of the cross-section for production of WZ with an associated heavy flavor jet  
7 is performed using  $140 \text{ fb}^{-1}$  of proton-proton collision data at  $\sqrt{s} = 13$  TeV from the ATLAS  
8 experiment at the LHC. A measurement of the fully leptonic decay mode,  $WZ \rightarrow l\nu ll$ , is  
9 performed. The cross-section of  $WZ + b$  and  $WZ + \text{charm}$  in various fiducial regions is  
10 measured.

11

© 2021 CERN for the benefit of the ATLAS Collaboration.

Reproduction of this article or parts of it is allowed as specified in the CC-BY-4.0 license.

## 12 Contents

13	<b>1 Changes and outstanding items</b>	<b>3</b>
14	1.1 Changelog	3
15	1.1.1 Changes relative to v9	3
16	1.1.2 Changes relative to v8	3
17	1.1.3 Changes relative to v7	3
18	1.1.4 Changes relative to v5	4
19	1.1.5 Changes relative to v4	4
20	1.1.6 Changes relative to v3	4
21	1.1.7 Changes relative to v2	5
22	1.1.8 Changes relative to v1	5
23	1.2 Outstanding Items	5
24	<b>2 Executive Summary</b>	<b>6</b>
25	<b>3 Data and Monte Carlo Samples</b>	<b>6</b>
26	3.1 Data Samples	7
27	3.2 Monte Carlo Samples	7
28	<b>4 Object Reconstruction</b>	<b>9</b>
29	4.1 Trigger	9
30	4.2 Light leptons	10
31	4.3 Jets	11
32	4.4 B-tagged Jets	11
33	4.5 Missing transverse energy	13
34	4.6 Overlap removal	13
35	<b>5 tZ Separation Multivariate Analysis</b>	<b>13</b>
36	5.1 Top Mass Reconstruction	14
37	5.2 tZ BDT	14
38	5.3 tZ Interference Studies	18
39	<b>6 Event Selection and Signal Region Definitions</b>	<b>20</b>
40	6.1 Event Preselection	20
41	6.2 Fit Regions	24
42	6.3 Non-Prompt Lepton Estimation	40
43	6.3.1 $t\bar{t}$ Validation	40
44	6.3.2 Z+jets Validation	43
45	<b>7 Systematic Uncertainties</b>	<b>47</b>
46	<b>8 Results</b>	<b>55</b>
47	8.1 Fit Procedure	55
48	8.2 Results of the Simultaneous Fit	56

---

49	8.3	Inclusive 1+2 Jet Fit	66
50	8.4	Alternate tZ Inclusive Fit	70
51	8.4.1	tZ Inclusive Fit	70
52	8.4.2	Floating tZ	70
53	<b>9</b>	<b>Conclusion</b>	<b>71</b>
54	<b>A</b>	<b>Appendices</b>	<b>74</b>
55	<b>Appendices</b>		<b>74</b>
56	A.1	Non-prompt lepton MVA	74
57	A.2	Non-prompt CR Modelling	76
58	A.3	DSID list	80

---

## 59 List of contributions

---

Aaron Webb	Main analyser. Responsible for ntuple production, fits, and note writing.
Peter Onyisi	Advisor to Aaron Webb. Analysis design and implementation strategy.

---

62 **1 Changes and outstanding items**

63 **1.1 Changelog**

64 This is version 10

65 **1.1.1 Changes relative to v9**

- 66 • Reordered note to put fiducial region definition in the intro, tZ BDT before the event  
67 selection  
68 •

69 **1.1.2 Changes relative to v8**

- 70 • Included more references to appendices in the text  
71 • Expanded explanation of fiducial region definition  
72 • Previous draft claimed that both standard and custom PLVs were used. Text is fixed to  
73 state that a custom PLV is used for lepton iso, but standard lepton id is used  
74 • Included plots of PLV output, included WPs used  
75 • specified that non-prompt CR plots are post correction  
76 • changed title of results section

77 **1.1.3 Changes relative to v7**

- 78 • Moved from LO to NLO tZ sample  
79 • Add additional plots of Z+jets and ttbar CRs in Section A.2  
80 • Clarified CDI file used, MC ptag, PFlow jet algorithm  
81 • Included overlap removal procedure  
82 • Included details on PLV  
83 • Added plots of missing tZ BDT input features for each fit region  
84 • Changed reference on PLV to recent ttH/ttW note  
85 • Included alternate fits with WZ+1-2 jet inclusive, tZ floating

---

86 **1.1.4 Changes relative to v5**

- 87     • added list of DSIDs to an appendix  
 88     • included systematics on jet migrations  
 89     • Updated results section to include simultaneous fit over 1-jet and 2-jet bins, describe  
 90        unfolding procedure  
 91     • Updated other sections to account for this change  
 92     • Included info about migrations in Section 5.2

93 **1.1.5 Changes relative to v4**

- 94     • Fixed various typos, clarified wording  
 95     • Expanded info about JER uncertainties, electron systematics, theory uncertainties  
 96     • removed a table on lepton selection, included information in the text instead  
 97     • Plotted lepton Pt Z and W for Zjet CR, rather than lep 1 and 2  
 98     • fixed binning in kinematic plots  
 99     • Included prefit and postfit yield tables  
 100     • added signal modelling systematics  
 101     • included alternate fit studies with tZ included in signal

102 **1.1.6 Changes relative to v3**

- 103     • Merged introduction into executive summary, including unblinding details and list of  
 104        SRs/CRs used  
 105     • listed ptag used (p4133), and release (AB 21.2.127)  
 106     • Included table reftab:xsecUnc listing x-sec uncertainties used  
 107     • Removed selection criteria listed in table ?? (QMisID, AmbiguityType) that were removed  
 108        from the analysis  
 109     • specified variable used to make truth jet flavor determination (HadronConeExclTruthLa-  
 110        belIID)  
 111     • fixed bug in MtLepMet calculation, updated selection/fits to account for this  
 112     • Included plots of MtLepMet and PtZ, swapped lep 1 and 2  $p_T$  plots for lep W and lep Z  
 113        plots

- 114     • updated tZ BDT training to reduce overfitting, updated plots to include error bars, feature  
115       importance
- 116     • updated table 8 to clarify selection, fix the tZ\_BDT cut used
- 117     • replace a few broken ntuples which included large weight events
- 118     • include DL1r distribution for Z+jets and  $t\bar{t}$  VRs
- 119     • Expanded section on fakes, included information on derived scale factors from VRs.
- 120     • Changed the kinematic plots to include  $p_T(Z)$  and  $m_T(W)$ , list lepton  $p_T$  based on W and  
121       Z candidates.

122     **1.1.7 Changes relative to v2**

- 123     • Added alternate VBS samples to include missing b-jet diagrams
- 124     • Included a section on tZ interference effects, ??.
- 125     • Updated to reflect changes for 2018, including the move to PFlow jets, DL1r, updated  
126       trigger, and updated AnalysisBase version (now 21.2.127)
- 127     • Revised fit regions, using separate 1-jet and 2-jet fits, with all 2-j regions included
- 128     • updated plots for tZ BDT, added details about the model
- 129     • Included truth jet information

130     **1.1.8 Changes relative to v1**

- 131     • Added GRL list
- 132     • Fixed latex issue in line 92, typo in line 172
- 133     • Added tables 6 and ??, summarizing the event and object selection
- 134     • Added table 2, which includes the DSID of samples used
- 135     • Included reference to WZ inclusive paper in introduction

136     **1.2 Outstanding Items**

- 137     • Unblind, update plots and fits to include data
- 138     • Add cross-section, significance once unblinded

## 139 2 Executive Summary

140 The production of  $WZ$  in association with a heavy flavor jet represents an important background  
 141 for many major analyses. This includes any process with leptons and b-jets in the final state,  
 142 such as  $t\bar{t}H$ ,  $t\bar{t}W$ , and  $t\bar{t}Z$ . While precise measurements have been made of  $WZ$  production  
 143 [1],  $WZ +$  heavy flavor remains poorly understood. This is largely because the QCD processes  
 144 involved in the production of the b-jet make it difficult to simulate accurately. This introduces a  
 145 large uncertainty for analyses that include this process as a background.

146 Motivated by its relevance to the  $t\bar{t}H$  multilepton analysis, we perform a study of the fully  
 147 leptonic decay mode of this channel; that is, events where both the W and Z decay leptonically.  
 148 Because  $WZ$  has no associated jets at leading order, while the major backgrounds for this channel  
 149 tend to have high jet multiplicity, events with more than two jets are rejected. This gives a final  
 150 state signature of three leptons and one or two jets.

151 Events that meet this selection criteria are sorted into pseudo-continuous b-tagging regions based  
 152 on the DL1r b-tag score of their associated jets. This is done to separate  $WZ +$  b-jet events from  
 153  $WZ +$  charm and  $WZ +$  light jets. These regions are fit to data in order make a more accurate  
 154 estimate of the contribution of  $WZ +$  heavy-flavor, where heavy-flavor jets include b-jets and  
 155 charm jets. The full Run-2 dataset collected by the ATLAS detector, representing  $139 \text{ fb}^{-1}$  of  
 156 data from pp collisions at  $\sqrt{s} = 13 \text{ TeV}$ , is used for this study.

157 Section 3 details the data and Monte Carlo (MC) samples used in the analysis. The reconstruction  
 158 of various physics objects is described in Section 4. Section 6 describes the event selection applied  
 159 to these samples, along with the definitions of the various regions used in the fit. The multivariate  
 160 analysis techniques used to separate the  $tZ$  background from  $WZ +$  heavy flavor are described in  
 161 Section 5. Section 7 describes the various sources of systematic uncertainties considered in the  
 162 fit. Finally, the results of the analysis are summarized in Section 8, followed by a brief conclusion  
 163 in Section 9.

164 **The current state of the analysis shows blinded results for the full Run-2 dataset. Regions  
 165 containing >5%  $WZ+b$  events are blinded, and results are from Asimov, MC only fits.**

## 166 3 Data and Monte Carlo Samples

167 Both data and Monte Carlo samples used in this analysis were prepared in the xAOD format,  
 168 which was used to produce a Dx AOD sample in the HIGG8D1 derivation framework. The HIGG8D1  
 169 framework is designed for the  $t\bar{t}H$  multi-lepton analysis, which targets events with multiple  
 170 leptons as well as tau hadrons. This framework reduces the size of the dataset by removing  
 171 events based on event topology and only keeping useful information for each event. Events are  
 172 removed from the derivations that do not meet one of the following selections:

- 173     • at least two light leptons within a range  $|\eta| < 2.6$ , with leading lepton  $p_T > 15 \text{ GeV}$  and  
 174       subleading lepton  $p_T > 5 \text{ GeV}$

- 175     • OR at least one light lepton with  $p_T > 15$  GeV within a range  $|\eta| < 2.6$ , and at least two  
 176       hadronic taus with  $p_T > 15$  GeV.

177     Samples were then generated from these HIGG8D1 derivations with p-tag of p4134 for data  
 178       and p4133 for Monte Carlo using AnalysisBase version 21.2.127 modified to include custom  
 179       variables.

### 180     3.1 Data Samples

181     The study uses a sample of proton-proton collision data collected by the ATLAS detector from  
 182       2015 through 2018 at an energy of  $\sqrt{s} = 13$  TeV, which represents an integrated luminosity of  
 183        $139 \text{ fb}^{-1}$  [2]. This data set was collected with a bunch-crossing rate of 25 ns. All data used in  
 184       this analysis was verified by data quality checks [3], having been included in the following Good  
 185       Run Lists:

- 186       • data15\_13TeV.periodAllYear\_DetStatus-v79-repro20-02\_DQDefects-00-02-02  
   187           \_PHYS\_StandardGRL\_All\_Good\_25ns.xml
- 188       • data16\_13TeV.periodAllYear\_DetStatus-v88-pro20-21\_DQDefects-00-02-04  
   189           \_PHYS\_StandardGRL\_All\_Good\_25ns.xml
- 190       • data17\_13TeV.periodAllYear\_DetStatus-v97-pro21-13\_Unknown\_PHYS\_StandardGRL  
   191           \_All\_Good\_25ns\_Triggerno17e33prim.xml
- 192       • data18\_13TeV.periodAllYear\_DetStatus-v102-pro22-04\_Unknown\_PHYS\_StandardGRL  
   193           \_All\_Good\_25ns\_Triggerno17e33prim.xml

194     Runs included from the AllYear period containers are included.

### 195     3.2 Monte Carlo Samples

196     Several different generators were used to produce Monte Carlo simulations of the signal and  
 197       background processes. For all samples, the response of the ATLAS detector is simulated using  
 198       GEANT4 [4]. The WZ signal samples are simulated using Sherpa 2.2.2 [5]. Signal events are  
 199       generated using NNPDF30NNLO PDF set with up to one parton at NLO and 2 to 3 partons at  
 200       LO [**Butterworth:2015oua**].

201     The tZ background is simulated at NLO with **MADGRAPH5\_AMC@NLO**, with **PYTHIA8** used to  
 202       perform parton showering and fragmentation. The NNPDF30NNLO PDF set is used.

203     Specific information about the Monte Carlo samples being used can be found in Table 1. A list  
 204       of the specific samples used by data set ID is shown in Table 2.

Table 1: The configurations used for event generation of signal and background processes, including the event generator, matrix element (ME) order, parton shower algorithm, and parton distribution function (PDF).

Process	Event generator	ME order	Parton Shower	PDF
WZ, VV	SHERPA 2.2.2	MEPS NLO	SHERPA	CT10 [6]
tZ	MG5_AMC [7]	NLO	PYTHIA 8	CTEQ6L1
t̄W	MG5_AMC (SHERPA 2.1.1)	NLO (LO multileg)	PYTHIA 8 (SHERPA)	NNPDF 3.0 NLO (NNPDF 3.0 NLO)
t̄(Z/γ* → ll)	MG5_AMC	NLO	PYTHIA 8	NNPDF 3.0 NLO
t̄H	MG5_AMC (MG5_AMC)	NLO (NLO)	PYTHIA 8 (HERWIG++) [9]	NNPDF 3.0 NLO [8] (CT10 [6])
tHqb	MG5_AMC	LO	PYTHIA 8	CT10
tHW	MG5_AMC (SHERPA 2.1.1)	NLO (LO multileg)	HERWIG++ (SHERPA)	CT10 (NNPDF 3.0 NLO)
tWZ	MG5_AMC	NLO	PYTHIA 8	NNPDF 2.3 LO
t̄t, t̄t̄t̄	MG5_AMC	LO	PYTHIA 8	NNPDF 2.3 LO [10]
t̄tW+W-	MG5_AMC	LO	PYTHIA 8	NNPDF 2.3 LO
t̄t	POWHEG-BOX v2 [11]	NLO	PYTHIA 8	NNPDF 3.0 NLO
t̄t̄γ	MG5_AMC	LO	PYTHIA 8	NNPDF 2.3 LO
s-, t-channel, Wt single top	POWHEG-BOX v1 [12]	NLO	PYTHIA 6	CT10
qqVV, VVV Z → l+l-	SHERPA 2.2.1	MEPS NLO	SHERPA	NNPDF 3.0 NLO

Sample	DSID
WZ	364253, 364739-42
VV	364250, 364254, 364255, 363355-60, 364890
t̄W	410155
t̄Z	410156, 410157, 410218-20
low mass t̄Z	410276-8
Rare Top	410397, 410398, 410399
single Top	410658-9, 410644-5
three Top	304014
four Top	410080
t̄WW	410081
Z + jets	364100-41
low mass Z + jets	364198-215
W + jets	364156-97
Vγ	364500-35
tZ	412063-5
tW	410013-4
WtZ	410408
VVV	364242-9
VH	342284-5
WtH	341998
t̄tγ	410389
t̄t	410470
t̄tH	345873-5, 346343-5

Table 2: List of Monte Carlo samples by data set ID used in the analysis.

## 205 4 Object Reconstruction

206 All regions defined in this analysis share a common lepton, jet, and overall event preselection.  
 207 The selection applied to each physics object is detailed here; the event preselection, and the  
 208 selection used to define the various fit regions, is described in Section 6.

### 209 4.1 Trigger

210 Events are required to be selected by dilepton triggers, as summarized in Table 3.

Dilepton triggers (2015)	
$\mu\mu$ (asymm.)	HLT_mu18_mu8noL1
$ee$ (symm.)	HLT_2e12_lhloose_L12EM10VH
$e\mu, \mu e$ ( $\sim$ symm.)	HLT_e17_lhloose_mu14
Dilepton triggers (2016)	
$\mu\mu$ (asymm.)	HLT_mu22_mu8noL1
$ee$ (symm.)	HLT_2e17_lhvloose_nod0
$e\mu, \mu e$ ( $\sim$ symm.)	HLT_e17_lhloose_nod0_mu14
Dilepton triggers (2017)	
$\mu\mu$ (asymm.)	HLT_mu22_mu8noL1
$ee$ (symm.)	HLT_2e24_lhvloose_nod0
$e\mu, \mu e$ ( $\sim$ symm.)	HLT_e17_lhloose_nod0_mu14
Dilepton triggers (2018)	
$\mu\mu$ (asymm.)	HLT_mu22_mu8noL1
$ee$ (symm.)	HLT_2e24_lhvloose_nod0
$e\mu, \mu e$ ( $\sim$ symm.)	HLT_e17_lhloose_nod0_mu14

Table 3: List of lowest  $p_T$ -threshold, un-prescaled dilepton triggers used for 2015–2018 data taking.

## 4.2 Light leptons

212 Electron candidates are reconstructed from energy clusters in the electromagnetic calorimeter  
 213 that are associated with charged particle tracks reconstructed in the inner detector [13]. Electron  
 214 candidates are required to have  $p_T > 10$  GeV and  $|\eta_{\text{cluster}}| < 2.47$ . Muon candidates are  
 215 reconstructed by combining inner detector tracks with track segments or full tracks in the muon  
 216 spectrometer [14]. Muon candidates are required to have  $p_T > 10$  GeV and  $|\eta| < 2.5$ . Candidates  
 217 in the transition region between different electromagnetic calorimeter components,  $1.37 <$   
 218  $|\eta_{\text{cluster}}| < 1.52$ , are rejected. A multivariate likelihood discriminant combining shower shape  
 219 and track information is used to distinguish real electrons from hadronic showers (fake electrons).  
 220 To further reduce the non-prompt electron contribution, the track is required to be consistent  
 221 with originating from the primary vertex; requirements are imposed on the transverse impact  
 222 parameter significance ( $|d_0|/\sigma_{d_0} < 5$ ) and the longitudinal impact parameter ( $|\Delta z_0 \sin \theta_\ell| < 0.5$   
 223 mm). Electron candidates are required to pass TightLH identification.

224 Muon candidates are reconstructed by combining inner detector tracks with track segments or  
 225 full tracks in the muon spectrometer [14]. Muon candidates are required to have  $p_T > 10$  GeV  
 226 and  $|\eta| < 2.5$ . The longitudinal impact parameter is the same for both electrons and muons, while  
 227 muons are required to pass a slightly tighter transverse impact parameter,  $|d_0|/\sigma_{d_0} < 3$ . Muons  
 228 are also required to pass Medium ID requirements.

229 Leptons are additionally required to pass a non-prompt BDT selection developed by the  $t\bar{t}H$   
230 multilepton/ $t\bar{t}W$  analysis group. This BDT and the WPs used are summarized in Appendix A.1,  
231 and described in detail in [15]. Optimized working points and scale factors for this BDT are  
232 taken from that analysis.

233 **4.3 Jets**

234 Jets are reconstructed from calibrated topological clusters built from energy deposits in the  
235 calorimeters [16], as well as information from the inner tracking detector, using the anti- $k_t$   
236 algorithm with a radius parameter  $R = 0.4$ . Particle Flow, or PFlow, jets are used in the analysis.  
237 Jets with energy contributions likely arising from noise or detector effects are removed from  
238 consideration [17], and only jets satisfying  $p_T > 25$  GeV and  $|\eta| < 2.5$  are used in this analysis.  
239 For jets with  $p_T < 60$  GeV and  $|\eta| < 2.4$ , a jet-track association algorithm is used to confirm  
240 that the jet originates from the selected primary vertex, in order to reject jets arising from pileup  
241 collisions [18].

242 **4.4 B-tagged Jets**

243 In order to make a measurement of  $WZ +$  heavy flavor it is necessary to distinguish these events  
244 from  $WZ +$  light jets. For this purpose, the DL1r b-tagging algorithm is used to distinguish  
245 heavy flavor jets from lighter ones. The DL1r algorithm [19] uses jet kinematics, particularly  
246 jet vertex information, as input for a neural network which assigns each jet a score designed to  
247 reflect how likely that jet is to have originated from a b-quark.

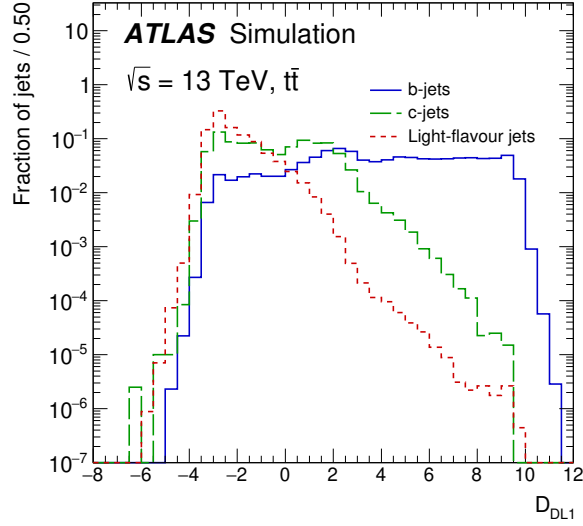


Figure 1: Output distribution of the DL1r algorithm for pure samples of b-jets, charm jets, and light jets, with each normalized to unity [19]

From the output of the BDT, working points (WPs) are developed based on the efficiency of truth b-jets at particular values of the DL1r algorithm. These WPs are taken from the March 2020 CDI file, 2020-21-13TeV-MC16-CDI-2020-03-11\_v2.root. The working points used in this analysis are summarized in Table 4.

WP	Rejection		
	b-jet eff.	c-jet	light jet
85%	2.6	29	
77%	4.9	130	
70%	9.4	390	
60%	27	1300	

Table 4: c-jet and light-flavor jet rejections corresponding to each b-tagging Working Point by b-jet efficiency, evaluated on  $t\bar{t}$  events.

As shown in table 4, a tighter WP will accept fewer b-jets, but reject a higher fraction of charm and light jets. Generally, analyses that include b-jets will use a fixed working point, for example, requiring that a jet pass the 70% threshold. By instead treating these working points as bins, e.g. events with jets that fall between the 85% and 77% WPs fall into one bin, while events with jets passing the 60% WP fall into another, additional information can be gained. This analysis uses each of these working points to form orthogonal regions in order to provide separation between  $WZ + b$ ,  $WZ + c$ , and  $WZ + \text{light}$ .

259 **4.5 Missing transverse energy**

260 Missing transverse momentum ( $E_T^{\text{miss}}$ ) is used as part of the event selection. The missing  
 261 transverse momentum vector is defined as the negative of the vector sum of the transverse  
 262 momenta of all reconstructed physics objects as well as remaining unclustered energy, the latter  
 263 of which is estimated from low- $p_T$  tracks associated with the primary vertex but not assigned  
 264 to a hard object, with object definitions taken from [20]. Light leptons considered in the  $E_T^{\text{miss}}$   
 265 reconstruction are required to have  $p_T > 10 \text{ GeV}$ , while jets are required to have  $p_T > 20 \text{ GeV}$ .

266 **4.6 Overlap removal**

267 To avoid double counting objects and remove leptons originating from decays of hadrons, overlap  
 268 removal is performed in the following order: any electron candidate within  $\Delta R = 0.1$  of another  
 269 electron candidate with higher  $p_T$  is removed; any electron candidate within  $\Delta R = 0.1$  of a muon  
 270 candidate is removed; any jet within  $\Delta R = 0.2$  of an electron candidate is removed; if a muon  
 271 candidate and a jet lie within  $\Delta R = \min(0.4, 0.04 + 10[\text{GeV}]/p_T(\text{muon}))$  of each other, the jet  
 272 is kept and the muon is removed if the jet has at least three associated tracks, otherwise the jet is  
 273 removed and the muon is kept.

274 This algorithm is applied to the preselected objects. The overlap removal procedure is summarized  
 275 in Table 5.

Keep	Remove	Cone size ( $\Delta R$ )
electron	electron (low $p_T$ )	0.1
muon	electron	0.1
electron	jet	0.2
jet	muon	$\min(0.4, 0.04 + 10[\text{GeV}]/p_T(\text{muon}))$ , $n_{\text{track}} > 3$
muon	jet	$\min(0.4, 0.04 + 10[\text{GeV}]/p_T(\text{muon}))$ , $n_{\text{track}} < 3$
electron	tau	0.2

Table 5: Summary of the overlap removal procedure between electrons, muons, and jets.

276 **5 tZ Separation Multivariate Analysis**

277 Because tZ produces a final state identical to signal, it represents a predominant background in  
 278 the most signal enriched regions. That is, the region with one jet passing the 60% DL1r WP.  
 279 Therefore, a boosted decision tree (BDT) algorithm is trained to separate WZ + heavy flavor  
 280 from tZ.

281 Separation between tZ and WZ + heavy flavor is achieved in part by reconstructing the invariant  
 282 mass of the top candidate, which clusters more closely to the top mass for tZ than WZ + heavy

283 flavor. The result of this BDT is used to create a tZ enriched region in the fit, reducing its impact  
 284 on the measurement of WZ + heavy flavor.

285 **5.1 Top Mass Reconstruction**

286 The reconstruction of the top mass follows the procedure described in detail in section 6.1 of  
 287 [21]. The mass of the top quark candidate is reconstructed from the jet, the lepton not included  
 288 in the Z-candidate, and a reconstructed neutrino. In the case that there is one jet in the event,  
 289 there is only possible b-jet candidate. For events with two jets, the jet with the highest DL1r  
 290 score is used.

291 The neutrino from the W decay is expected to be the only source of  $E_T^{\text{miss}}$ . Therefore, the  $E_T$   
 292 and  $\phi$  of the neutrino are taken from the  $E_T^{\text{miss}}$  measurement. This leaves the z-component of  
 293 the neutrino momentum,  $p_{\nu z}$  as the only unknown.

294 This unknown is solved for by taking the combined invariant mass of the lepton and neutrino to  
 295 give the invariant mass of the W boson:

$$296 \quad (p_l + p_\nu)^2 = m_W^2$$

297 Expanding this out into components, this equation gives:

$$298 \quad \sqrt{p_{T\nu}^2 + p_{z\nu}^2} E_l = \frac{m_W^2 - m_l^2}{2} + p_{T\nu}(p_{lx}\cos\phi_\nu + p_{ly}\sin\phi_\nu) + p_{lz}p_{\nu z}$$

299 This equation gives two solutions for  $p_{\nu z}$ . For cases where only one of these solutions is real,  
 300 that is taken as the value of  $p_{\nu z}$ . For instances with two real solutions, the one which is shown  
 301 to be correct in the largest fraction of simulations is taken. For cases when no real solution is  
 302 found, often because of detector effects, the value of  $E_T^{\text{miss}}$  is varied in decreasing increments of  
 303 100 MeV until a real solution is found.

304 The reconstructed top mass distribution for tZ and WZ + b can be seen in figure 2.

305 **5.2 tZ BDT**

306 A Boosted Decision Tree (BDT), specifically XGBoost [22], is used to provide separation between  
 307 tZ and WZ+b. The following kinematic variables are used as inputs:

- 308     • The invariant mass of the reconstructed top candidate
- 309     •  $p_T$  of each of the leptons, jet
- 310     • The invariant mass of each combination of lepton pairs,  $M(l\bar{l})$

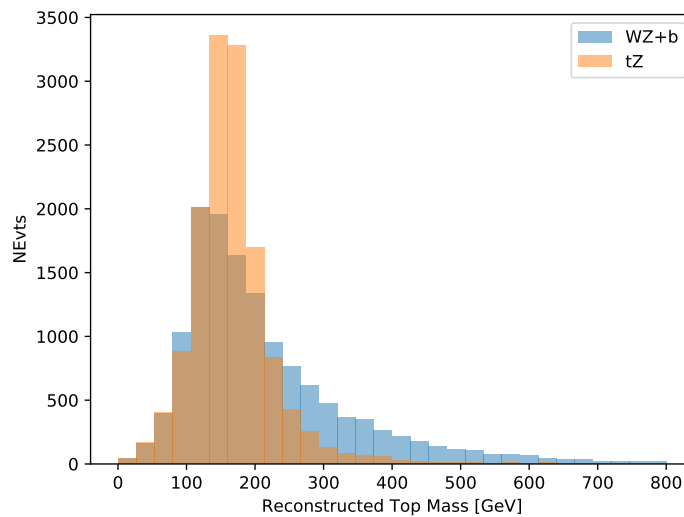


Figure 2: Reconstructed top mass distributions for tZ and WZ + b, measured in MeV.

311     •  $E_T^{\text{miss}}$

312     • Distance between each combination of leptons,  $\Delta R(ll)$

313     • Distance between each lepton and the jet,  $\Delta R(lj)$

314     The training samples included only events meeting the requirements of the 1-jet, >60% region,  
 315     i.e. passing all the selection described in section 6 and having exactly one jet which passes the  
 316     tightest (60%) DL1r working point.

317     The distributions of a few of these features for both signal and background is shown in figure  
 318     3.

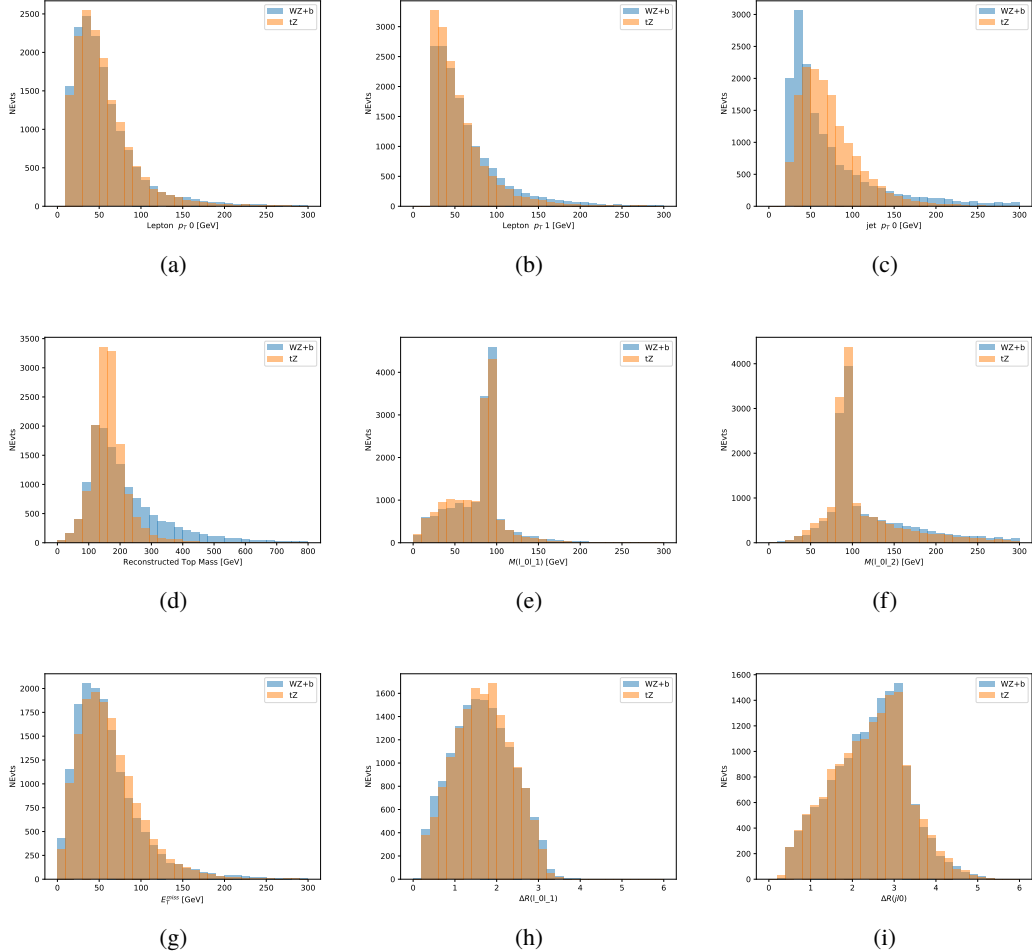


Figure 3: Distribution of input features of the BDT for signal (WZ) and background (tZ). Both are scaled to an equal number of events. (a), (b) and (c) show the  $p_T$  of lepton 0, lepton 1, and the jet, (d) show the reconstructed top mass, (e) and (f) show the invariant mass of leptons 0 and 1, leptons 0 and 2. (g) shows the  $E_T^{\text{miss}}$  of each event. (h) and (i) show the  $\Delta R$  between lepton 0 and lepton 1, and the jet.

319 A sample of 20,000 background (tZ) and signal (WZ+b) Monte Carlo events are used to train  
 320 the BDT. And additional 5,000 events are reserved for testing the model, in order to prevent  
 321 over-fitting. A total of 750 decision trees with a maximum depth of 6 branches are used to build  
 322 the model. These parameters are chosen empirically, by training several models with different  
 323 parameters and selecting the one that gave the best separation for the test sample.

324 The results of the BDT training are shown in figure 4. The output scores for both signal and  
 325 background events is shown on the left. The right shows the receiving operating characteristic  
 326 (ROC) curve that results from the MVA. The ROC curve represents the background rejection  
 327 as a function of signal efficiency, where each point on the curve represents a different response

328 score.

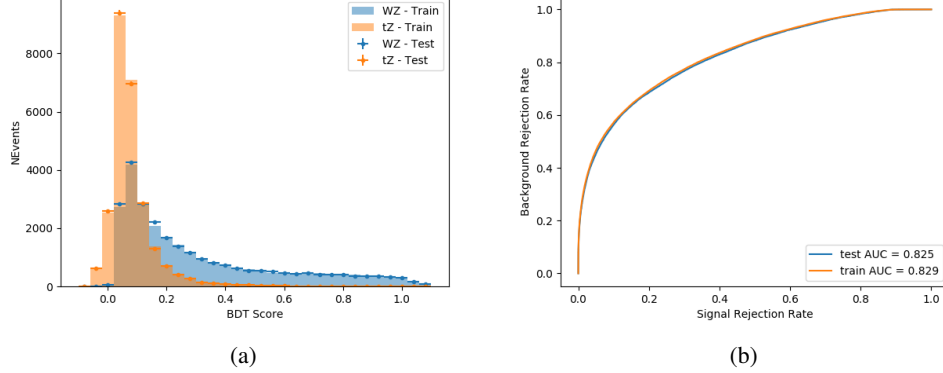


Figure 4: Distribution of the BDT response for signal and background events on the left, the ROC curve for the BDT on the right.

329 The relative important of each input feature in the model, measured by how often they appeared  
330 in the decision trees, is shown in figure 5.

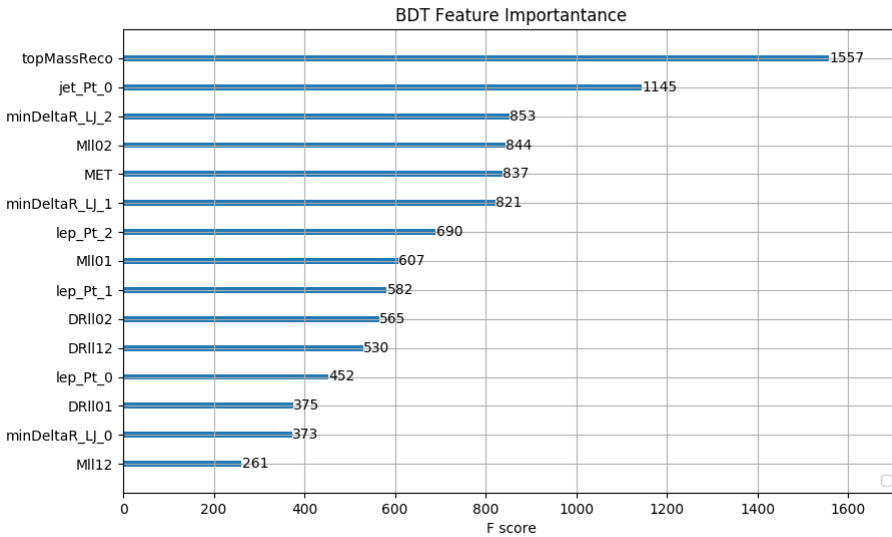


Figure 5: Relative importance of each input feature in the model.

331 These results suggest that some amount of separation can be achieved between these two pro-  
332 cesses, with a high BDT score selecting a set of events that is pure in WZ + b. A BDT score

333 of 0.12 is selected as a cutoff, where events with scores higher than this form a signal enriched  
334 region, and events with scores lower than this form a tZ control region. This cutoff is selected by  
335 varying the value of this cutoff in stat-only Asimov fits, and selecting the value that minimizes  
336 the statistical uncertainty on WZ + b. A working point of 0.12 produces a background rejection  
337 rate of 74%, compared to a signal acceptance of 78%.

### 338 5.3 tZ Interference Studies

339 Because it includes an on-shell Z boson as well as a b-jet and W from the top decay, tZ  
340 production represents an identical final state to WZ + b-jet. This implies the possibility of matrix  
341 level interference between these two processes not accounted for in the Monte Carlo simulations,  
342 which consider the two processes independently. Truth level studies are performed in order to  
343 estimate the impact of these interference effects.

344 In order to estimate the matrix level interference effects between tZ and WZ + b-jet, two different  
345 sets of simulations are produced using MadGraph 5 [**Madgraph**] - one which simulates these  
346 two processes independently, and another where they are produced simultaneously, such that  
347 interference effects are present. These two sets of samples are then compared, and the difference  
348 between them can be taken to represent any interference effects.

349 MadGraph simulations of 10,000 tZ and 10,000 WZ + b-jet events are produced, along with  
350 20,000 events where both are present, in the fiducial region where three leptons and at least one  
351 jet are produced.

352 A selection mimicking the preselection used in the main analysis is applied to the samples: The  
353 SS leptons are required to have  $p_T > 20$  GeV, and  $> 10$  GeV is required for the OS lepton. The  
354 associated b-jet is required to have  $p_T > 25$  GeV, and all physics objects are required to fall in a  
355 range of  $|\eta| < 2.5$ .

356 The kinematics of these samples after the selection has been applied are shown below:

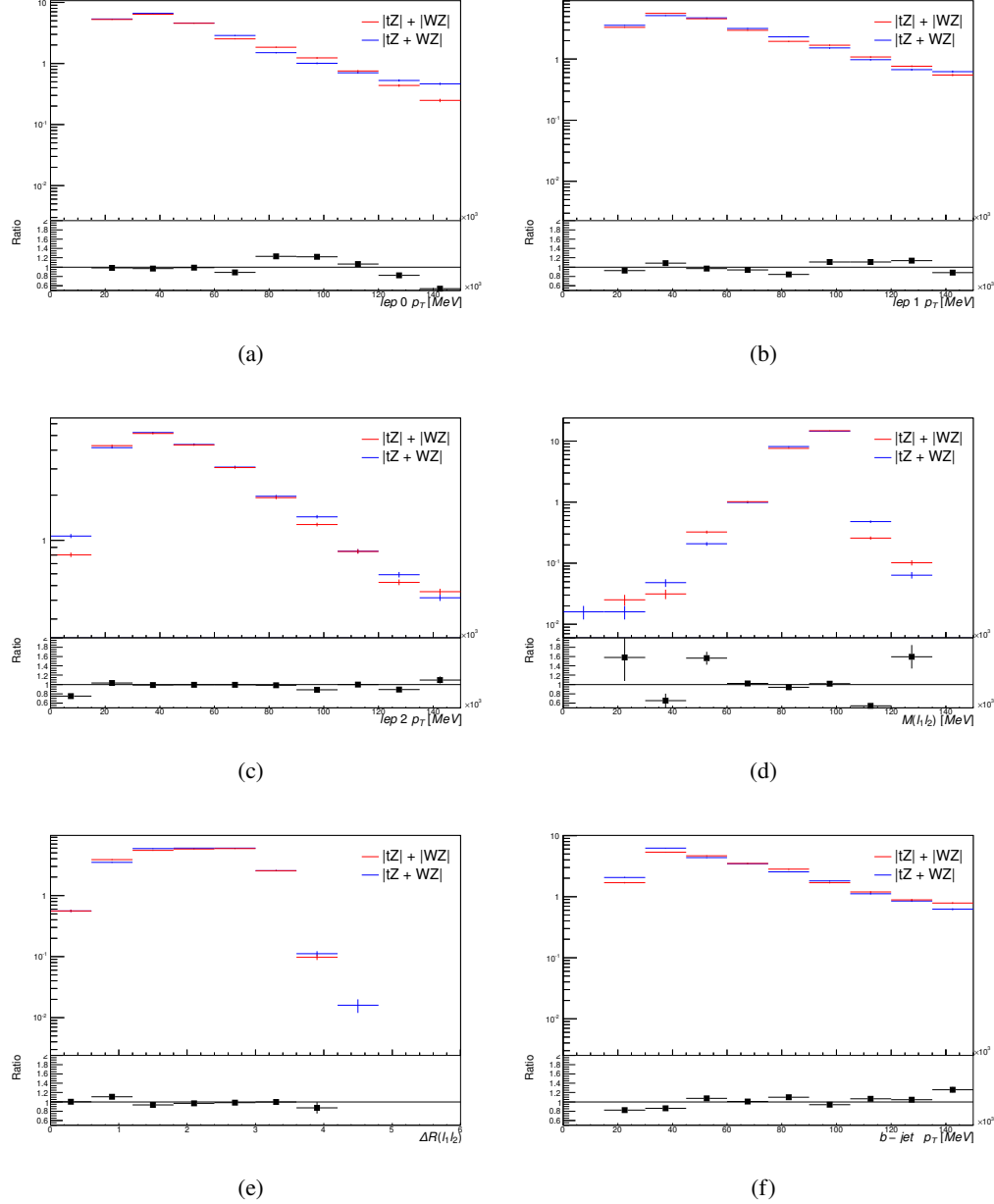


Figure 6: Comparisons between (a) the  $p_T$  of the lepton from the W, (b) and (c) show the  $p_T$  of the lepton from the Z, (d) the invariant mass of the Z-candidate, (e)  $\Delta R$  of the leptons from the Z, and (f) the  $p_T$  of the b-jet, for WZ and tZ events generated with interference effects (blue) and without interference effects (red).

357 The overall cross-section of the two methods agree within error, and no significant differences  
358 in the kinematic distributions are seen. It is therefore concluded that interference effects do not

359 significantly impact the results.

## 360 6 Event Selection and Signal Region Definitions

361 Event are required to pass a preselection described in Section 6.1 and summarized in Table 6.  
362 Those that pass this preselection are divided into various fit regions described in Section 6.2,  
363 based on the number of jets in the event, and the b-tag score of those jets.

### 364 6.1 Event Preselection

365 Events are required to include exactly three reconstructed light leptons passing the requirement  
366 described in 4.2, which have a total charge of  $\pm 1$ .

367 The leptons are ordered in the analysis code as 0, 1, and 2. Lepton 0 is the lepton whose charge  
368 is opposite the other two. Lepton 1 is the lepton closest to the opposite charge lepton, i.e. the  
369 smallest  $\Delta R$ , leaving lepton 2 as the lepton further from the opposite charge lepton. Lepton 0 is  
370 required to have  $p_T > 10$  GeV, as it is found to be prompt the vast majority of the time, while  
371 the same sign leptons, 1 and 2, are required to have  $p_T > 20$  GeV to reduce the contribution of  
372 non-prompt leptons, as non-prompt leptons tend to be soft.

373 The invariant mass of at least one pair of opposite sign, same flavor leptons is required to fall  
374 within 10 GeV of the mass of the Z boson, 91.2 GeV. Events where one of the opposite sign pairs  
375 have an invariant mass less than 12 GeV are rejected in order to suppress low mass resonances.

376 An additional requirement is placed on the missing transverse energy,  $E_T^{\text{miss}} > 20$  GeV, and the  
377 transverse mass of the W candidate,  $m(E_T^{\text{miss}} + l_{\text{other}}) > 30$  GeV, defined as  $\sqrt{2 p_T^{\text{lep}} E_T^{\text{miss}} * (1 - \cos(\phi_{\text{lep}} - \phi_{E_T^{\text{miss}}}))}$ .  
378 Here  $E_T^{\text{miss}}$  is the missing transverse energy, and  $l_{\text{other}}$  is the lepton not included in the Z-  
379 candidate.

380 Events are required to have one or two reconstructed jets passing the selection described in  
381 Section 4.3. Events with more than two jets are rejected in order to reduce the contribution of  
382 backgrounds such as  $t\bar{t}Z$  and  $t\bar{t}W$ , which tend to have higher jet multiplicity.

Event Selection
Exactly three leptons with total charge $\pm 1$
Two same-charge leptons with $p_T > 20$ GeV
One opposite charge lepton with $p_T > 10$ GeV
$m(l^+l^-)$ within 10 GeV of 91.2 GeV
Transverse mass of W-candidate, $\sqrt{2p_T^{lep}E_T^{\text{miss}} * (1 - \cos(\phi_{lep} - \phi_{E_T^{\text{miss}}}))} > 30$ GeV
Missing transverse energy, $E_T^{\text{miss}} > 20$ GeV
One or two jets with $p_T > 25$ GeV

Table 6: Summary of the selection applied to events for inclusion in the fit

383 The event yields in the preselection region for both data and Monte Carlo are summarized in  
 384 Table 6.1, which shows good agreement between data and Monte Carlo, and demonstrates that  
 385 this region consists primarily of WZ + jets events. The WZ events are split into WZ + b, WZ  
 386 + c, and WZ + l based on the truth flavor of the associated jet in the event. Specifically, this  
 387 determination is made based on the HadronConeExclTruthLabelID of the jet, as recommended  
 388 by the b-tagging working group [23]. In this ordering b-jet supersedes charm, which supersedes  
 389 light. That is, WZ + light events contain no charm and no b jets at truth level, WZ + c contain at  
 390 least one truth charm and no b-jets, and WZ + b contains at least one truth b-jet.

Process	Events
WZ + b	$167.6 \pm 6.5$
WZ + c	$1080 \pm 40$
WZ + l	$7220 \pm 310$
Other VV	$850 \pm 140$
t̄tW	$16.8 \pm 2.3$
t̄tZ	$115 \pm 17$
rare Top	$2.2 \pm 0.1$
Single top	$0.10 \pm 0.45$
Three top	$0.01 \pm 0.01$
Four top	$0.02 \pm 0.01$
t̄tWW	$0.23 \pm 0.05$
Z + jets	$600 \pm 260$
V + $\gamma$	$37 \pm 54$
tZ	$190 \pm 70$
tW	$5.5 \pm 1.2$
WtZ	$25.8 \pm 1.1$
VVV	$26.2 \pm 0.9$
VH	$94 \pm 7$
t̄t	$108.68 \pm 8$
t̄tH	$4.3 \pm 0.5$
Total	$10600 \pm 530$
Data	10574

Table 7: Event yields in the preselection region at  $139.0 \text{ fb}^{-1}$ 

<sup>391</sup> Here Other VV represents diboson processes other than WZ, and consists predominantly of  
<sup>392</sup>  $ZZ \rightarrow ll\bar{l}\bar{l}$  events where one of the leptons is not reconstructed.

<sup>393</sup> Simulations are further validated by comparing the kinematic distributions of the Monte Carlo  
<sup>394</sup> with data, which are shown in Figure 7. Here, bins with 5% or more WZ+b are blinded.

## WZ Fit Region - Inclusive

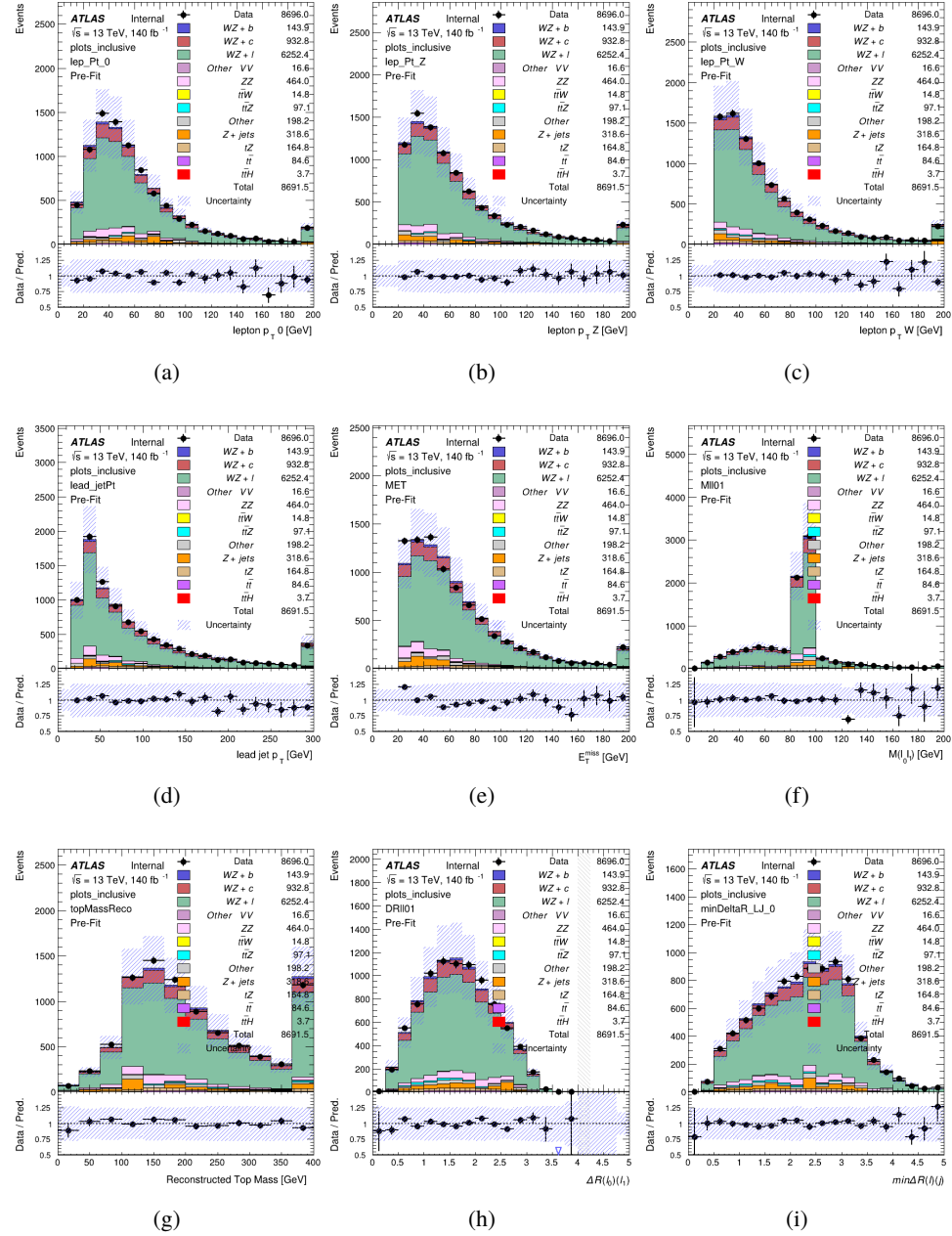


Figure 7: Comparisons between the data and MC distributions in the preselection region for (a) the  $p_T$  of the opposite sign lepton, (b) the  $p_T$  of the other lepton from the Z candidate, (c) the  $p_T$  of the lepton from the W candidate, (d) the leading jet  $p_T$ , (e) the  $E_T^{\text{miss}}$ , and (f) the invariant mass of leptons 0 and 1, (g) the reconstructed top mass, (h)  $\Delta(R)$  between lepton 0 and 1, (i) the  $\Delta(R)$  between the closest lepton and jet.

395 **6.2 Fit Regions**

396 Once preselection has been applied, the remaining events are categorized into one of twelve  
 397 orthogonal regions. The regions used in the fit are summarized in Table 8.

Table 8: A list of the regions used in the fit and the selection used for each.

Region	Selection
1j, <85%	$N_{\text{jets}} = 1, n_{\text{Jets\_DL1r\_85}} = 0$
1j, 85%-77%	$N_{\text{jets}} = 1, n_{\text{Jets\_DL1r\_85}} = 1, n_{\text{Jets\_DL1r\_77}} = 0$
1j, 77%-70%	$N_{\text{jets}} = 1, n_{\text{Jets\_DL1r\_77}} = 1, n_{\text{Jets\_DL1r\_70}} = 0$
1j, 70%-60%	$N_{\text{jets}} = 1, n_{\text{Jets\_DL1r\_70}} = 1, n_{\text{Jets\_DL1r\_60}} = 0$
1j, >60%	$N_{\text{jets}} = 1, n_{\text{Jets\_DL1r\_60}} = 1, tZ \text{ BDT} > 0.12$
1j tZ CR	$N_{\text{jets}} = 1, n_{\text{Jets\_DL1r\_60}} = 1, tZ \text{ BDT} < 0.12$
2j, <85%	$N_{\text{jets}} = 2, n_{\text{Jets\_DL1r\_85}} = 0$
2j, 85%-77%	$N_{\text{jets}} = 2, n_{\text{Jets\_DL1r\_85}} \geq 1, n_{\text{Jets\_DL1r\_77}} = 0$
2j, 77%-70%	$N_{\text{jets}} = 2, n_{\text{Jets\_DL1r\_77}} \geq 1, n_{\text{Jets\_DL1r\_70}} = 0$
2j, 70%-60%	$N_{\text{jets}} = 2, n_{\text{Jets\_DL1r\_70}} \geq 1, n_{\text{Jets\_DL1r\_60}} = 0$
2j, >60%	$N_{\text{jets}} = 2, n_{\text{Jets\_DL1r\_60}} \geq 1, tZ \text{ BDT} > 0.12$
2j tZ CR	$N_{\text{jets}} = 2, n_{\text{Jets\_DL1r\_60}} \geq 1, tZ \text{ BDT} < 0.12$

398 The working points discussed in Section 4.4 are used to separate events into fit regions based on  
 399 the highest working point reached by a jet in each event. Because the background composition  
 400 differs significantly based on the number of b-jets, events are further subdivided into 1-jet and  
 401 2-jet regions in order to minimize the impact of background uncertainties.

402 An unfolding procedure is performed to account for differences in the number of reconstructed  
 403 jets compared to the number of truth jets in each event. The `AntiKt4TruthDressedWZJets`  
 404 truth jet collection is used to make this determination. In order to account for migration of  
 405 WZ+1-jet and WZ+2-jet events between the 1-jet and 2-jet bins at reco level, the signal samples  
 406 are separated based on the number of truth jets. Events with 0 jets or more than 3 jets at truth  
 407 level, yet fall within one of the categories listed in Table 8, are categorized as WZ + other, and  
 408 treated as a background. The migration matrix in the number of jets at truth level versus reco  
 409 level is shown in Figure 8. The composition of the number of truth jets in each reco jet bin is  
 410 taken from MC, with uncertainties in these estimates described in detail in Section 7.

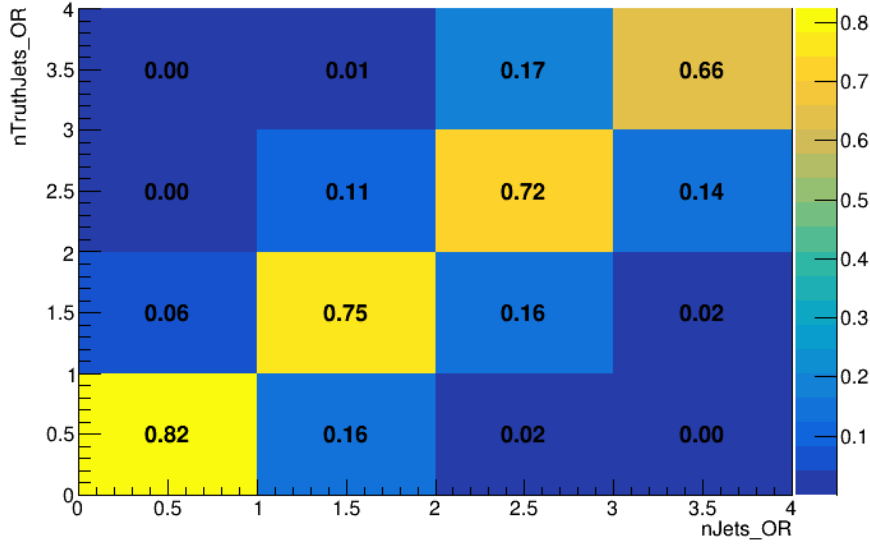


Figure 8: Number of truth jets compared to the number of reconstructed jets in each WZ event falling in the preselection region. Each row is normalized to unity.

- 411 An additional tZ control region is created based on the BDT described in Section 5. The region  
 412 with 1-jet passing the 60% working point is split in two - a signal enriched region of events with  
 413 a BDT score greater than 0.12, and a tZ control region including events with a score less than  
 414 0.12. This cutoff is arrived at by performing a fit an Asimov dataset with a variety of cutoffs,  
 415 and selecting the value that produces the highest significance for the measurement of WZ + b.  
 416 The modeling in each region is validated by comparing data and MC predictions for various  
 417 kinematic distributions. Events containing 5% or more WZ + b are blinded. These plot are  
 418 shown in Figures 9-22.

## WZ Fit Region - 1j Inclusive

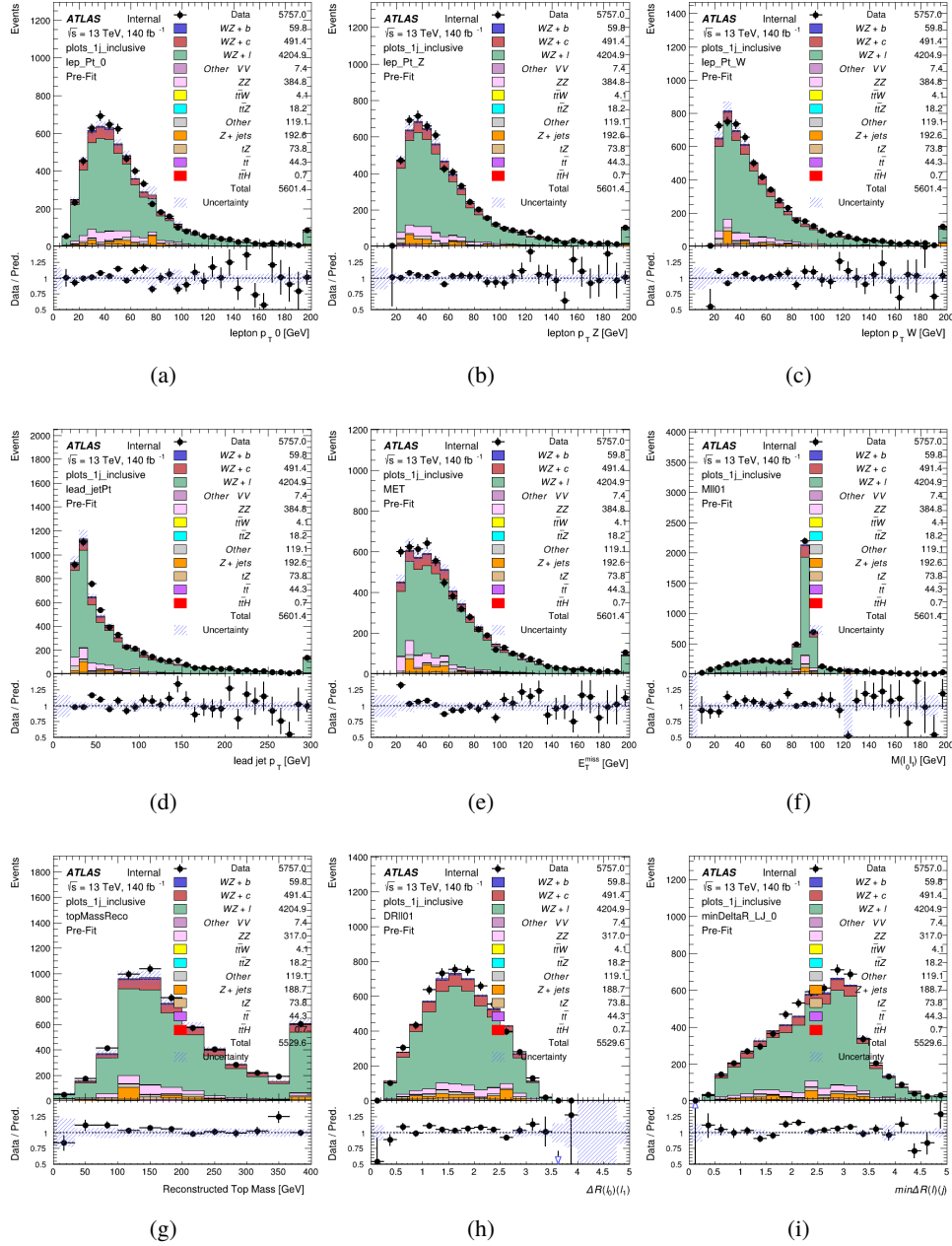


Figure 9: Comparisons between the data and MC distributions in the preselection region for (a) the  $p_T$  of the opposite sign lepton, (b) the  $p_T$  of the other lepton from the Z candidate, (c) the  $p_T$  of the lepton from the W candidate, (d) the leading jet  $p_T$ , (e) the  $E_T^{\text{miss}}$ , and (f) the invariant mass of leptons 0 and 1, (g) the reconstructed top mass, (h)  $\Delta(R)$  between lepton 0 and 1, (i) the  $\Delta(R)$  between the closest lepton and jet.

## WZ Fit Region - 1j &lt; 85% WP

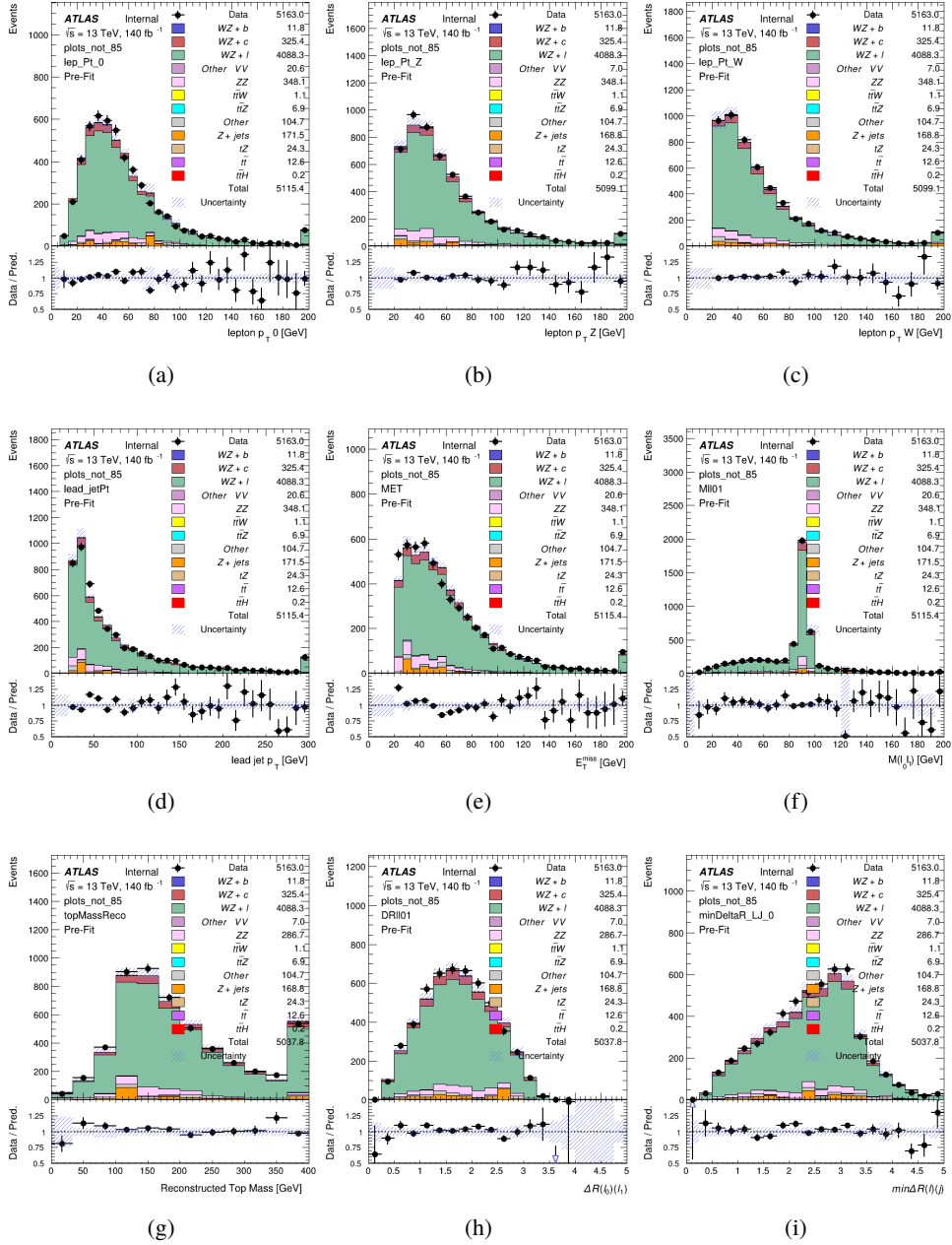


Figure 10: Comparisons between the data and MC distributions in the preselection region for (a) the  $p_T$  of the opposite sign lepton, (b) the  $p_T$  of the other lepton from the Z candidate, (c) the  $p_T$  of the lepton from the W candidate, (d) the leading jet  $p_T$ , (e) the  $E_T^{\text{miss}}$ , and (f) the invariant mass of leptons 0 and 1, (g) the reconstructed top mass, (h)  $\Delta(R)$  between lepton 0 and 1, (i) the  $\Delta(R)$  between the closest lepton and jet.

## WZ Fit Region - 1j 77-85% WP

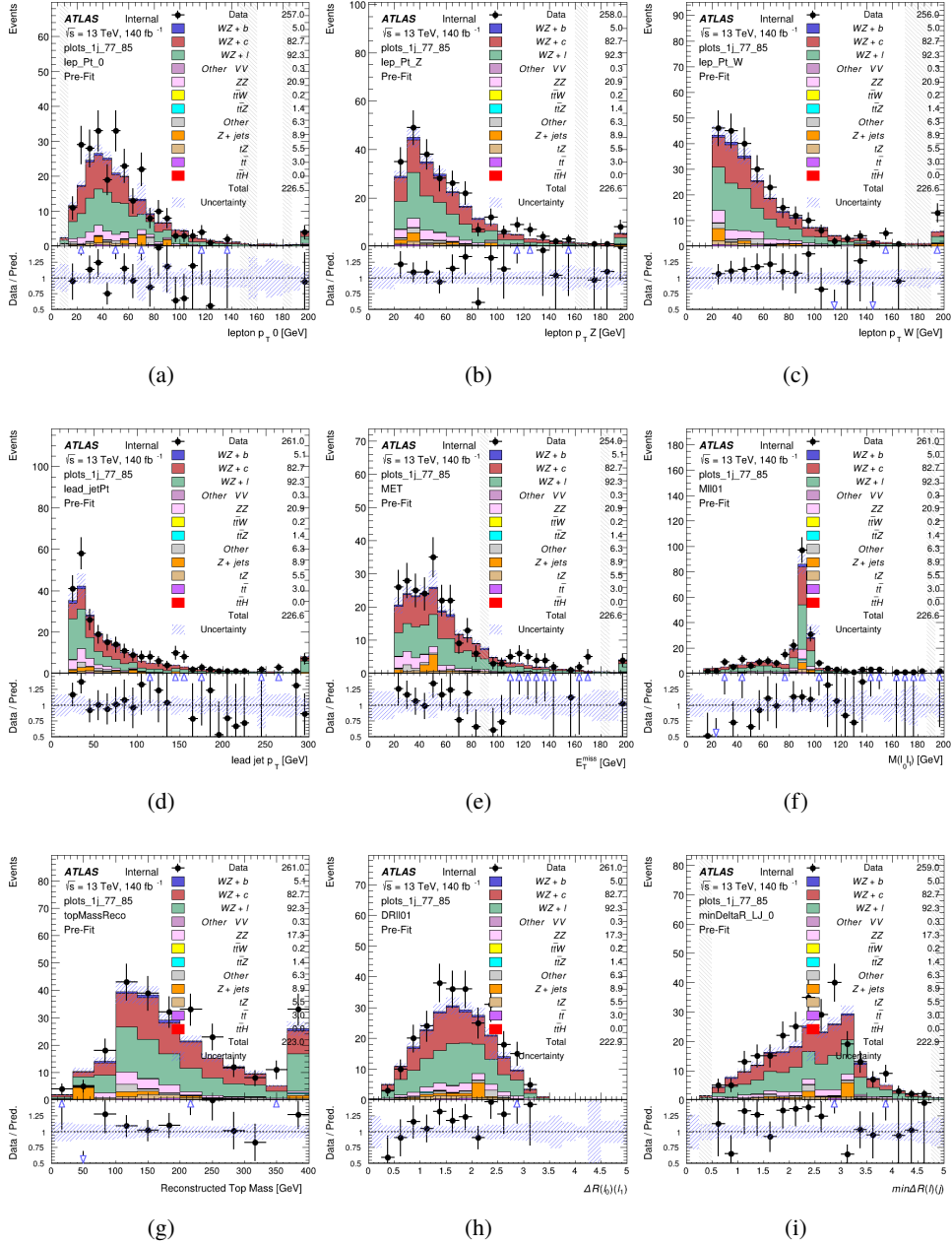


Figure 11: Comparisons between the data and MC distributions in the preselection region for (a) the  $p_T$  of the opposite sign lepton, (b) the  $p_T$  of the other lepton from the Z candidate, (c) the  $p_T$  of the lepton from the W candidate, (d) the leading jet  $p_T$ , (e) the  $E_T^{\text{miss}}$ , and (f) the invariant mass of leptons 0 and 1, (g) the reconstructed top mass, (h)  $\Delta(R)$  between lepton 0 and 1, (i) the  $\Delta(R)$  between the closest lepton and jet.

## WZ Fit Region - 1j 70-77% WP

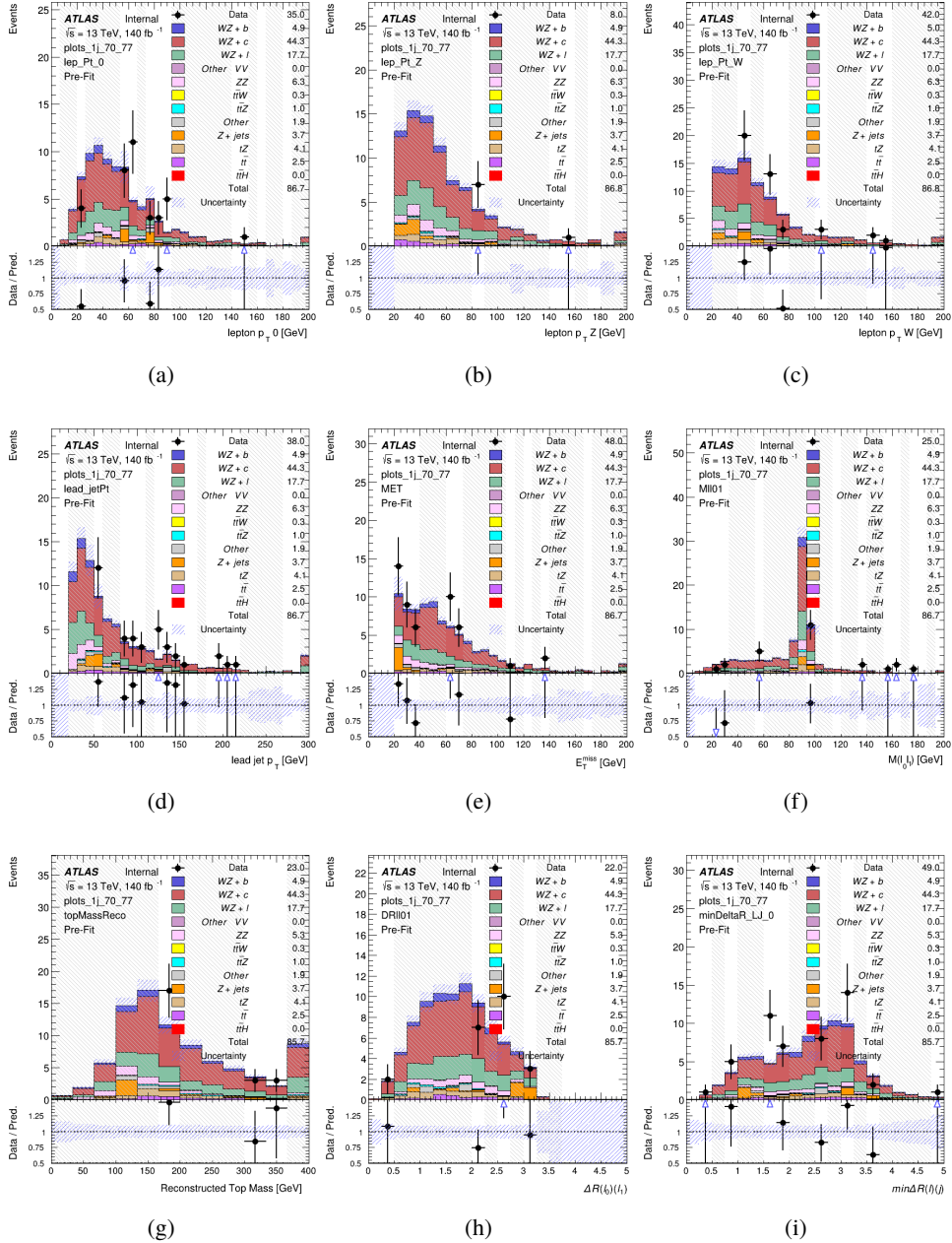


Figure 12: Comparisons between the data and MC distributions in the preselection region for (a) the  $p_T$  of the opposite sign lepton, (b) the  $p_T$  of the other lepton from the  $Z$  candidate, (c) the  $p_T$  of the lepton from the  $W$  candidate, (d) the leading jet  $p_T$ , (e) the  $E_T^{\text{miss}}$ , and (f) the invariant mass of leptons 0 and 1, (g) the reconstructed top mass, (h)  $\Delta(R)$  between lepton 0 and 1, (i) the  $\Delta(R)$  between the closest lepton and jet.

## WZ Fit Region - 1j 60-70% WP

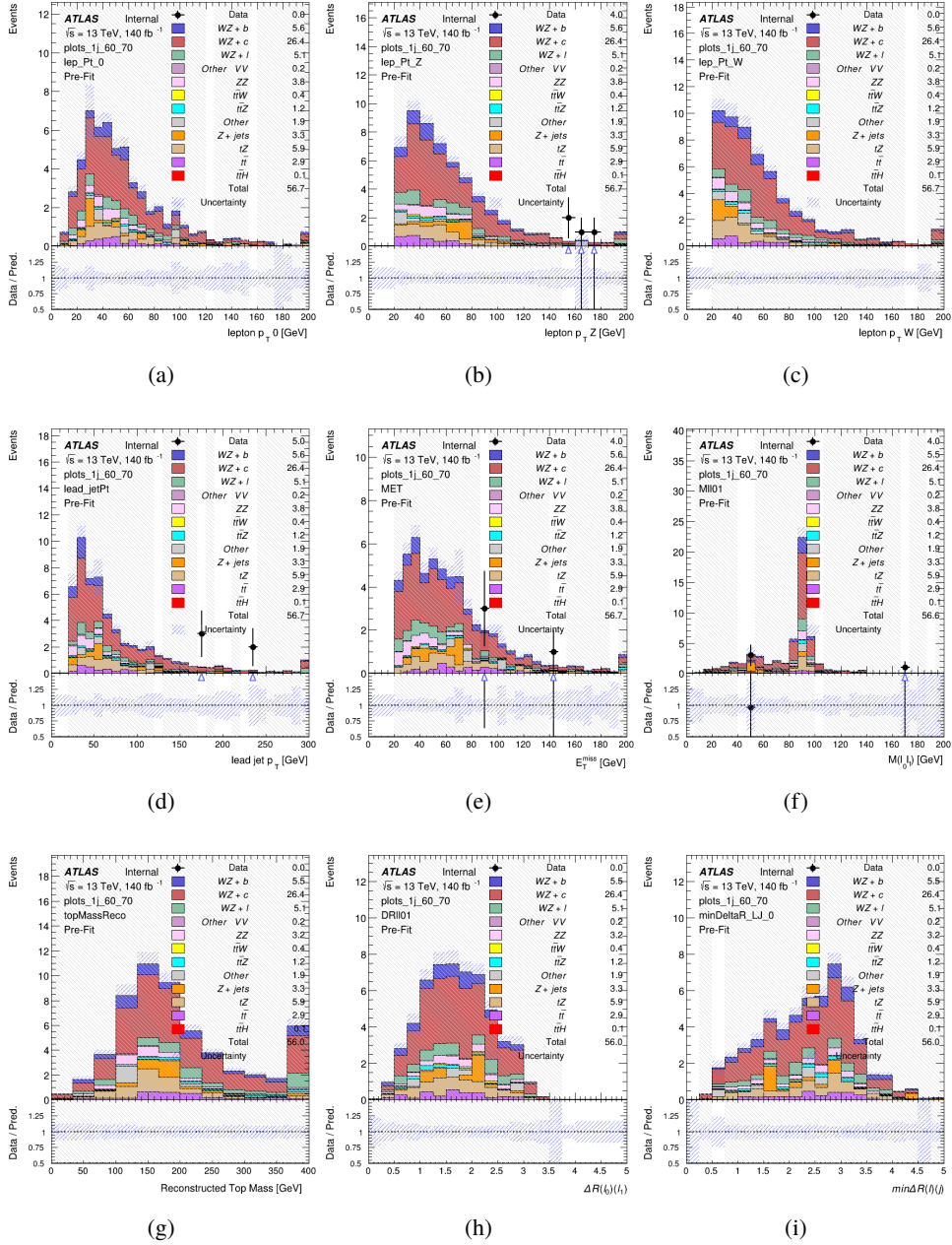


Figure 13: Comparisons between the data and MC distributions in the preselection region for (a) the  $p_T$  of the opposite sign lepton, (b) the  $p_T$  of the other lepton from the Z candidate, (c) the  $p_T$  of the lepton from the W candidate, (d) the leading jet  $p_T$ , (e) the  $E_T^{\text{miss}}$ , and (f) the invariant mass of leptons 0 and 1, (g) the reconstructed top mass, (h)  $\Delta(R)$  between lepton 0 and 1, (i) the  $\Delta(R)$  between the closest lepton and jet.

## WZ Fit Region - 1j 60% WP

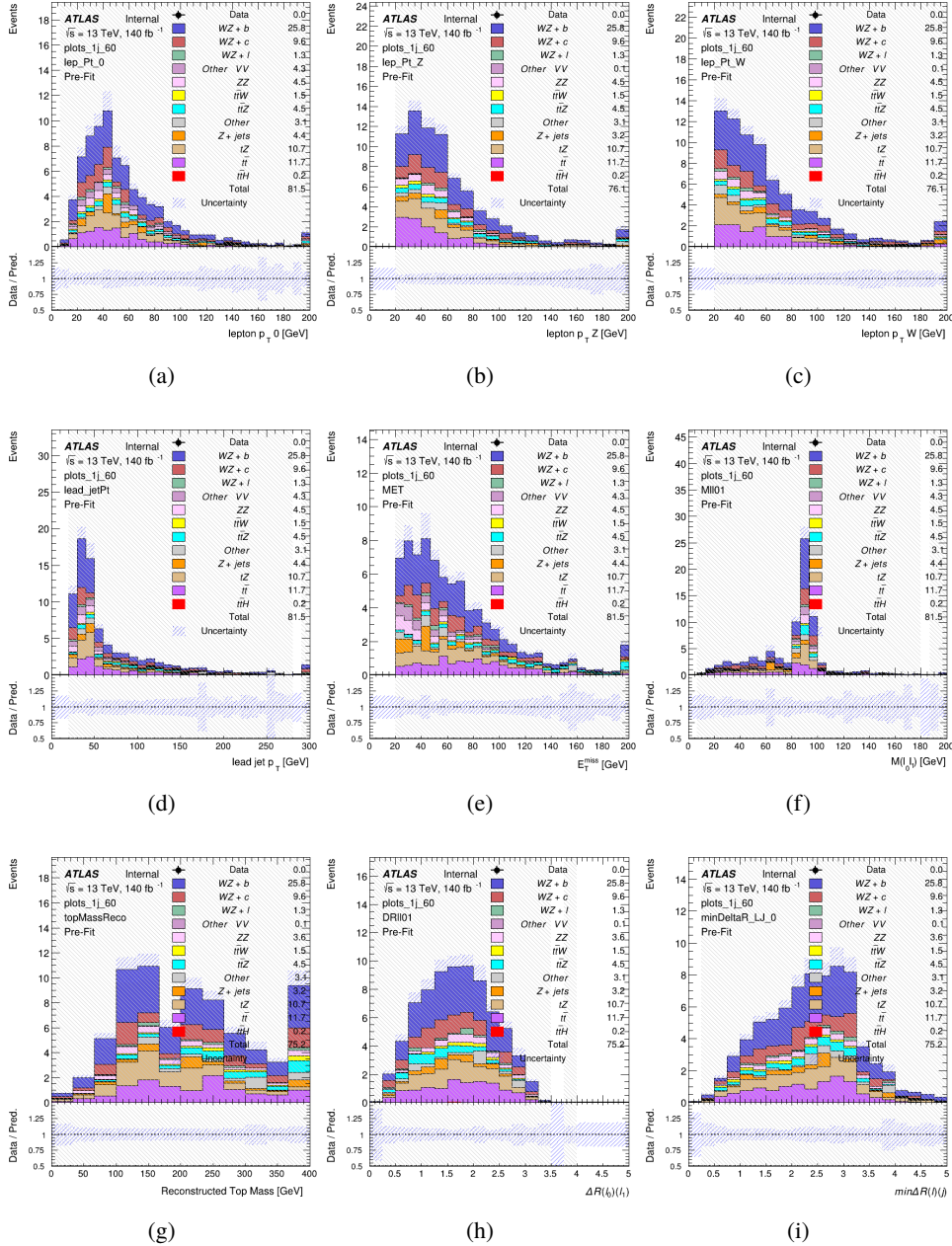


Figure 14: Comparisons between the data and MC distributions in the preselection region for (a) the  $p_T$  of the opposite sign lepton, (b) the  $p_T$  of the other lepton from the Z candidate, (c) the  $p_T$  of the lepton from the W candidate, (d) the leading jet  $p_T$ , (e) the  $E_T^{\text{miss}}$ , and (f) the invariant mass of leptons 0 and 1, (g) the reconstructed top mass, (h)  $\Delta(R)$  between lepton 0 and 1, (i) the  $\Delta(R)$  between the closest lepton and jet.

## WZ Fit Region - tZ-CR

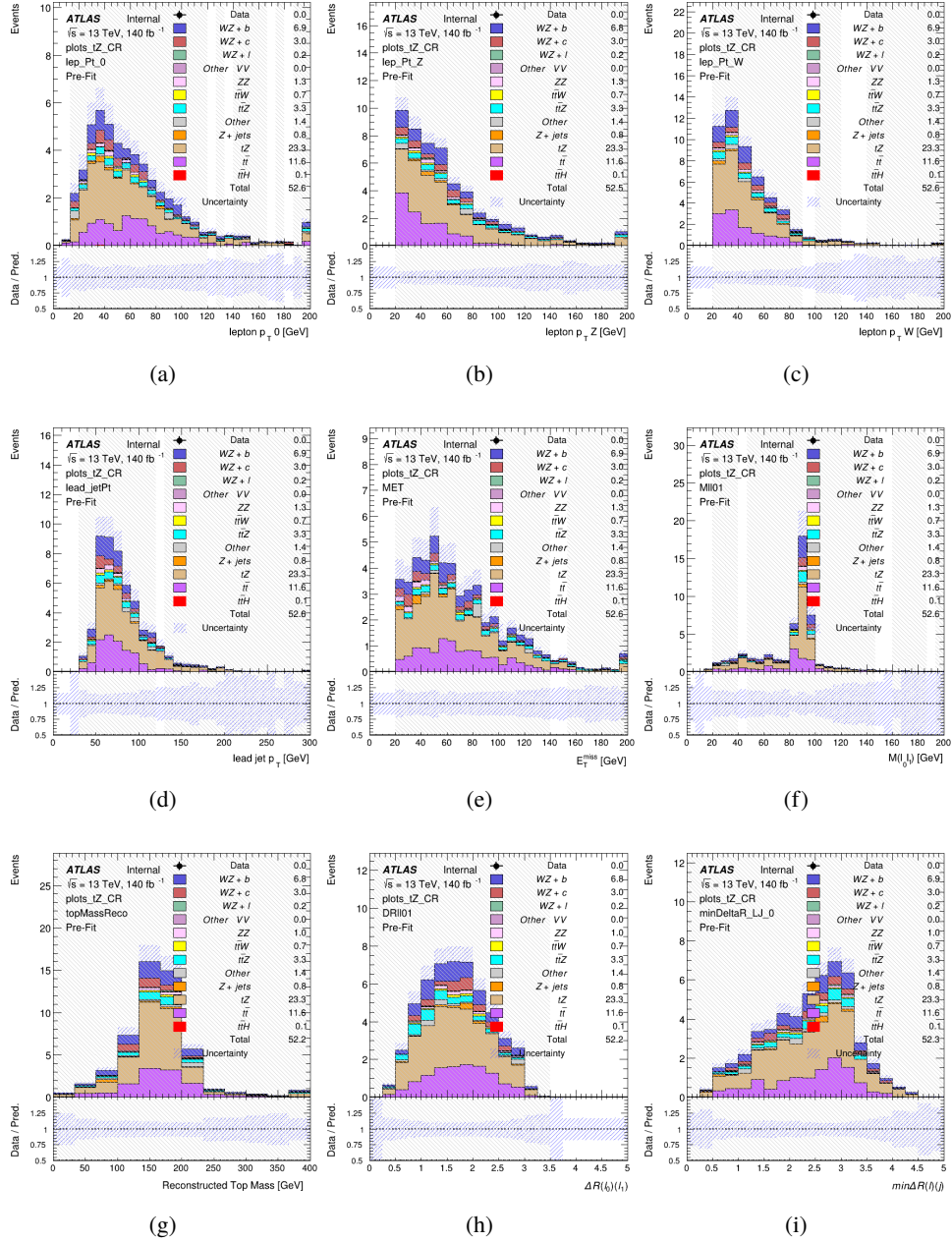


Figure 15: Comparisons between the data and MC distributions in the preselection region for (a) the  $p_T$  of the opposite sign lepton, (b) the  $p_T$  of the other lepton from the Z candidate, (c) the  $p_T$  of the lepton from the W candidate, (d) the leading jet  $p_T$ , (e) the  $E_T^{\text{miss}}$ , and (f) the invariant mass of leptons 0 and 1, (g) the reconstructed top mass, (h)  $\Delta(R)$  between lepton 0 and 1, (i) the  $\Delta(R)$  between the closest lepton and jet.

## WZ Fit Region - 2j Inclusive

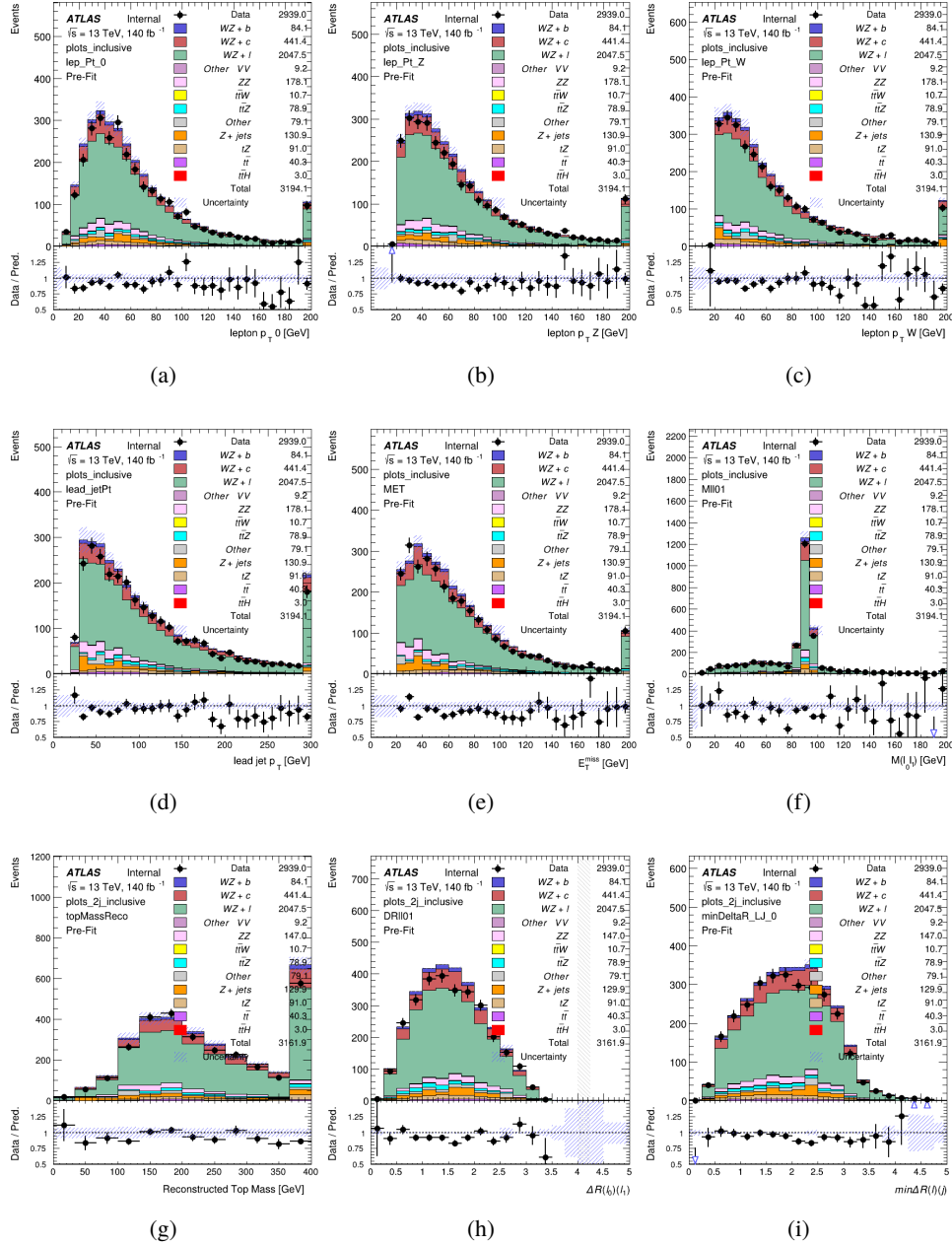


Figure 16: Comparisons between the data and MC distributions in the preselection region for (a) the  $p_T$  of the opposite sign lepton, (b) the  $p_T$  of the other lepton from the Z candidate, (c) the  $p_T$  of the lepton from the W candidate, (d) the leading jet  $p_T$ , (e) the  $E_T^{\text{miss}}$ , and (f) the invariant mass of leptons 0 and 1, (g) the reconstructed top mass, (h)  $\Delta(R)$  between lepton 0 and 1, (i) the  $\Delta(R)$  between the closest lepton and jet.

## WZ Fit Region - 2j &lt; 85% WP

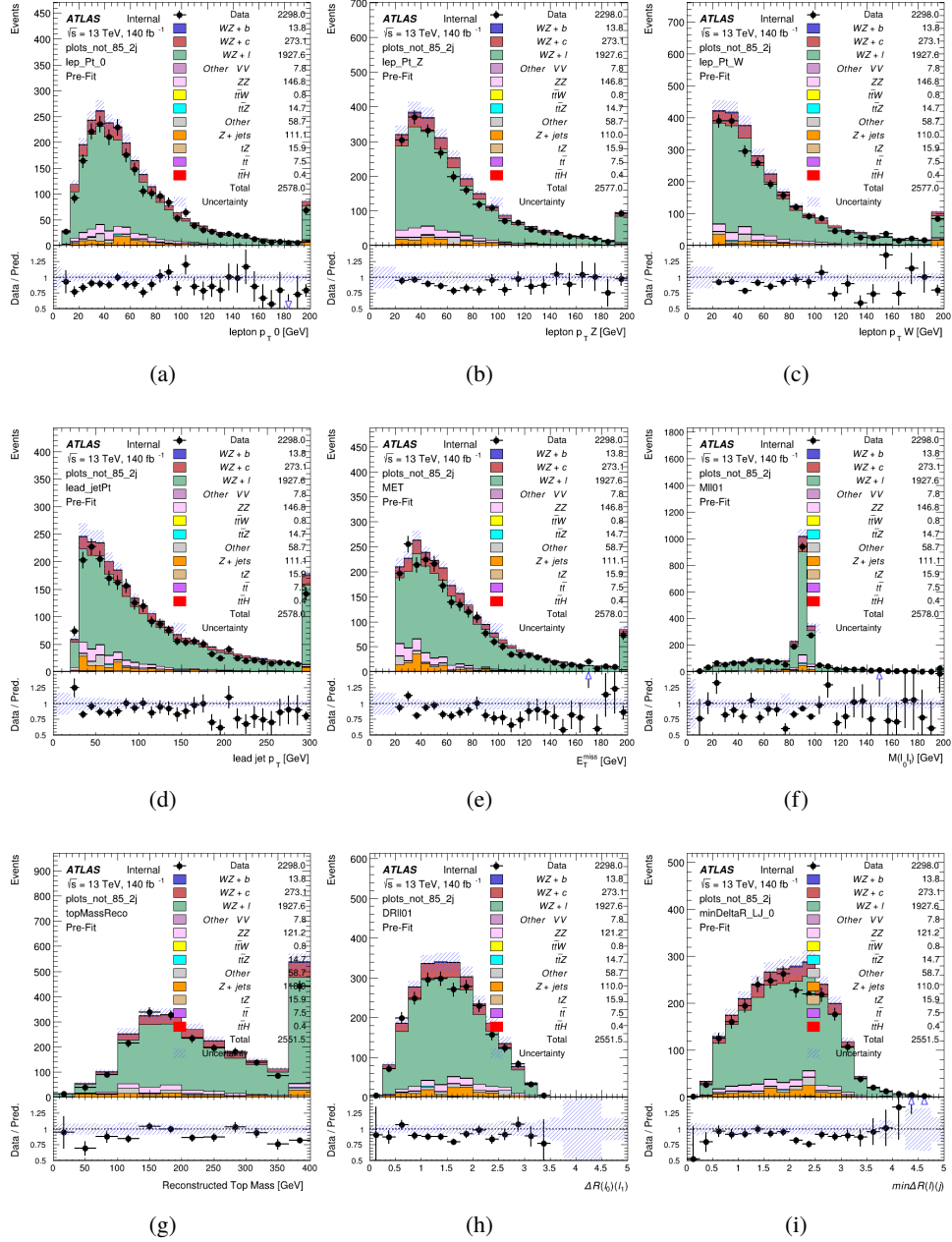


Figure 17: Comparisons between the data and MC distributions in the preselection region for (a) the  $p_T$  of the opposite sign lepton, (b) the  $p_T$  of the other lepton from the Z candidate, (c) the  $p_T$  of the lepton from the W candidate, (d) the leading jet  $p_T$ , (e) the  $E_T^{\text{miss}}$ , and (f) the invariant mass of leptons 0 and 1, (g) the reconstructed top mass, (h)  $\Delta(R)$  between lepton 0 and 1, (i) the  $\Delta(R)$  between the closest lepton and jet.

## WZ Fit Region - 2j 77-85% WP

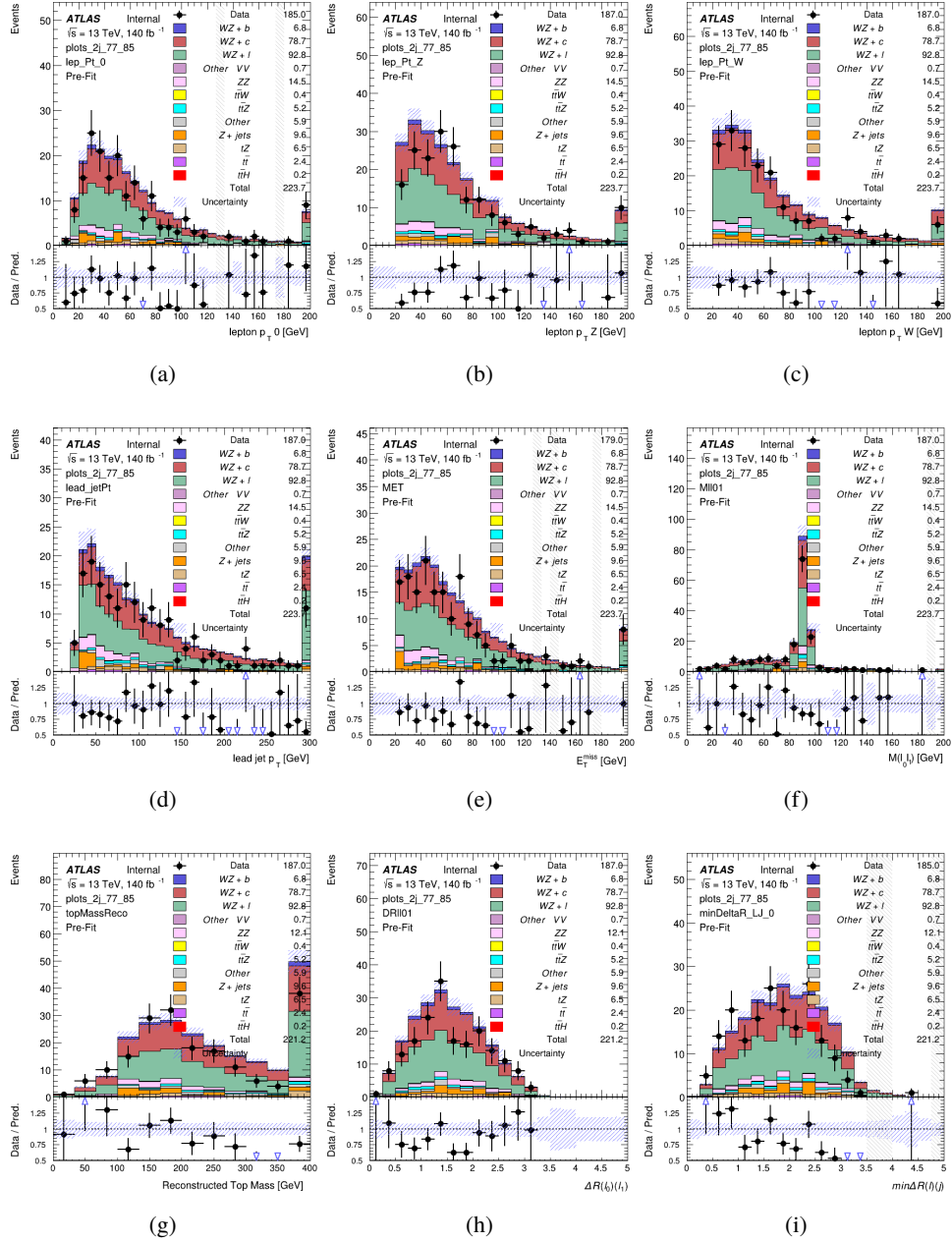


Figure 18: Comparisons between the data and MC distributions in the preselection region for (a) the  $p_T$  of the opposite sign lepton, (b) the  $p_T$  of the other lepton from the Z candidate, (c) the  $p_T$  of the lepton from the W candidate, (d) the leading jet  $p_T$ , (e) the  $E_T^{\text{miss}}$ , and (f) the invariant mass of leptons 0 and 1, (g) the reconstructed top mass, (h)  $\Delta(R)$  between lepton 0 and 1, (i) the  $\Delta(R)$  between the closest lepton and jet.

## WZ Fit Region - 2j 70-77% WP

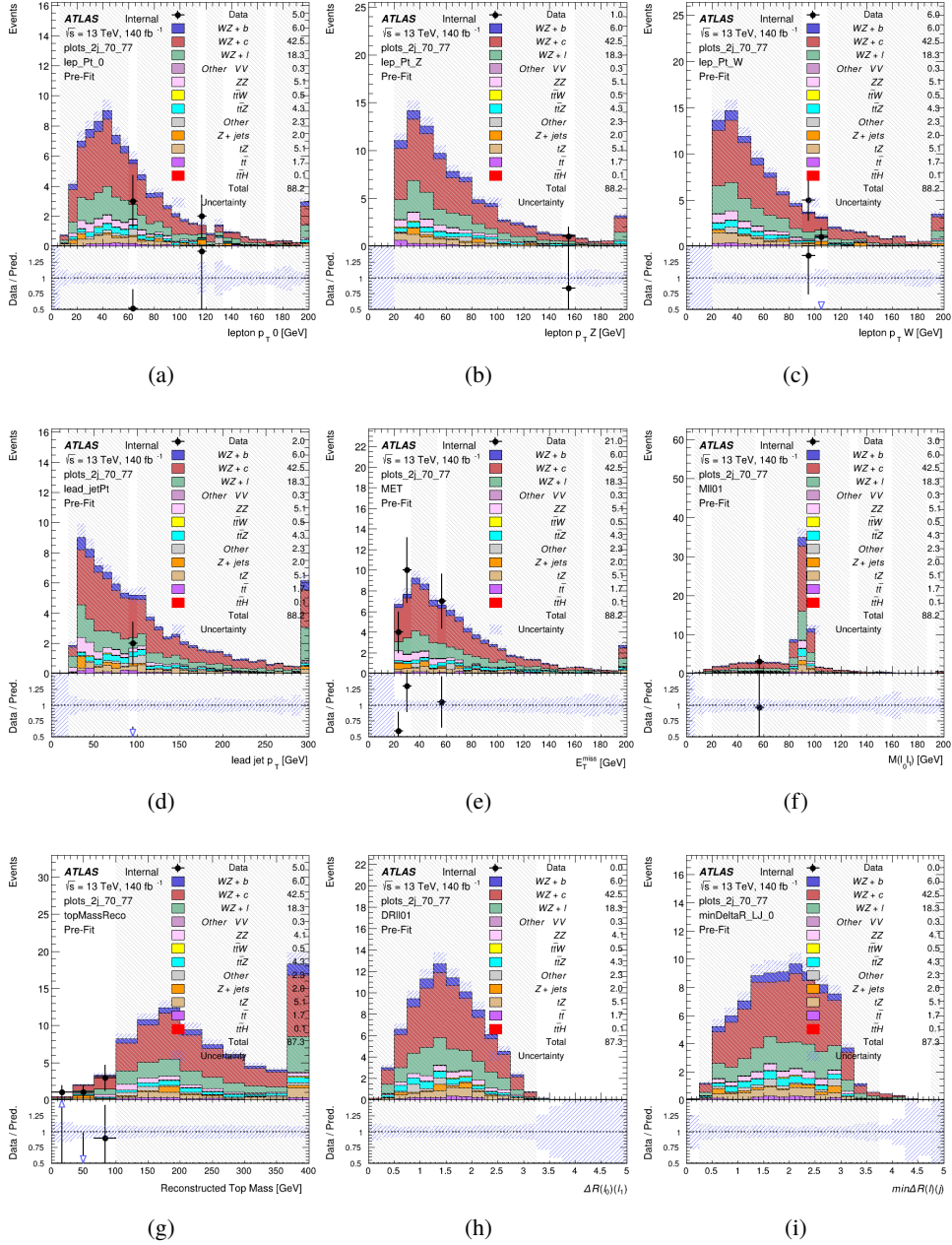


Figure 19: Comparisons between the data and MC distributions in the preselection region for (a) the  $p_T$  of the opposite sign lepton, (b) the  $p_T$  of the other lepton from the Z candidate, (c) the  $p_T$  of the lepton from the W candidate, (d) the leading jet  $p_T$ , (e) the  $E_T^{\text{miss}}$ , and (f) the invariant mass of leptons 0 and 1, (g) the reconstructed top mass, (h)  $\Delta(R)$  between lepton 0 and 1, (i) the  $\Delta(R)$  between the closest lepton and jet.

## WZ Fit Region - 2j 60-70% WP

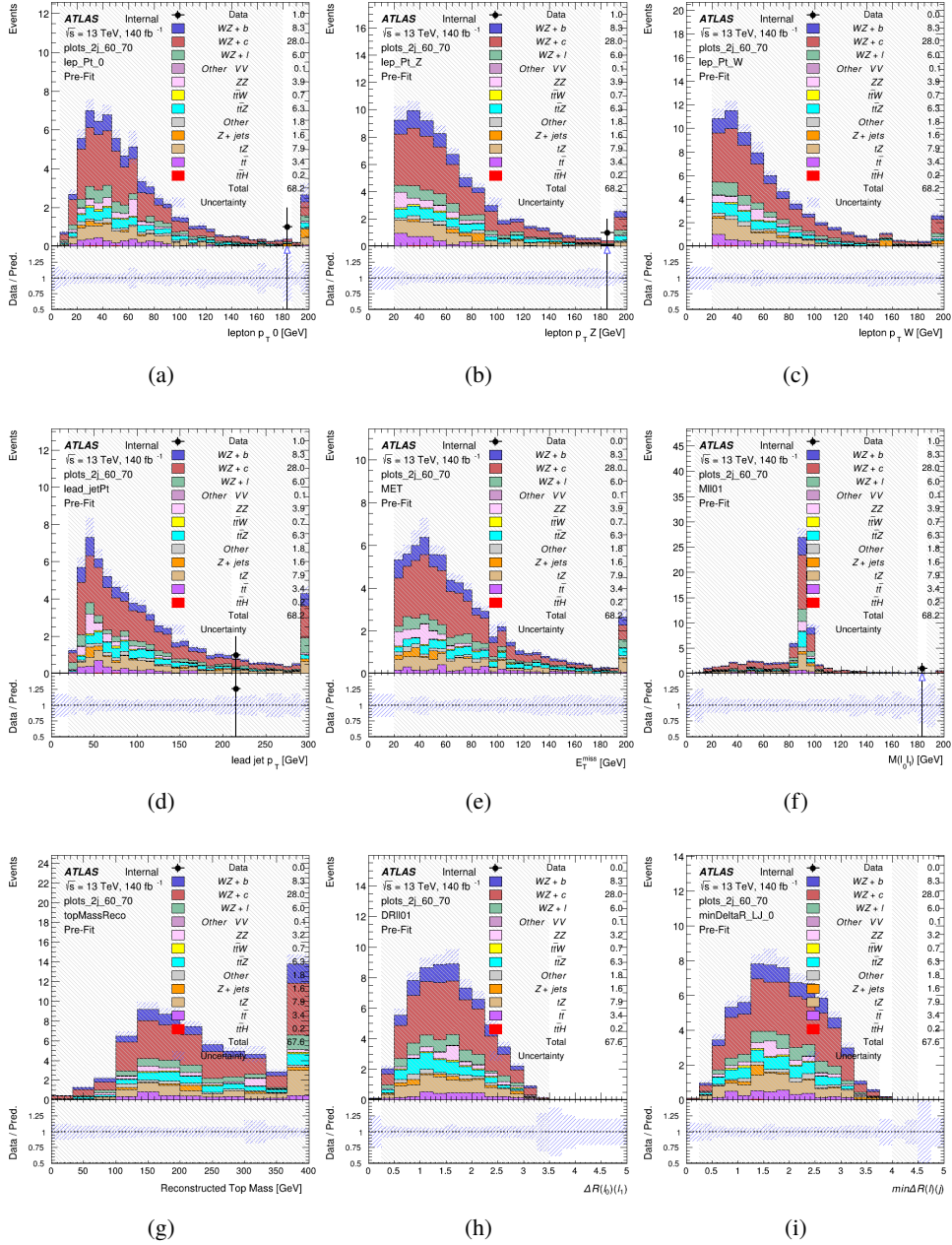


Figure 20: Comparisons between the data and MC distributions in the preselection region for (a) the  $p_T$  of the opposite sign lepton, (b) the  $p_T$  of the other lepton from the Z candidate, (c) the  $p_T$  of the lepton from the W candidate, (d) the leading jet  $p_T$ , (e) the  $E_T^{\text{miss}}$ , and (f) the invariant mass of leptons 0 and 1, (g) the reconstructed top mass, (h)  $\Delta(R)$  between lepton 0 and 1, (i) the  $\Delta(R)$  between the closest lepton and jet.

## WZ Fit Region - 2j 60% WP

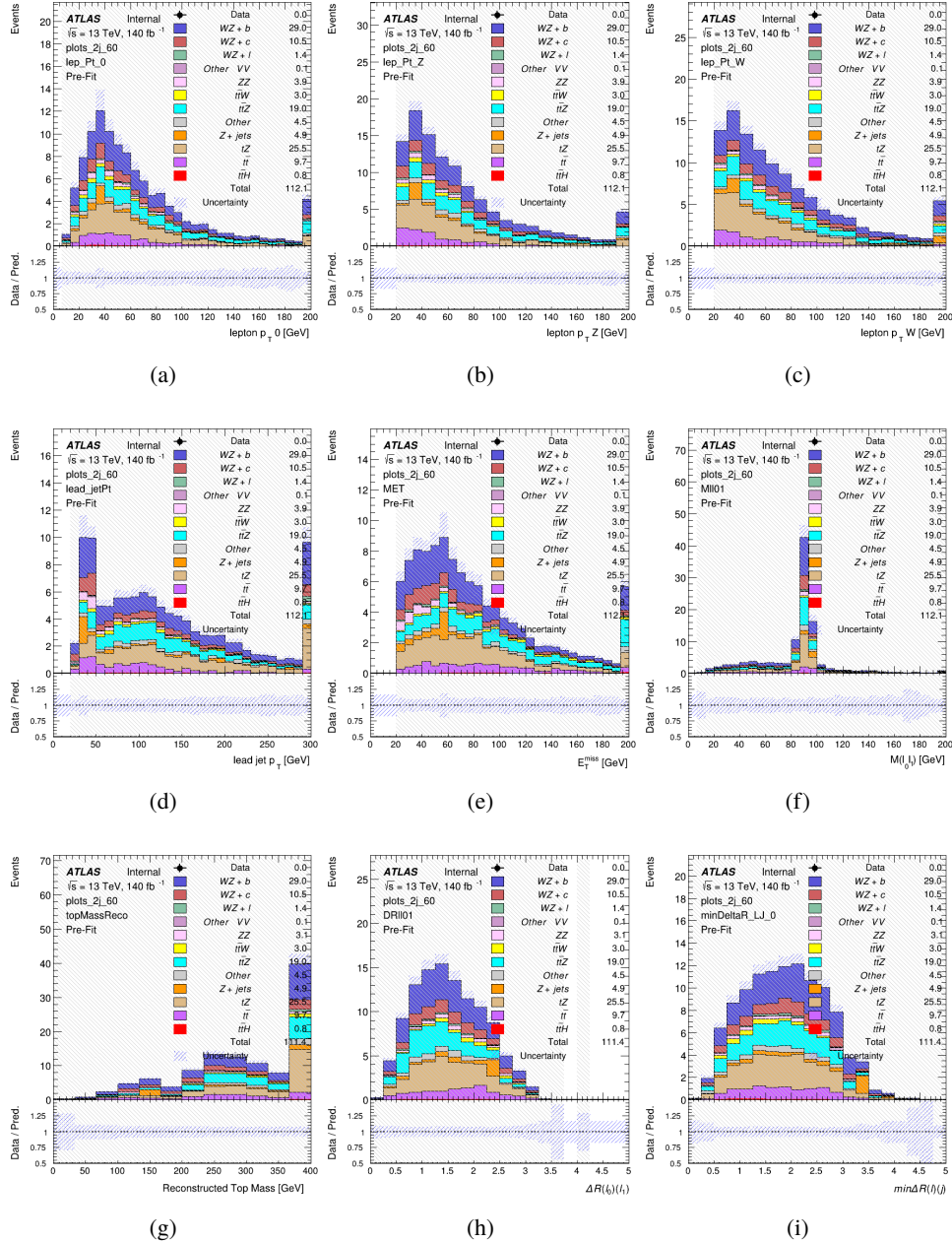


Figure 21: Comparisons between the data and MC distributions in the preselection region for (a) the  $p_T$  of the opposite sign lepton, (b) the  $p_T$  of the other lepton from the Z candidate, (c) the  $p_T$  of the lepton from the W candidate, (d) the leading jet  $p_T$ , (e) the  $E_T^{\text{miss}}$ , and (f) the invariant mass of leptons 0 and 1, (g) the reconstructed top mass, (h)  $\Delta(R)$  between lepton 0 and 1, (i) the  $\Delta(R)$  between the closest lepton and jet.

## WZ Fit Region - tZ-CR-2j

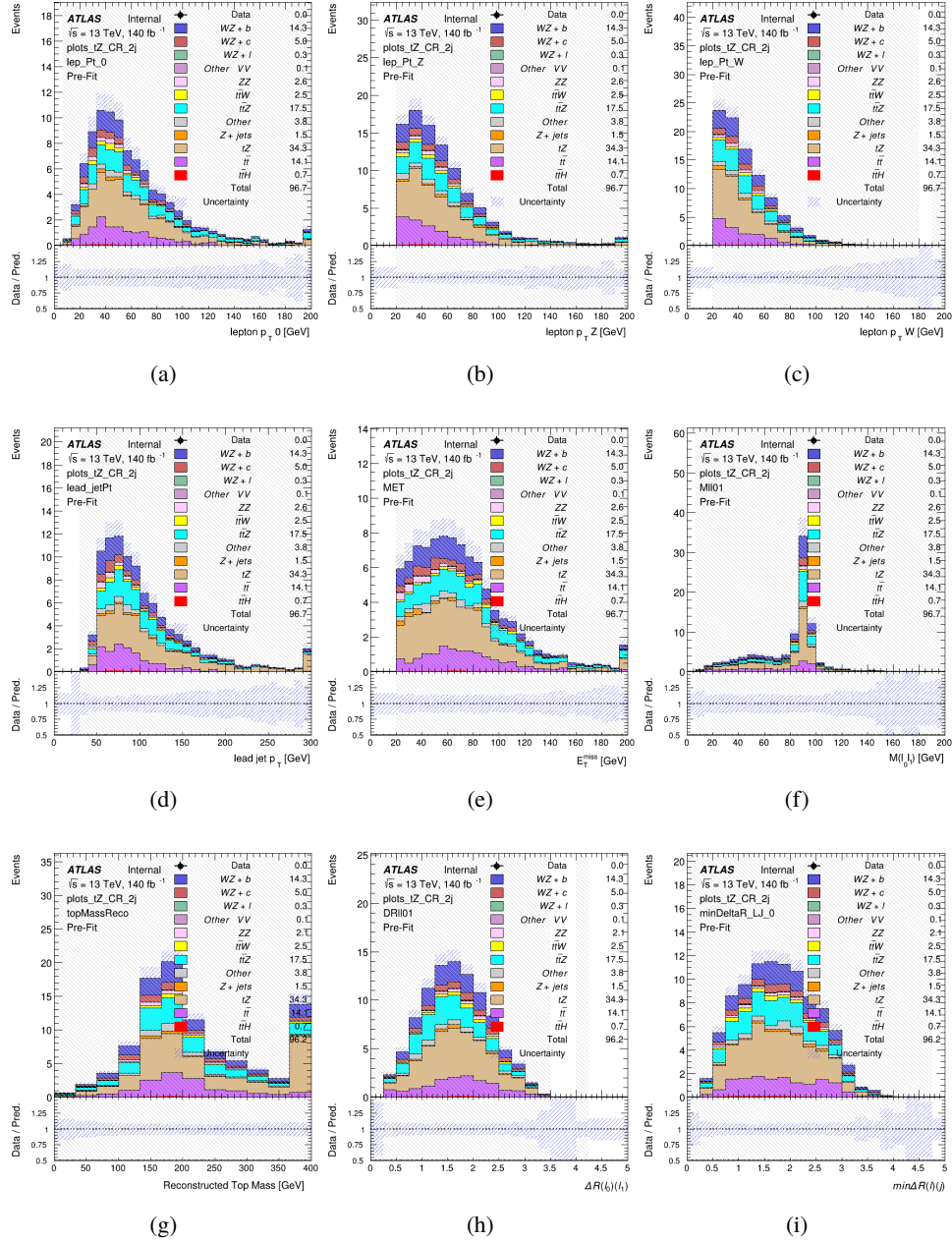


Figure 22: Comparisons between the data and MC distributions in the preselection region for (a) the  $p_T$  of the opposite sign lepton, (b) the  $p_T$  of the other lepton from the Z candidate, (c) the  $p_T$  of the lepton from the W candidate, (d) the leading jet  $p_T$ , (e) the  $E_T^{\text{miss}}$ , and (f) the invariant mass of leptons 0 and 1, (g) the reconstructed top mass, (h)  $\Delta(R)$  between lepton 0 and 1, (i) the  $\Delta(R)$  between the closest lepton and jet.

419 **6.3 Non-Prompt Lepton Estimation**

420 Two processes act as sources of non-prompt leptons appear in the analysis:  $t\bar{t}$  and Z+jet  
 421 production both produce two prompt leptons, and each contribute to the 31 region when an  
 422 additional non-prompt lepton appears in the event. The contribution of these processes is  
 423 estimated with Monte Carlo simulations, which are validated using enriched validation regions.

424 The modelling in the Z+jets and  $t\bar{t}$  CRs is further validated for each of the pseudo-continuous  
 425 b-tag regions used in the analysis. The relevant lepton  $p_T$  spectrum in each b-tag region is shown  
 426 in Appendix A.2 for these CRs after the correction factors derived below have been applied.

427 **6.3.1  $t\bar{t}$  Validation**

428  $t\bar{t}$  events can produce two prompt leptons from the decay of each of the tops. These top decays  
 429 produce two b-quarks, the decay of which can produce additional non-prompt leptons, which  
 430 occasionally pass the event preselection. In order to validate that the Monte Carlo accurately  
 431 simulates this process accurately, the MC prediction in a non-prompt  $t\bar{t}$  enriched validation  
 432 region is compared to data.

433 The  $t\bar{t}$  validation region is similar to the preselection region - three leptons meeting the criteria  
 434 described in Section 6 are required, and the requirements on  $E_T^{\text{miss}}$  remain the same. However,  
 435 the selection requiring that a lepton pair form a Z-candidate are reversed. Events where the  
 436 invariant mass of any two opposite sign, same flavor leptons falls within 10 GeV of 91.2 GeV are  
 437 rejected. This ensures the  $t\bar{t}$  validation region is orthogonal to the preselection region.

438 Further, because the jet multiplicity of  $t\bar{t}$  events tends to be higher than WZ + jets, the number  
 439 of jets in each event is required to be greater than 1. As b-jets are almost invariably produced  
 440 from top decays, at least one b-tagged jet passing the 70% DL1r WP in each event is required.  
 441 Various kinematic plots of this region are shown in Figure 23.

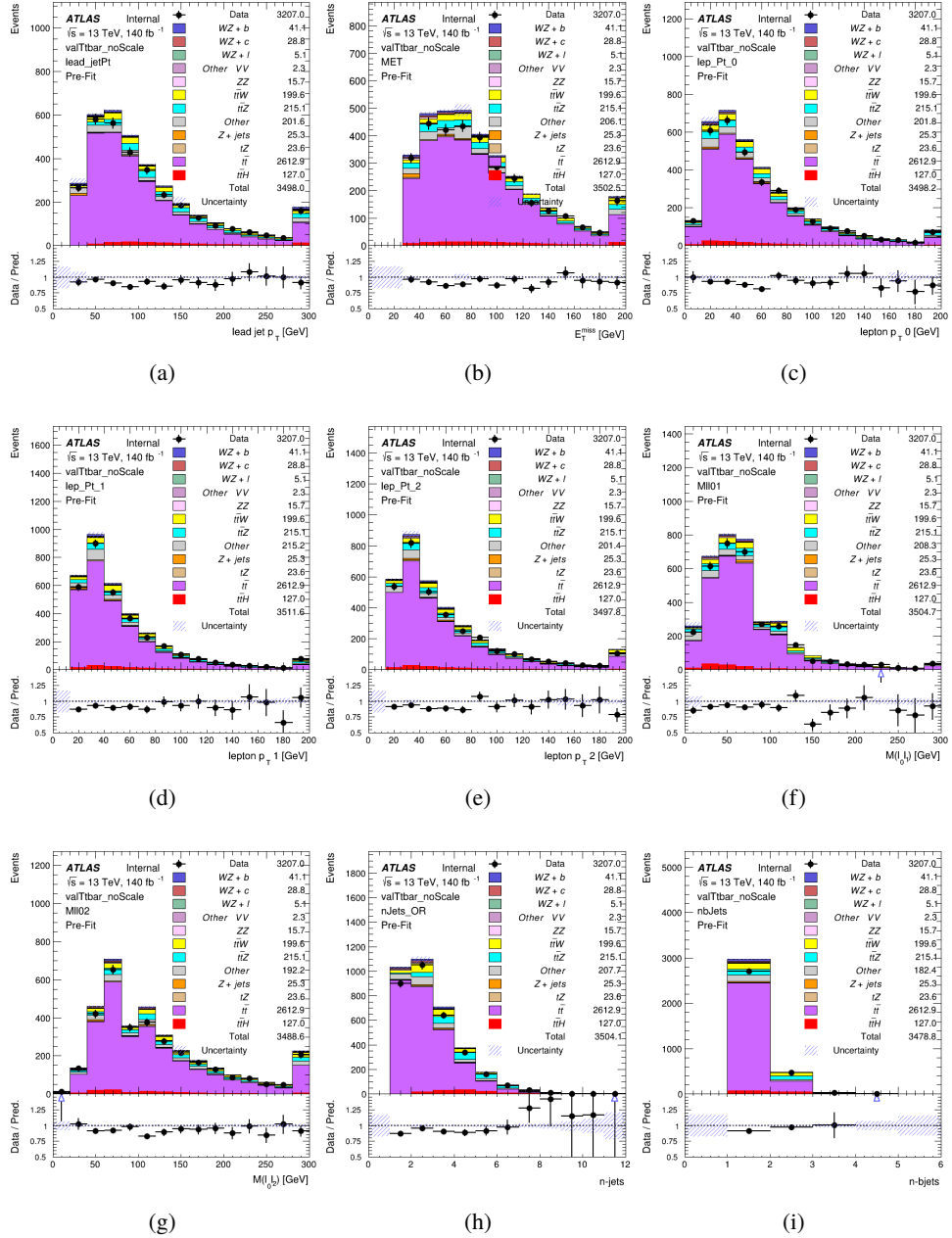


Figure 23: Comparisons between the data and MC distributions in the  $t\bar{t}$  validation region for (a) the  $p_T$  of the leading jet, (b) the missing transverse energy, (c) the  $p_T$  of lepton 0, (d)  $p_T$  of lepton 1, (e)  $p_T$  of lepton 2, (f) the invariant mass of leptons 0 and 1, (g) the invariant mass of leptons 0 and 2, (h) the number of jets, (i) the number of b-tagged jets.

The shape of each distribution agrees quite well between data and MC, with a constant offset between the two. This is accounted for by applying a constant correction factor of 0.9 to the  $t\bar{t}$

444 MC prediction. Plots showing the kinematics of the  $t\bar{t}$  VR after this correction factor has been  
 445 applied are shown in Figure 24.

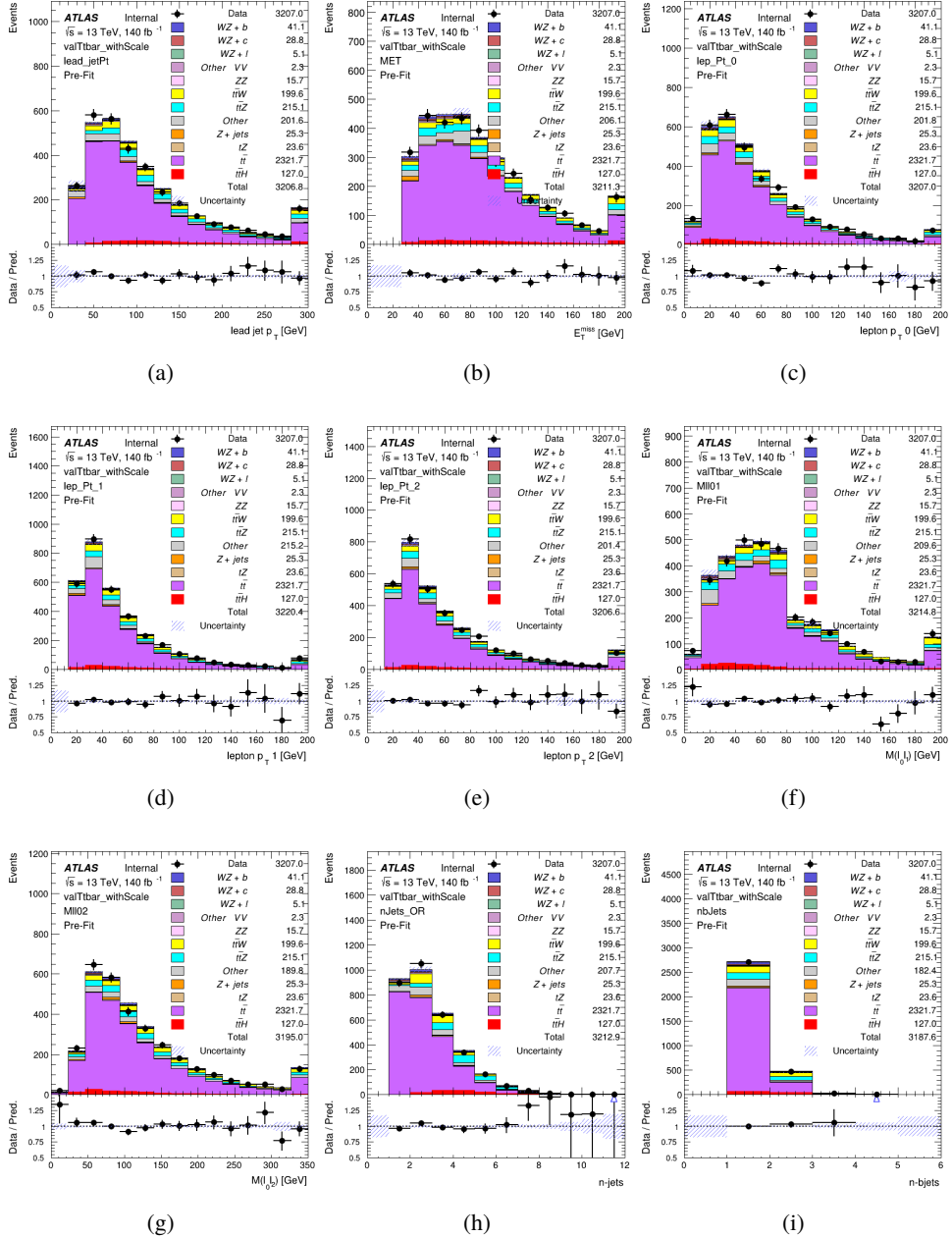


Figure 24: Comparisons between the data and MC distributions in the  $t\bar{t}$  validation region after the correction factor has been applied for (a) the  $p_T$  of the leading jet, (b) the missing transverse energy, (c) the  $p_T$  of lepton 0, (d)  $p_T$  of lepton 1, (e)  $p_T$  of lepton 2, (f) the invariant mass of leptons 0 and 1, (g) the invariant mass of leptons 0 and 2, (h) the number of jets, (i) the number of b-tagged jets.

446 The modeling is further validated by looking at the yield in the  $t\bar{t}$  VR for each DL1r WP, giving  
 447 a clearer correspondence to the signal regions used in the fit. For these plots, the requirement  
 448 that each event contain at least one b-tagged jet is removed. Each region shown in Figure 25  
 449 requires one or more jets pass the listed WP, with no jets passing the next highest WP.

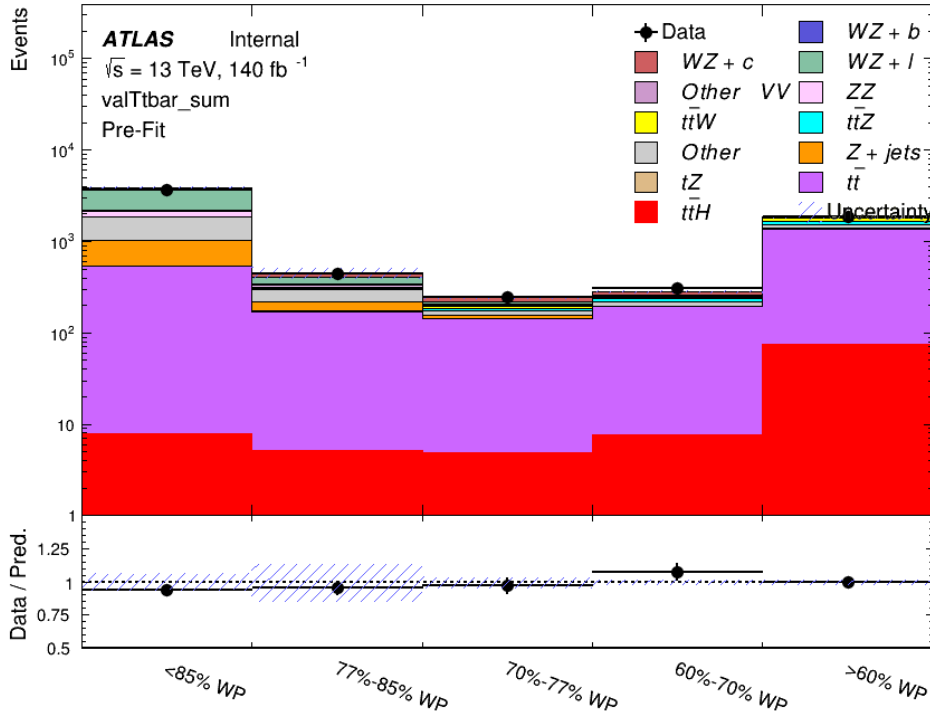


Figure 25: Data and MC comparisons for each DL1r WP for both 1-jet and 2-jet regions, after the  $t\bar{t}$  VR selection and correction factor have been applied

450 As data and MC are found to agree within 20% for each of these working points, a 20% systematic  
 451 uncertainty on the  $t\bar{t}$  prediction is included for the analysis.

### 452 6.3.2 Z+jets Validation

453 Similar to  $t\bar{t}$ , a non-prompt Z+jets validation region is produced in order to validate the MC  
 454 predictions. The lepton requirements remain the same as the preselection region. Because no  
 455 neutrinos are present for this process, the  $E_T^{\text{miss}}$  cut is reversed, requiring  $E_T^{\text{miss}} < 30 \text{ GeV}$ . This  
 456 also ensures this validation region is orthogonal to the preselection region. Further, the number  
 457 of jets in each event is required to be greater than or equal to one. Various kinematic plots of this  
 458 region are shown below. The general agreement between data and MC in each of these suggests  
 459 that the non-prompt contribution of Z+jets is well modeled by Monte Carlo.

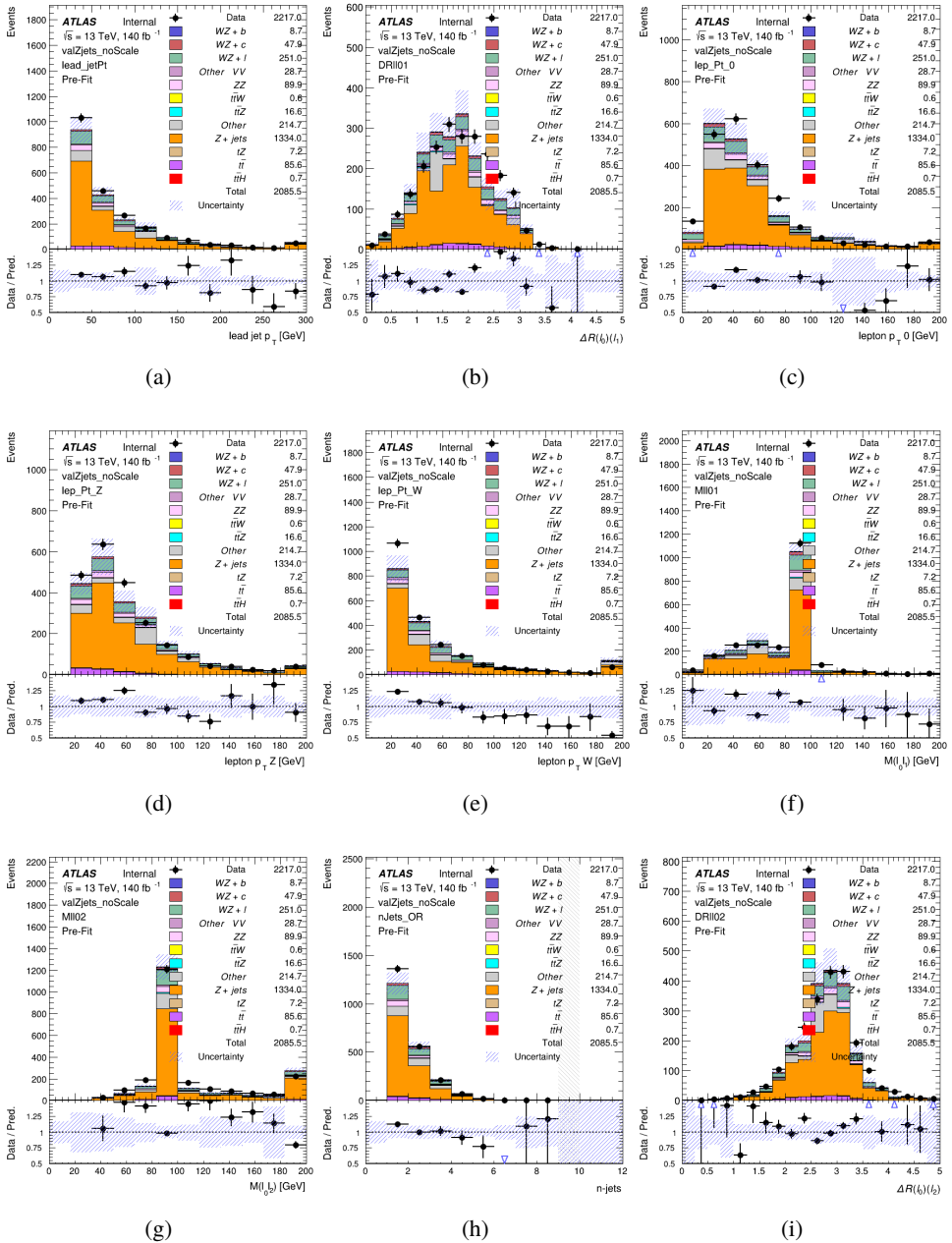


Figure 26: Comparisons between the data and MC distributions in the Z+jets validation region for (a) the  $p_T$  of the leading jet, (b)  $\Delta R$  between leptons 0 and 1, (c) the  $p_T$  of lepton 0, (d)  $p_T$  of SS lepton from the Z candidate, (e)  $p_T$  of the SS lepton from the W candidate, (f) the invariant mass of leptons 0 and 1, (g) the invariant mass of leptons 0 and 2, (h) the number of jets, (i)  $\Delta R$  between leptons 0 and 2. Includes only statistical uncertainties

460 While there is general agreement between data and MC within statistical uncertainty, the shape

of the  $p_T$  spectrum of the lepton from the W candidate is found to differ. As this is the lepton not included in the Z-candidate, in the case of Z+jets, this lepton is most often the non-prompt lepton. A similar effect is seen for both non-prompt muons and electrons in the Z+jets validation region, as shown in Figure 27.

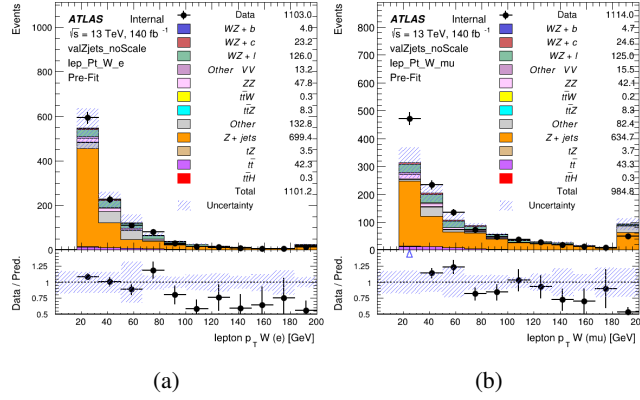


Figure 27:  $p_T$  spectrum of the lepton from the W candidate for (a) electrons and (b) muons

To account for this discrepancy, a variable correction factor is applied to Z+jets.  $\chi^2$  minimization of the W lepton  $p_T$  spectrum is performed to derive a correction factor as a function of this  $p_T$ . Kinematic plots of the Z + jets validation region after this correction factor has been applied are shown in Figure 28.

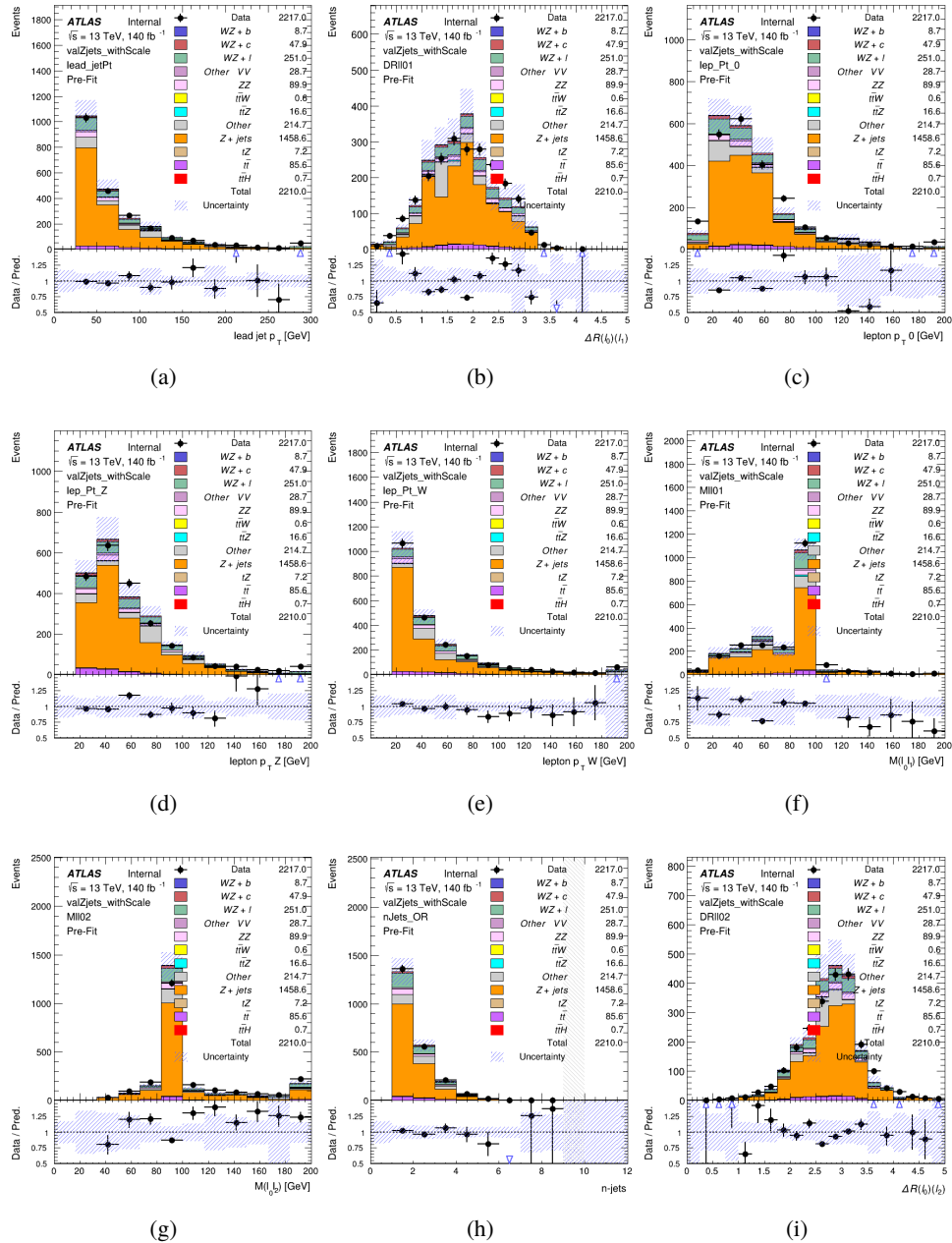


Figure 28: Comparisons between the data and MC distributions in the Z+jets validation region after the correction factor has been applied for (a) the  $p_T$  of the leading jet, (b)  $\Delta R$  between leptons 0 and 1, (c) the  $p_T$  of lepton 0, (d)  $p_T$  of SS lepton from the Z candidate, (e)  $p_T$  of the SS lepton from the W candidate, (f) the invariant mass of leptons 0 and 1, (g) the invariant mass of leptons 0 and 2, (h) the number of jets, (i)  $\Delta R$  between leptons 0 and 2

469 The modeling is further validated by looking at the yield in the Z+jets VR for each DL1r WP,

470 giving a clearer correspondence to the signal regions used in the fit. Each region shown in Figure  
 471 29 requires one or more jets pass the listed WP, with no jets passing the next highest WP.

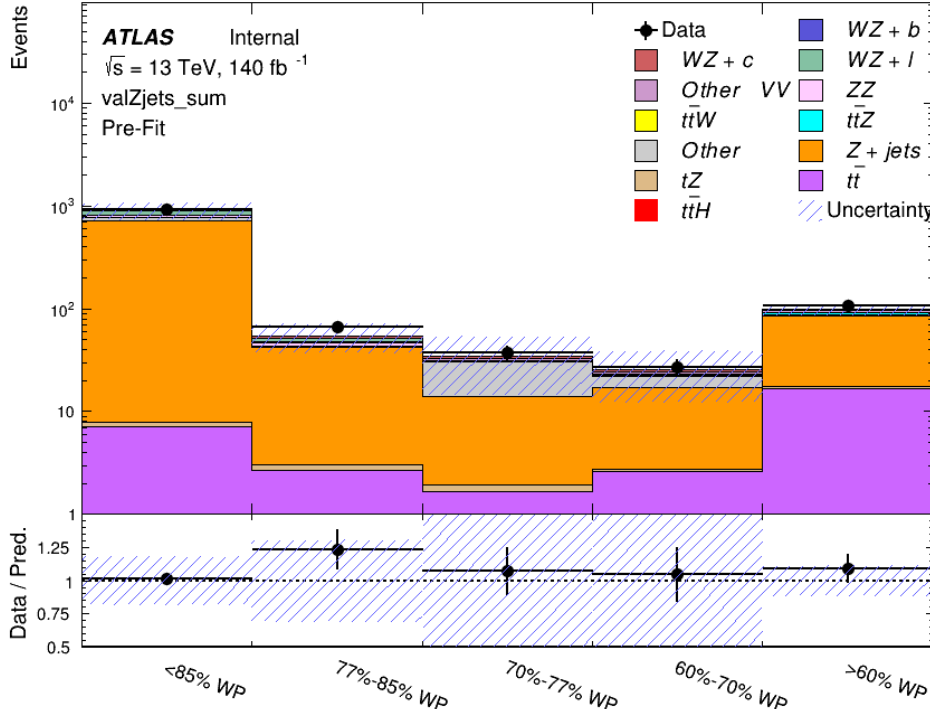


Figure 29: Data and MC comparisons for each DL1r WP for both 1-jet and 2-jet regions, after the Z+jets VR selection and correction factor have been applied

472 For each of the b-tagging working points considered, the data falls within 25% of the MC  
 473 prediction once this correction factor has been applied. Therefore, a 25% systematic uncertainty  
 474 is applied to Z + jets in the analysis.

## 475 7 Systematic Uncertainties

476 The systematic uncertainties that are considered are summarized in Table 9. These are imple-  
 477 mented in the fit either as a normalization factors or as a shape variation or both in the signal  
 478 and background estimations. The numerical impact of each of these uncertainties is outlined in  
 479 Section 8.

Table 9: Sources of systematic uncertainty considered in the analysis.

Systematic uncertainty	Components
Luminosity	1
Pileup reweighting	1
<b>Physics Objects</b>	
Electron	6
Muon	15
Jet energy scale	28
Jet energy resolution	8
Jet vertex fraction	1
Jet flavor tagging	131
$E_T^{\text{miss}}$	3
Total (Experimental)	194
<b>Signal Modeling</b>	
Shape modelling	3
Renormalization and factorization scales	5
nJet Migration	5
<b>Background Modeling</b>	
Cross section	15
Renormalization and factorization scales	12
Parton shower and hadronization model	2
Shower tune	4
Total (Signal and background modeling)	41
Total (Overall)	236

<sup>480</sup> The uncertainty in the combined 2015–2018 integrated luminosity is 1.7% [24], obtained using  
<sup>481</sup> the LUCID-2 detector [25] for the primary luminosity measurements.

<sup>482</sup> The experimental uncertainties are related to the reconstruction and identification of light  
<sup>483</sup> leptons and b-tagging of jets, and to the reconstruction of  $E_T^{\text{miss}}$ . The TOTAL electron ID  
<sup>484</sup> correlation model is used, corresponding to 1 electron ID systematic [26]. Electron ID is found  
<sup>485</sup> to be a subleading systematic that is unconstrained by the fit, making it an appropriate choice for  
<sup>486</sup> this analysis.

<sup>487</sup> The sources which contribute to the uncertainty in the jet energy scale (JES) [27] are decom-  
<sup>488</sup> posed into uncorrelated components and treated as independent sources in the analysis. The  
<sup>489</sup> CategoryReduction model is used to account for JES uncertainties, which decomposes the uncer-  
<sup>490</sup> tainties into 30 nuisance parameters included in the fit. The SimpleJER model is used to account  
<sup>491</sup> for jet energy resolution (JER) uncertainties, and 8 JER uncertainty components included as NPs  
<sup>492</sup> in the fit.

493     The uncertainties in the b-tagging efficiencies measured in dedicated calibration analyses  
 494 [19] are also decomposed into uncorrelated components. The large number of components for  
 495 b-tagging is due to the calibration of the distribution of the MVA discriminant.

496     The full list of systematic uncertainties considered in the analysis is summarized in Tables 10,  
 497 11 and 12.

498

Experimental Systematics on Leptons and $E_T^{\text{miss}}$			
Type	Description	Systematics Name	Application
<b>Trigger</b>			
Scale Factors	Trigger Efficiency	lepSFTrigTight_MU(EL)_SF_Trigger_STAT(SYST)	Event Weight
<b>Muons</b>			
Efficiencies	Reconstruction and Identification	lepSFObjTight_MU_SF_ID_STAT(SYST)	Event Weight
	Isolation	lepSFObjTight_MU_SF_Isol_STAT(SYST)	Event Weight
	Track To Vertex Association	lepSFObjTight_MU_SF_TTVA_STAT(SYST )	Event Weight
$p_T$ Scale	$p_T$ Scale	MUONS_SCALE	$p_T$ Correction
Resolution	Inner Detector Energy Resolution	MUONS_ID	$p_T$ Correction
	Muon Spectrometer Energy Resolution	MUONS_MS	$p_T$ Correction
<b>Electrons</b>			
Efficiencies	Reconstruction	lepSFObjTight_EL_SF_ID	Event Weight
	Identification	lepSFObjTight_EL_SF_Reco	Event Weight
	Isolation	lepSFObjTight_EL_SF_Isol	Event Weight
Scale Factor	Energy Scale	EG_SCALE_ALL	Energy Correction
Resolution	Energy Resolution	EG_RESOLUTION_ALL	Energy Correction
<b><math>E_T^{\text{miss}}</math></b>			
Soft Tracks Terms	Resolution	MET_SoftTrk_ResoPerp	$p_T$ Correction
	Resolution	MET_SoftTrk_ResoPara	$p_T$ Correction
	Scale	MET_SoftTrk_ScaleUp	$p_T$ Correction
	Scale	MET_SoftTrk_ScaleDown	$p_T$ Correction

Table 10: Summary of experimental systematics considered for leptons and  $E_T^{\text{miss}}$ . Includes type, description, name of systematic as used in the fit, and mode of application. The mode of application indicates the systematic evaluation, e.g. as an overall event re-weighting (Event Weight) or rescaling ( $p_T$  Correction).

Experimental Systematics on Jets			
Type	Origin	Systematics Name	Application
Jet Vertex Tagger		JVT	Event Weight
Energy Scale	Calibration Method	JET_21NP_ JET_EffectiveNP_1-19	$p_T$ Correction $p_T$ Correction
	$\eta$ inter-calibration	JET_EtaIntercalibration_Modelling JET_EtaIntercalibration_NonClosure JET_EtaIntercalibration_TotalStat	$p_T$ Correction $p_T$ Correction $p_T$ Correction
	High $p_T$ jets	JET_SingleParticle_HighPt	$p_T$ Correction
	Pile-Up	JET_Pileup_OffsetNPV JET_Pileup_OffsetMu JET_Pileup_PtTerm JET_Pileup_RhoTopology	$p_T$ Correction $p_T$ Correction $p_T$ Correction $p_T$ Correction
	Non Closure	JET_PunchThrough_MC15	$p_T$ Correction
	Flavour	JET_Flavor_Response JET_BJES_Response JET_Flavor_Composition	$p_T$ Correction $p_T$ Correction $p_T$ Correction
Resolution		JET_JER_SINGLE_NP	Event Weight

Table 11: Jet systematics take into account effects of jets calibration method,  $\eta$  inter-calibration, high  $p_T$  jets, pile-up, and flavor response. They are all diagonalised into effective parameters.

Experimental Systematics on b-tagging		
Type	Origin	Systematic Name
Scale Factors	DL1r b-tagger efficiency on b originated jets in bins of $\eta$	DL1r_Continuous_EventWeight_B0-29
	DL1r b-tagger efficiency on c originated jets in bins of $\eta$	DL1r_Continuous_EventWeight_C0-19
	DL1r b-tagger efficiency on light flavoured originated jets in bins of $\eta$ and $p_T$	DL1r_Continuous_EventWeight_Light0-79
	DL1r b-tagger extrapolation efficiency	DL1r_Continuous_EventWeight_extrapolation DL1r_Continuous_EventWeight_extrapolation_from_charm

Table 12: Summary of experimental systematics to be included for b-tagging of jets in the analysis, using the continuous DL1r tagging algorithm. All of the b-tagging related systematics are applied as event weights. From left: type, description, and the name of systematic used in the fit.

499     Theoretical uncertainties applied to MC predictions, including cross section, PDF, and scale  
 500    uncertainties are taken from theory calculations, with the exception of non-prompt and diboson  
 501    backgrounds. The cross-section uncertainty on tZ is taken from [28]. Derivation of the non-  
 502    prompt background uncertainties, Z+jets and tt}, are explained in detail in Section 6.3. These  
 503    normalization uncertainties are chosen so as to account for the complete uncertainty in the  
 504    non-prompt contribution, and therefore no additional modelling uncertainties are considered for  
 505    Z+jets and tt}.

506    The other VV + heavy flavor processes (namely VV+b and VV+charm, which primarily consist  
 507    of ZZ events) are also poorly understood, because these processes involve the same physics as  
 508    WZ + heavy flavor, and have also not been measured. Therefore, a conservative 50% uncertainty  
 509    is applied to those samples. While this uncertainty is large, it is found to have little impact on  
 510    the significance of the final result.

511    The theory uncertainties applied to the predominate background estimates are summarized in  
 512    Table 13.

Process	X-section [%]
tZ	X-sec: $\pm 15.2$
t̄ H (aMC@NLO+Pythia8)	QCD Scale: $^{+5.8}_{-9.2}$ PDF( $+\alpha_S$ ): $\pm 3.6$
t̄ Z (aMC@NLO+Pythia8)	QCD Scale: $^{+9.6}_{-11.3}$ PDF( $+\alpha_S$ ): $\pm 4$
t̄ W (aMC@NLO+Pythia8)	QCD Scale: $^{+12.9}_{-11.5}$ PDF( $+\alpha_S$ ): $\pm 3.4$
VV + b/charm (Sherpa 2.2.1)	$\pm 50$
VV + light (Sherpa 2.2.1)	$\pm 6$
t̄ t	$\pm 20$
Z + jets	$\pm 25$
Others	$\pm 50$

Table 13: Summary of theoretical uncertainties for MC predictions in the analysis.

513 Due to its importance as a background, additional modelling uncertainties are considered for tZ.  
 514 Alternative tZ samples with variations in scale (DSID 412064-5) and shower modelling (DSID  
 515 501046) are included as systematics..

516 The fit involves varying the overall normalization of signal templates over the regions de-  
 517 scribed in Section 6.2, which are defined by the flavor and number of associated jets at truth-  
 518 level. The modelling of these template shapes therefore significantly impacts the final result.  
 519 Additional signal uncertainties, probing the shape of the signal templates as well as the rate of  
 520 migrations between the number of truth-jets and reconstructed jets, are estimated by comparing  
 521 estimates from the nominal Sherpa WZ samples with alternative WZ samples generated with  
 522 POWHEG+PYTHIA8 (DSID 361601). Separate systematics are included in the fit for WZ + b, WZ  
 523 + c and WZ + light, where the distribution among each of the fit regions is varied based on the  
 524 prediction of the Powheg sample.

525 The variations in the signal templates are shown in Figures 30 and 31. Each of these plots are  
 526 normalized to unity in order to capture the relevant differences in shape.

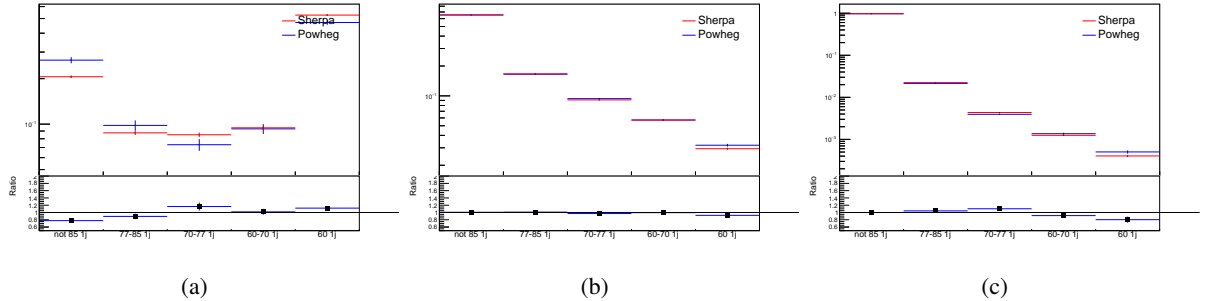


Figure 30: Comparison between Sherpa and Powheg predictions of the distribution of (a) WZ + b, (b) WZ + charm, and (c) WZ + light among the various b-tag WPs used in the 1-jet fit.

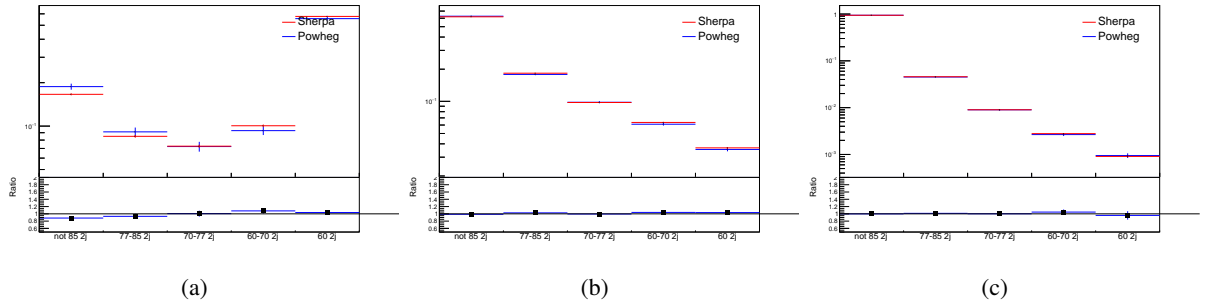


Figure 31: Comparison between Sherpa and Powheg predictions of the distribution of (a) WZ + b, (b) WZ + charm, and (c) WZ + light among the various b-tag WPs used in the 2-jet fit.

527 Separate systematics are included in the fit for WZ + b, WZ + charm and WZ + light,  
 528 where  
 529 the distribution among each of the fit regions is varied based on the prediction of the Powheg  
 sample.

530 A similar approach is taken to account for uncertainties in migrations between the number of  
 531 reco and truth jets. The fraction of events with 1 truth jet which fall into the 1 jet bin versus the  
 532 2 jet bin at reco level is compared for Sherpa and Powheg. The same is done for events with 2  
 533 truth jets. This comparison is shown in figure 32.

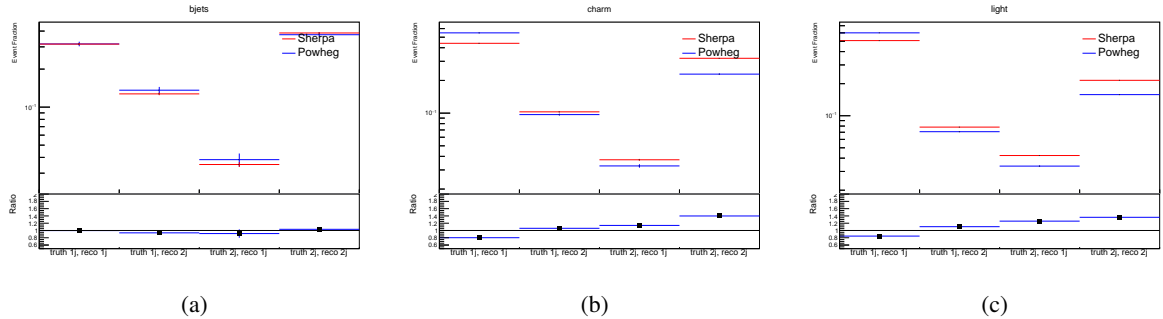


Figure 32: Comparison between Sherpa and Powheg predictions for truth jet migrations between the 1 and 2 jet reco bins for (a) WZ + b, (b) WZ + charm, and (c) WZ + light

534 A systematic is included where events are shifted between the 1-jet and 2-jet regions based on  
 535 the differences between these two shapes. This is done independently for each of the WZ + b,  
 536 WZ + charm, and WZ + light templates.

537 Additional systematics are included to account for the uncertainty in the contamination of 0 jet  
 538 and 3 or more jet events (at truth level) in the 1 and 2 reco jet bins. Because these events fall  
 539 outside the scope of this measurement, these events are included as a background. As such, a  
 540 normalization, rather than a shape, uncertainty is applied for this background.

541 The number of WZ events with 0-jets and  $>=3$ -jets in the reconstructed 1-jet and 2-jet regions  
 542 are compared for Sherpa and Powheg, as seen in figure 33. These differences are taken as separate  
 543 normalization systematics on the yield of WZ+0-jet and WZ+ $>=3$ -jet events.

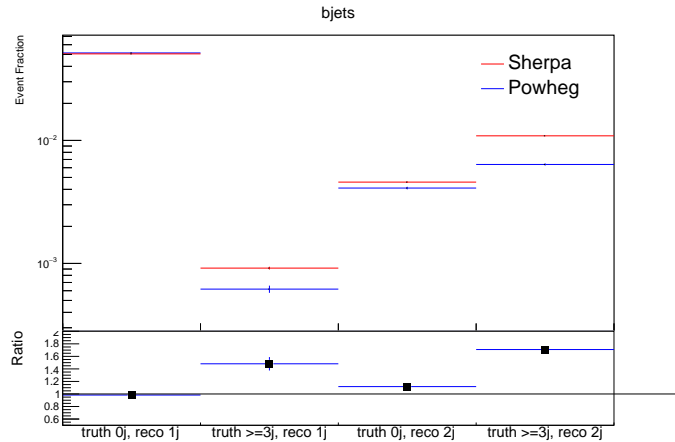


Figure 33: Comparison between Sherpa and Powheg predictions for 0 and  $>=3$  truth jet contributions in the 1 and 2 jet reco bins

---

**544 8 Results****545 8.1 Fit Procedure**

546 A maximum-likelihood fit is performed over the unfolded signal templates in the various fit  
547 regions described in Section 6 in order to extract the best-fit value of the WZ + b-jet and WZ +  
548 charm jet contributions for events with both 1 and 2 associated jets.

549 Because the fit regions are defined by the number of associated jets at reco-level, an unfolding  
550 procedure is applied to the signal in order to account for differences in the number of truth jets  
551 compared to the number of reco-jets. The WZ + b, WZ + charm and WZ + light contributions  
552 are separated into independent samples based on the number of truth jets in each event. WZ + 1  
553 truth-jet and WZ + 2 truth-jets are treated as signal samples, while WZ + 0 truth-jets and WZ +  
554 >=3 truth-jets are treated as an additional background.

555 A maximum likelihood fit to data is performed simultaneously in the regions described in Section  
556 6, summarized in figure 34. The six signal templates, which include WZ+b 1-jet, WZ+c 1-jet,  
557 WZ+l 1-jet, WZ+b 2-jets, WZ+c 2-jets, WZ+l 2-jets, are allowed to float, while the remaining  
558 background contributions are held fixed. The parameters  $\mu_{WZ+b-1-jet}$ ,  $\mu_{WZ+charm1-jet}$ ,  
559  $\mu_{WZ+light-1-jet}$ ,  $\mu_{WZ+b-2-jet}$ ,  $\mu_{WZ+charm2-jet}$ ,  $\mu_{WZ+light-2-jet}$ , where  $\mu = \sigma_{\text{observed}}/\sigma_{\text{SM}}$ ,  
560 are extracted from the fit. A simultaneous fit is performed over all 1-jet and 2-jet regions.

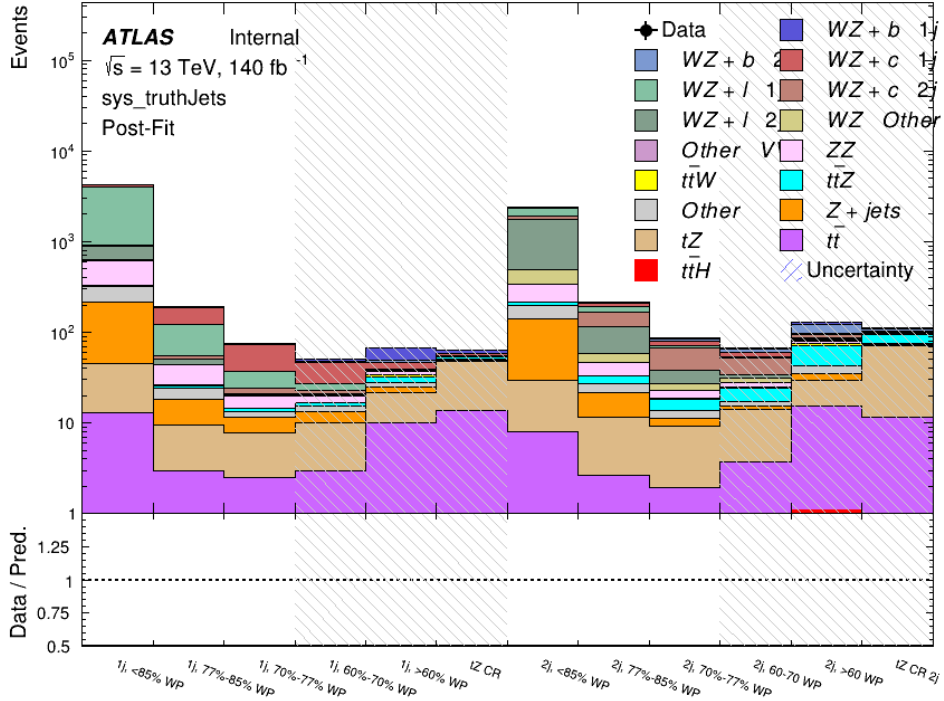


Figure 34: Post-fit summary of the fit regions.

As described in Section 7, there are 230 systematic uncertainties that are considered as NPs in the fit. These NPs are constrained by Gaussian or log-normal probability density functions. The latter are used for normalisation factors to ensure that they are always positive. The expected number of signal and background events are functions of the likelihood. The prior for each NP is added as a penalty term, decreasing the likelihood as it is shifted away from its nominal value. The correlations between these nuisance parameters are summarized in Figure ??.

Several alternative fit strategies are documented in Appendices 8.3-8.4.1. These include a measurement of WZ + 1 or 2 jets inclusively, a fit where tZ is allowed to float, and a case where tZ is included as part of the signal.

## 8.2 Results of the Simultaneous Fit

The Asimov fit for 1-jet events gives an expected  $\mu$  value of  $1.00^{+0.47}_{-0.43}(\text{stat})^{+0.30}_{-0.27}(\text{sys})$  for  $WZ + b$ . The normalization factors extracted from the fit for  $WZ + \text{charm}$  and  $WZ + \text{light}$  are  $1.00 \pm 0.17 \pm 0.17$  and  $1.00 \pm 0.06 \pm 0.14$ , respectively.

The expected cross-section of  $WZ+b$  with 1-jet is  $1.74^{+0.82}_{-0.75}(\text{stat})^{+0.53}_{-0.48}(\text{sys})$  fb, and  $14.6 \pm 2.5(\text{stat}) \pm 2.3(\text{sys})$  fb for  $WZ + \text{charm}$ , with a correlation of -0.15 between them. An expected

576 significance of 2.0 is observed for WZ + b in this region.

577 For 2-jet events, the fit gives an expected  $\mu$  value of  $1.00^{+0.53}_{-0.51}(\text{stat})^{+0.39}_{-0.34}(\text{sys})$  for WZ + b.  
 578 The fitted cross-section modifiers for WZ + charm and WZ + light are  $1.00 \pm 0.25 \pm 0.21$  and  
 579  $1.00 \pm 0.06 \pm 0.16$ , respectively.

580 The expected WZ + b cross-section in the 2-jet region is  $2.5^{+1.3}_{-1.3}(\text{stat})^{+0.95}_{-0.83}(\text{sys})$  fb with an  
 581 expected significance of  $1.7\sigma$ . The 2-jet expected cross-section of WZ + charm is  $12.7 \pm$   
 582  $3.2(\text{stat}) \pm 2.7(\text{sys})$  fb, and the correlation between WZ + charm and WZ + b is -0.22.

583 A summary of the correlation between the various WZ components is summarized in Table 14.

584

	WZ + b - 1-jet	WZ + c - 1-jet	WZ + l - 1-jet	WZ + b - 2-jet	WZ + c - 2-jet	WZ + l - 2-jet
WZ + b - 1-jet	1.00	-0.15	0.28	-0.13	-0.22	0.17
WZ + c - 1-jet	-	1.00	0.36	0.13	-0.14	-0.16
WZ + l - 1-jet	-	-	1.00	0.10	-0.20	-0.39
WZ + b - 2-jet	-	-	-	1.00	-0.22	0.17
WZ + c - 2-jet	-	-	-	-	1.00	0.23
WZ + l - 2-jet	-	-	-	-	-	1.00

Table 14: Correlations between the various components of WZ

585 The pre-fit yields in each of the 1-jet regions used in the fit are shown in Table 8.2.

586

Sample	1j, <85% WP	1j, 77%-85% WP	1j, 70%-77% WP	1j, 60%-70% WP	1j, 60%+ WP	tZ CR
WZ + b - 1j	$8.1 \pm 1.6$	$4.7 \pm 0.5$	$4.6 \pm 0.4$	$5.1 \pm 0.4$	$18.1 \pm 2.4$	$5.0 \pm 0.6$
WZ + c - 1j	$260 \pm 22$	$81 \pm 6$	$43.1 \pm 3.6$	$25.8 \pm 2.6$	$9.4 \pm 1.8$	$2.9 \pm 0.6$
WZ + l - 1j	$3090 \pm 250$	$91 \pm 13$	$17 \pm 3$	$4.9 \pm 1.6$	$1.3 \pm 0.4$	$0.2 \pm 0.1$
WZ + b - 2j	$1.10 \pm 0.37$	$0.44 \pm 0.11$	$0.39 \pm 0.06$	$0.62 \pm 0.14$	$2.1 \pm 0.5$	$0.59 \pm 0.14$
WZ + c - 2j	$21 \pm 5$	$5.6 \pm 1.2$	$3.0 \pm 0.7$	$2.0 \pm 0.5$	$0.70 \pm 0.20$	$0.30 \pm 0.08$
WZ + l - 2j	$250 \pm 60$	$5.7 \pm 1.6$	$0.73 \pm 0.53$	$0.31 \pm 0.15$	$0.07 \pm 0.06$	$0.01 \pm 0.01$
WZ - Other	$13 \pm 5$	$1.4 \pm 0.4$	$0.42 \pm 0.08$	$0.2 \pm 0.01$	$0.30 \pm 0.05$	$0.67 \pm 0.15$
Other VV	$6.2 \pm 0.6$	$0.2 \pm 0.4$	$0.2 \pm 0.04$	$0.07 \pm 0.1$	$0.1 \pm 0.1$	$0.1 \pm 0.2$
ZZ	$336 \pm 26$	$17.8 \pm 2.1$	$4.3 \pm 0.6$	$1.7 \pm 0.5$	$0.36 \pm 0.08$	$0.10 \pm 0.03$
t̄W	$1.1 \pm 0.2$	$0.2 \pm 0.1$	$0.3 \pm 0.1$	$0.4 \pm 0.1$	$1.5 \pm 0.3$	$0.7 \pm 0.2$
t̄Z	$6.8 \pm 1.2$	$1.4 \pm 0.3$	$1.0 \pm 0.2$	$1.2 \pm 0.2$	$4.4 \pm 0.8$	$3.2 \pm 0.6$
Z + jets	$169 \pm 38$	$8.9 \pm 1.9$	$3.7 \pm 0.8$	$3.3 \pm 0.7$	$3.2 \pm 0.7$	$0.8 \pm 0.17$
V + $\gamma$	$45 \pm 28$	$1.9 \pm 2.4$	$0.1 \pm 0.1$	$0.02 \pm 0.01$	$1.0 \pm 0.9$	$0.02 \pm 0.03$
tZ	$31.8 \pm 4.3$	$6.4 \pm 1.1$	$5.3 \pm 0.8$	$7.2 \pm 1.1$	$11.8 \pm 2.0$	$33.9 \pm 4.5$
tW	$1.4 \pm 0.8$	$0.2 \pm 0.5$	$0.0 \pm 0.2$	$0.7 \pm 0.6$	$0.26 \pm 0.42$	$0.39 \pm 0.41$
WtZ	$2.3 \pm 1.2$	$0.6 \pm 0.3$	$0.3 \pm 0.21$	$0.27 \pm 0.2$	$1.1 \pm 0.7$	$0.6 \pm 0.5$
VVV	$12.4 \pm 0.5$	$0.93 \pm 0.06$	$0.35 \pm 0.03$	$0.13 \pm 0.02$	$0.14 \pm 0.03$	$0.02 \pm 0.01$
VH	$40 \pm 6$	$2.6 \pm 1.4$	$0.9 \pm 0.8$	$0.7 \pm 0.8$	$0.5 \pm 0.6$	$0.0 \pm 0.0$
t̄t	$12.1 \pm 1.6$	$2.9 \pm 0.6$	$2.5 \pm 0.5$	$2.8 \pm 0.5$	$11.2 \pm 1.4$	$10.9 \pm 1.5$
t̄tH	$0.24 \pm 0.03$	$0.05 \pm 0.01$	$0.04 \pm 0.01$	$0.06 \pm 0.01$	$0.20 \pm 0.03$	$0.13 \pm 0.02$
Total	$5010 \pm 260$	$227 \pm 24$	$88 \pm 12$	$57 \pm 8$	$76 \pm 16$	$53 \pm 8$

Table 15: Pre-fit yields in each of the 1-jet regions.

<sup>587</sup> Here <85% includes jets that fail to pass the 85% WP, and 60%+ includes jets that pass the  
<sup>588</sup> highest, 60%, WP. The post-fit yields in each region are summarized in Figure 8.2.

589

	1j, <85% WP	1j, 77%-85% WP	1j, 70%-77% WP	1j, 60%-70% WP	1j, 60%+ WP	tZ CR
WZ + b – 1j	$8.1 \pm 4.9$	$4.7 \pm 2.0$	$4.6 \pm 2.0$	$5.1 \pm 2.1$	$18 \pm 10$	$5.0 \pm 2.5$
WZ + c – 1j	$260 \pm 60$	$80 \pm 14$	$43 \pm 7$	$26 \pm 5$	$7.4 \pm 2.3$	$2.1 \pm 0.7$
WZ + l – 1j	$3090 \pm 130$	$90 \pm 11$	$17.3 \pm 2.8$	$4.9 \pm 1.6$	$1.3 \pm 0.4$	$0.23 \pm 0.13$
WZ + b – 2j	$1.10 \pm 0.37$	$0.44 \pm 0.11$	$0.39 \pm 0.06$	$0.62 \pm 0.14$	$2.1 \pm 0.5$	$0.59 \pm 0.14$
WZ + c – 2j	$21 \pm 5$	$5.6 \pm 1.2$	$3.0 \pm 0.7$	$2.0 \pm 0.5$	$0.70 \pm 0.20$	$0.30 \pm 0.08$
WZ + l – 2j	$250 \pm 60$	$5.7 \pm 1.6$	$0.73 \pm 0.53$	$0.31 \pm 0.15$	$0.07 \pm 0.06$	$0.01 \pm 0.01$
WZ – Other	$13 \pm 5$	$1.4 \pm 0.4$	$0.42 \pm 0.08$	$0.2 \pm 0.01$	$0.30 \pm 0.05$	$0.67 \pm 0.15$
Other VV	$6.2 \pm 0.6$	$0.92 \pm 0.07$	$0.02 \pm 0.01$	$0.01 \pm 0.01$	$0.01 \pm 0.01$	$0.01 \pm 0.01$
ZZ	$346 \pm 57$	$19 \pm 5$	$4.3 \pm 0.8$	$2.7 \pm 0.5$	$2.4 \pm 0.1$	$2.1 \pm 0.6$
t̄tW	$1.09 \pm 0.21$	$0.2 \pm 0.1$	$0.1 \pm 0.1$	$0.4 \pm 0.1$	$1.5 \pm 0.3$	$0.1 \pm 0.2$
t̄tZ	$6.8 \pm 1.2$	$1.4 \pm 0.3$	$1.0 \pm 0.2$	$1.2 \pm 0.2$	$4.4 \pm 0.7$	$3.2 \pm 0.5$
rare Top	$0.14 \pm 0.04$	$0.04 \pm 0.02$	$0.04 \pm 0.0$	$0.1 \pm 0.03$	$0.14 \pm 0.04$	$0.15 \pm 0.05$
t̄tWW	$0.04 \pm 0.03$	$0.01 \pm 0.02$	$0.01 \pm 0.01$	$0.01 \pm 0.01$	$0.01 \pm 0.02$	$0.01 \pm 0.01$
Z + jets	$169 \pm 37$	$8.9 \pm 1.9$	$3.7 \pm 0.8$	$3.3 \pm 0.7$	$3.2 \pm 0.7$	$0.8 \pm 0.2$
W + jets	$0.01 \pm 0.01$					
V + $\gamma$	$46 \pm 28$	$1.9 \pm 2.4$	$0.1 \pm 0.1$	$0.0 \pm 0.2$	$1.0 \pm 0.9$	$0.0 \pm 0.0$
tZ	$31 \pm 4$	$6.0 \pm 1.0$	$5.3 \pm 0.8$	$7.2 \pm 1.0$	$11.8 \pm 1.8$	$33.9 \pm 4.5$
tW	$1.37 \pm 0.82$	$0.18 \pm 0.26$	$0.01 \pm 0.12$	$0.67 \pm 0.64$	$0.26 \pm 0.42$	$0.39 \pm 0.41$
WtZ	$2.3 \pm 1.2$	$0.6 \pm 0.3$	$0.3 \pm 0.2$	$0.3 \pm 0.2$	$1.1 \pm 0.6$	$0.6 \pm 0.3$
VVV	$12.4 \pm 0.4$	$0.9 \pm 0.1$	$0.4 \pm 0.1$	$0.13 \pm 0.02$	$0.14 \pm 0.03$	$0.02 \pm 0.01$
VH	$40 \pm 6$	$2.6 \pm 1.4$	$0.9 \pm 0.8$	$0.7 \pm 0.8$	$0.4 \pm 0.6$	$0.01 \pm 0.01$
t̄t	$12.1 \pm 1.6$	$2.9 \pm 0.6$	$2.5 \pm 0.5$	$2.8 \pm 0.5$	$11.2 \pm 1.5$	$10.9 \pm 1.4$
t̄tH	$0.24 \pm 0.03$	$0.05 \pm 0.01$	$0.04 \pm 0.01$	$0.06 \pm 0.01$	$0.20 \pm 0.03$	$0.13 \pm 0.02$
Total	$5100 \pm 110$	$227 \pm 12$	$87 \pm 6$	$56.7 \pm 4.4$	$76 \pm 9$	$52.5 \pm 4.2$

Table 16: Post-fit yields in each of the 1-jet regions.

590 The impact of each NP is calculated by performing the fit with the parameter of interest held  
 591 fixed, varied from its fitted value by its uncertainty, and calculating  $\Delta\mu$  relative to the baseline  
 592 fit. The impact of the most significant sources of systematic uncertainties on WZ + b with one  
 593 associated jet is summarized in Table 17.

Uncertainty Source	$\Delta\mu$	
WZ + 1-jet light cross-section	0.13	-0.15
WZ + 1-jet charm cross-section	-0.10	0.12
Jet Energy Scale	0.1	-0.13
Other Diboson + b cross-section	-0.09	0.09
tZ cross-section	-0.08	0.08
WZ 1-jet/2-jet Migration	0.08	-0.07
Jet Energy Resolution	-0.07	0.08
Luminosity	-0.06	0.07
Flavor tagging	0.05	0.05
t <bar>t} cross-section</bar>	-0.05	0.05
Total Systematic Uncertainty	0.28	0.33

Table 17: Summary of the most significant sources of systematic uncertainty on the measurement of WZ + b with exactly one associated jet.

Uncertainty Source	$\Delta\sigma/\sigma_{\text{nominal}}$	
WZ + c 1j/2j migration	0.12	-0.09
Flavor Tagging	0.09	0.08
WZ + b, 1-jet cross-section	-0.04	0.05
Luminosity	-0.04	0.04
Jet Energy Resolution	0.04	0.04
WZ + b, 2-jet cross-section	0.04	-0.03
WZ cross-section - QCD scale	-0.04	0.04
Jet Energy Scaling	0.04	0.02
WZ cross-section - PDF	-0.03	0.03
WZ + light, 1-jet cross-section	0.03	-0.03
total	0.1879	0.1753

Table 18: Summary of the most significant sources of systematic uncertainty on the measurement of WZ + c with exactly one associated jet.

594 The ranking and impact of those nuisance parameters with the largest contribution to the overall  
 595 uncertainty is shown in Figure 35.

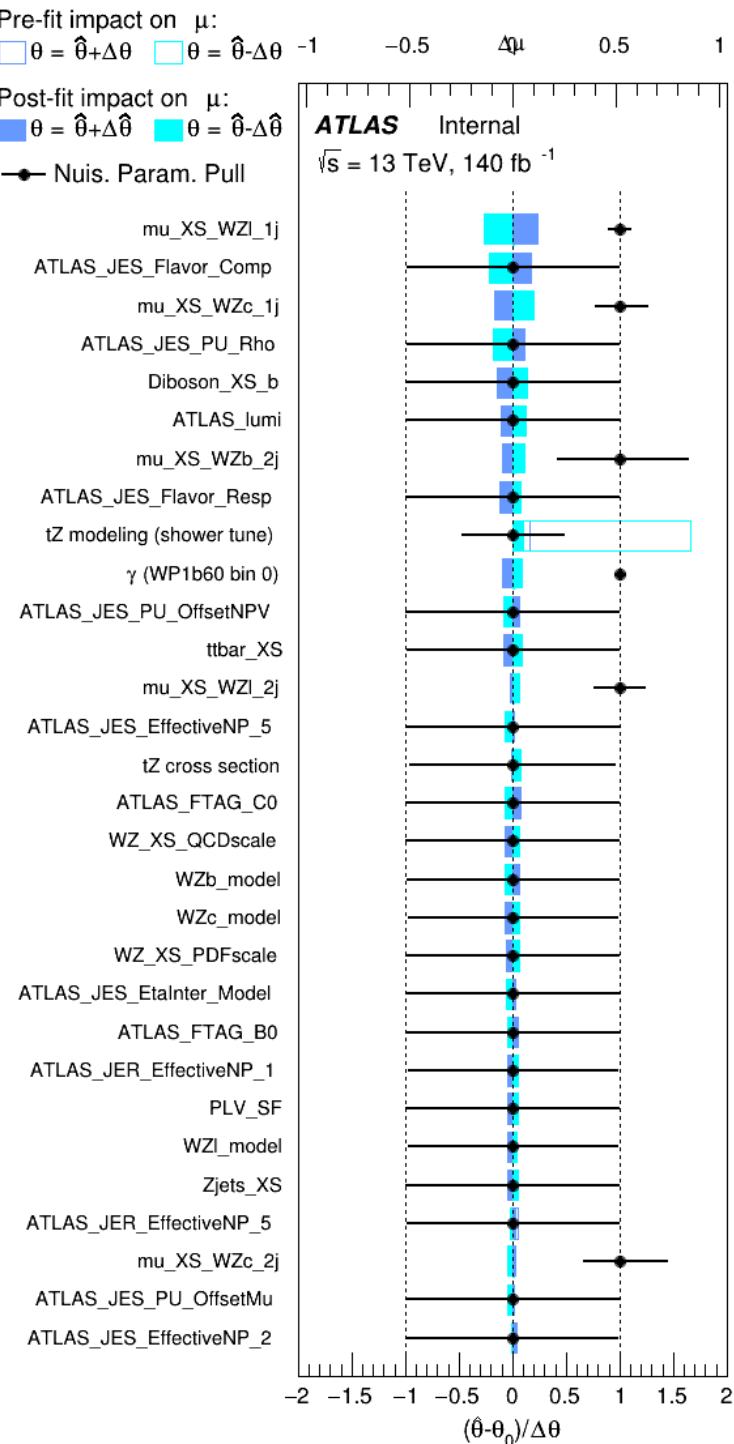


Figure 35: Impact of systematic uncertainties on the signal-strength of  $WZ + b$  for events with exactly one jet

<sup>596</sup> The large impact of the Jet Energy Scale and Jet Flavor Tagging is unsurprising, as the definition  
<sup>597</sup> of the fit regions depends heavily on the modeling of the jets. The other major sources of  
<sup>598</sup> uncertainty come from background modelling and cross-section uncertainty.

<sup>599</sup> Pre-fit yields in each of the 2-jet fit are shown in Table 8.2.

	2j, <85% WP	2j, 77%-85% WP	2j, 70%-77% WP	2j, 60%-70% WP	2j, 60%+ WP	tZ CR 2j
WZ + b - 2j	$3.1 \pm 1.6$	$6.7 \pm 0.5$	$5.6 \pm 0.4$	$8.0 \pm 0.6$	$24 \pm 2$	$5 \pm 1$
WZ + c - 2j	$180 \pm 20$	$54 \pm 6$	$41 \pm 3$	$24 \pm 3$	$17 \pm 2$	$7.0 \pm 0.6$
WZ + l - 2j	$1250 \pm 150$	$90 \pm 14$	$18 \pm 3$	$5.8 \pm 1.4$	$1.4 \pm 0.4$	$0.25 \pm 0.15$
WZ + b - 1j	$3.4 \pm 0.6$	$1.52 \pm 0.35$	$1.58 \pm 0.23$	$1.95 \pm 0.39$	$7.8 \pm 1.1$	$0.8 \pm 0.6$
WZ + c - 1j	$56 \pm 14$	$17.6 \pm 4.0$	$8.6 \pm 2.2$	$6.3 \pm 1.8$	$3.0 \pm 0.9$	$0.7 \pm 0.2$
WZ + l - 1j	$427 \pm 120$	$24 \pm 7$	$4.7 \pm 2.3$	$1.6 \pm 0.7$	$0.3 \pm 0.2$	$0.01 \pm 0.01$
WZ - Other	$129 \pm 29$	$6.1 \pm 4.6$	$1.2 \pm 0.3$	$0.3 \pm 0.2$	$2.9 \pm 0.5$	$3.6 \pm 0.6$
Other VV	$7.63 \pm 0.63$	$0.6 \pm 0.5$	$0.16 \pm 0.03$	$0.01 \pm 0.01$	$0.1 \pm 0.1$	$0.1 \pm 0.1$
ZZ	$135 \pm 20$	$14.1 \pm 3.2$	$4.7 \pm 0.8$	$4.0 \pm 0.6$	$4.1 \pm 0.7$	$3.1 \pm 0.5$
t̄W	$0.8 \pm 0.2$	$0.4 \pm 0.1$	$0.5 \pm 0.1$	$0.7 \pm 0.2$	$4.3 \pm 0.6$	$3.9 \pm 0.6$
t̄Z	$14.7 \pm 2.2$	$5.6 \pm 0.8$	$4.5 \pm 0.7$	$6.5 \pm 1.1$	$25.4 \pm 4.0$	$21.9 \pm 3.4$
rare Top	$0.14 \pm 0.04$	$0.07 \pm 0.03$	$0.03 \pm 0.02$	$0.09 \pm 0.03$	$0.37 \pm 0.07$	$0.6 \pm 0.1$
t̄WW	$0.04 \pm 0.03$	$0.02 \pm 0.02$	$0.01 \pm 0.01$	$0.01 \pm 0.00$	$0.03 \pm 0.03$	$0.01 \pm 0.01$
Z + jets	$110.0 \pm 22.9$	$9.6 \pm 2.0$	$2.1 \pm 0.50$	$1.6 \pm 0.4$	$5.1 \pm 1.1$	$1.5 \pm 0.3$
W + jets	$0.0 \pm 0.0$	$0.0 \pm 0.0$	$0.0 \pm 0.0$	$0.0 \pm 0.0$	$0.0 \pm 0.0$	$0.0 \pm 0.0$
V + γ	$25 \pm 18$	$0.5 \pm 0.2$	$0.1 \pm 0.1$	$0.1 \pm 0.1$	$0.0 \pm 0.02$	$0.05 \pm 0.07$
tZ	$21.9 \pm 2.9$	$9.6 \pm 1.3$	$9.1 \pm 1.0$	$10.0 \pm 1.5$	$14.7 \pm 3.2$	$60 \pm 6$
tW	$0.9 \pm 0.7$	$0.2 \pm 0.3$	$0.0 \pm 0.1$	$0.0 \pm 0.0$	$0.8 \pm 0.6$	$0.2 \pm 0.2$
WtZ	$4.9 \pm 2.5$	$1.5 \pm 0.8$	$1.1 \pm 0.6$	$1.3 \pm 0.7$	$4.6 \pm 2.4$	$3.3 \pm 1.7$
VVV	$7.4 \pm 0.3$	$1.0 \pm 0.1$	$0.4 \pm 0.1$	$0.2 \pm 0.1$	$0.13 \pm 0.03$	$0.04 \pm 0.01$
VH	$19.5 \pm 4.2$	$2.8 \pm 1.6$	$0.7 \pm 0.7$	$0.1 \pm 0.2$	$0.0 \pm 0.0$	$0.0 \pm 0.0$
t̄t	$0.7 \pm 0.4$	$0.1 \pm 0.1$	$0.05 \pm 0.06$	$0.15 \pm 0.13$	$0.8 \pm 0.5$	$2.3 \pm 1.2$
t̄t̄	$6.8 \pm 1.0$	$2.4 \pm 0.5$	$1.8 \pm 0.4$	$3.3 \pm 0.6$	$8.4 \pm 1.2$	$13.6 \pm 1.7$
t̄tH	$0.4 \pm 0.1$	$0.2 \pm 0.1$	$0.16 \pm 0.02$	$0.23 \pm 0.03$	$0.94 \pm 0.11$	$1.03 \pm 0.12$
Total	$2580 \pm 160$	$229 \pm 24$	$89 \pm 13$	$69 \pm 11$	$120 \pm 15$	$108 \pm 11$

Table 19: Pre-fit yields in each of the 2-jet regions.

<sup>600</sup> The post-fit yields in each region are summarized in Table 8.2.

	2j, <85% WP	2j, 77%-85% WP	2j, 70%-77% WP	2j, 60%-70% WP	2j, 60%+ WP	tZ CR 2j
WZ + b	$13 \pm 6$	$6.7 \pm 2.9$	$5.8 \pm 2.5$	$8.0 \pm 3.5$	$31 \pm 13$	$14 \pm 5$
WZ + c	$260 \pm 60$	$77 \pm 15$	$41 \pm 8$	$26 \pm 5$	$10.9 \pm 2.4$	$4.8 \pm 1.1$
WZ + l	$1860 \pm 90$	$90 \pm 12$	$17.6 \pm 2.8$	$5.8 \pm 1.3$	$1.4 \pm 0.4$	$0.3 \pm 0.2$
WZ + b - 1j	$3.4 \pm 0.6$	$1.52 \pm 0.35$	$1.58 \pm 0.23$	$1.95 \pm 0.39$	$6.7 \pm 1.1$	$1.9 \pm 0.6$
WZ + c - 1j	$56 \pm 14$	$17.6 \pm 4.0$	$8.6 \pm 2.2$	$6.3 \pm 1.8$	$3.0 \pm 0.9$	$0.7 \pm 0.2$
WZ + l - 1j	$427 \pm 120$	$24 \pm 7$	$4.7 \pm 2.3$	$1.6 \pm 0.7$	$0.3 \pm 0.2$	$0.01 \pm 0.01$
WZ - Other	$129 \pm 29$	$6.1 \pm 4.6$	$1.2 \pm 0.3$	$0.3 \pm 0.2$	$2.9 \pm 0.5$	$3.6 \pm 0.6$
Other VV	$7.6 \pm 0.6$	$0.3 \pm 0.3$	$0.3 \pm 0.1$	$0.1 \pm 0.06$	$0.03 \pm 0.02$	$0.1 \pm 0.1$
ZZ	$145 \pm 30$	$11.3 \pm 4.4$	$2.7 \pm 1.6$	$1.0 \pm 0.3$	$4.0 \pm 0.1$	$2.4 \pm 0.1$
t̄tW	$0.8 \pm 0.2$	$0.4 \pm 0.1$	$0.54 \pm 0.12$	$0.74 \pm 0.15$	$4.3 \pm 0.6$	$3.9 \pm 0.6$
t̄tZ	$14.7 \pm 2.2$	$5.6 \pm 0.8$	$4.5 \pm 0.7$	$6.5 \pm 1.0$	$25.4 \pm 3.9$	$21.9 \pm 3.3$
rare Top	$0.14 \pm 0.04$	$0.07 \pm 0.03$	$0.03 \pm 0.02$	$0.09 \pm 0.03$	$0.4 \pm 0.1$	$0.6 \pm 0.1$
t̄tWW	$0.04 \pm 0.03$	$0.02 \pm 0.02$	$0.01 \pm 0.01$	$0.01 \pm 0.01$	$0.03 \pm 0.03$	$0.01 \pm 0.01$
Z + jets	$110 \pm 23$	$9.6 \pm 2.0$	$2.1 \pm 0.5$	$1.6 \pm 0.4$	$5.1 \pm 1.1$	$1.5 \pm 0.3$
W + jets	$0.0 \pm 0.0$					
V + $\gamma$	$25 \pm 19$	$0.5 \pm 0.2$	$0.1 \pm 0.1$	$0.13 \pm 0.14$	$0.0 \pm 0.02$	$0.05 \pm 0.07$
tZ	$21.9 \pm 2.7$	$9.6 \pm 1.2$	$7.1 \pm 0.9$	$10.0 \pm 1.4$	$14.7 \pm 3.0$	$60 \pm 6$
tW	$0.1 \pm 0.7$	$0.2 \pm 0.3$	$0.0 \pm 0.1$	$0.0 \pm 0.0$	$0.8 \pm 0.6$	$0.2 \pm 0.2$
WtZ	$4.9 \pm 2.5$	$1.5 \pm 0.8$	$1.1 \pm 0.6$	$1.3 \pm 0.7$	$4.6 \pm 2.3$	$3.3 \pm 1.7$
VVV	$7.4 \pm 0.3$	$1.0 \pm 0.1$	$0.36 \pm 0.03$	$0.19 \pm 0.03$	$0.13 \pm 0.03$	$0.04 \pm 0.01$
VH	$19 \pm 4$	$2.8 \pm 1.6$	$0.7 \pm 0.7$	$0.1 \pm 0.2$	$0.0 \pm 0.0$	$0.0 \pm 0.0$
t̄t	$6.8 \pm 1.0$	$2.4 \pm 0.5$	$1.8 \pm 0.4$	$3.3 \pm 0.6$	$8.4 \pm 1.2$	$13.6 \pm 1.7$
t̄tH	$0.40 \pm 0.05$	$0.19 \pm 0.03$	$0.16 \pm 0.02$	$0.23 \pm 0.03$	$0.94 \pm 0.11$	$1.03 \pm 0.11$
Total	$2580 \pm 60$	$229 \pm 11$	$89 \pm 6$	$69.1 \pm 4.1$	$120 \pm 10$	$108 \pm 6$

Table 20: Post-fit yields in each of the 2-jet regions.

601 The same set of systematic uncertainties consider for the 1-jet fit are included in the 2-jet fit as  
 602 well. The impact of the most significant systematic uncertainties is summarized in Table 21.

Uncertainty Source	$\Delta\mu$	
WZ + c 2-jet cross-section	-0.13	0.16
WZ + l 2-jet cross-section	0.12	-0.09
ttZ cross-section - QCD scale	-0.10	0.13
WZ + b 1-jet cross-section	-0.11	0.10
Jet Energy Scale	-0.11	0.11
Luminosity	-0.11	0.12
tZ cross-section	-0.11	0.11
WtZ cross-section	-0.07	0.07
Flavor tagging	0.05	0.05
Other VV + b cross-section	-0.05	0.05
Total	0.35	0.37

Table 21: Summary of the most significant sources of systematic uncertainty on the measurement of WZ + b 2-jet events.

Uncertainty Source	$\Delta\sigma/\sigma_{\text{nominal}}$	
WZ + c 1j/2j migration	-0.17	0.25
Flavor Tagging	0.14	0.13
WZ + b, 1-jet cross-section	-0.09	0.09
Jet Energy Scale	0.06	0.08
Jet Energy Resolution	0.05	0.05
WZ $\geq 3j/2j$ migration	-0.04	0.04
WZ + c 2j/1j migration	-0.04	0.04
WZ cross-section - QCD scale	-0.04	0.04
WZ + light modelling	0.04	-0.03
Luminosity	-0.03	0.03
total	0.2694	0.3274

Table 22: Summary of the most significant sources of systematic uncertainty on the measurement of WZ + c with 2 associated jets.

603 The ranking and impact of those nuisance parameters with the largest contribution to the overall  
 604 uncertainty is shown in Figure 36.

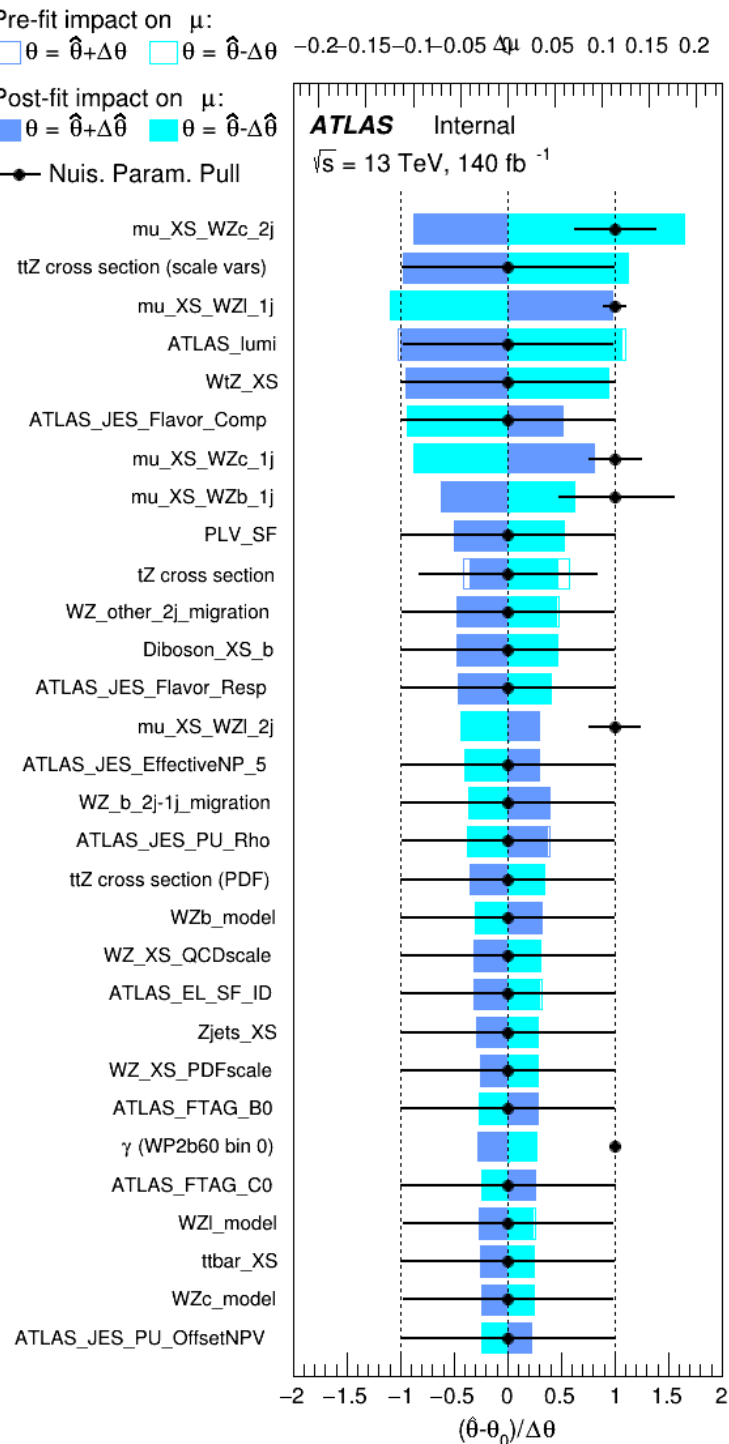


Figure 36: Impact of systematic uncertainties on the signal-strength of  $WZ + b$  in 2-jet events.

605 The large impact of the Jet Energy Scale and Jet Flavor Tagging is unsurprising, as the shape of  
606 the fit regions depends heavily on the modeling of the jets. The other major sources of uncertainty  
607 come from background modelling and cross-section uncertainty.

608 **8.3 Inclusive 1+2 Jet Fit**

609 An alternative fit is performed which combines the WZ + 1-jet and WZ + 2-jet samples rather than  
610 fitting them independently. This is done primarily as a cross-check of the nominal analysis, to  
611 see if measuring 1-jet and 2-jet events separately and combining them gives drastically different  
612 results than measuring them together.

613 For this study, three signal templates, WZ + b, WZ + charm and WZ + light, are fit to data, and  
614 the systematics accounting for migrations between 1-jet and 2-jet bins are removed. All other  
615 background and nuisance parameters remain the same as the nominal fit.

616 The measured  $\mu$  value for WZ + b is  $\mu = 1.00^{+0.30}_{-0.29}(\text{stat})^{+0.25}_{-23}(\text{sys})$ , with a significance of  $2.8\sigma$ ,  
617 and the uncertainty on WZ + charm is  $\mu = 1.00 \pm 0.12(\text{stat}) \pm 0.13(\text{sys})$ . This is compared to  
618 combined uncertainty of  $\mu = 1.00^{+0.32}_{-0.30}(\text{stat})^{+0.24}_{-23}(\text{sys})$  for WZ + b when 1-jet and 2-jet events  
619 are measured separately and then combined.

620 A post-fit summary plot of the fit regions is shown in Figure 37:

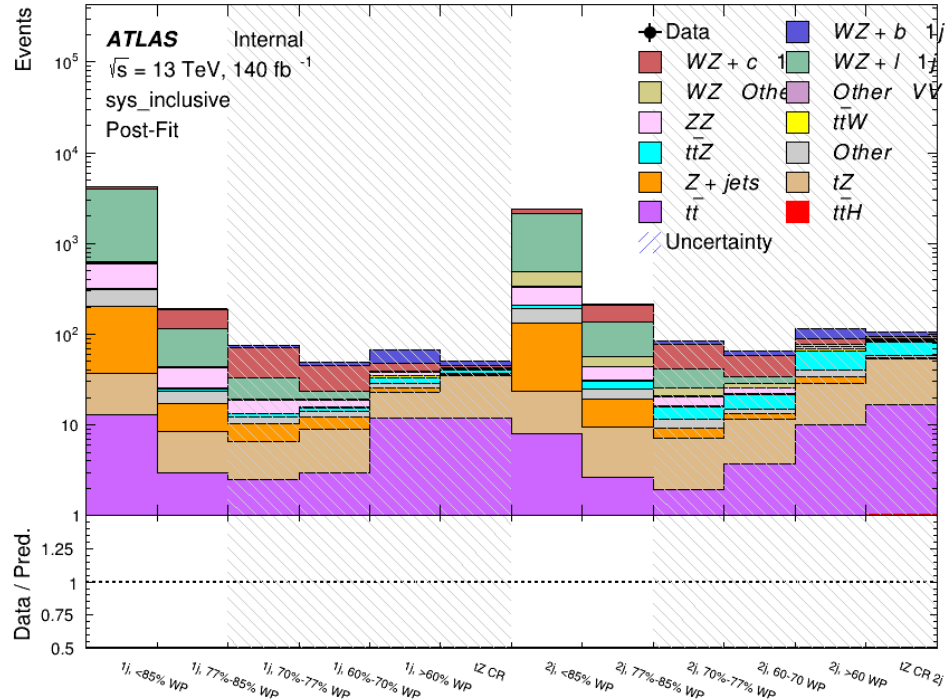


Figure 37: Post-fit summary of the 1-jet fit regions.

621 The impact of the most significant sources of systematic uncertainties on the measurement of  
 622 WZ+b is summarized in Table 23.

Uncertainty Source	$\Delta\mu$
WZ + light cross-section	0.13 -0.12
WZ + charm cross-section	-0.10 0.12
Jet Energy Scale	0.08 0.13
tZ cross-section	-0.10 0.10
Jet Energy Resolution	-0.10 0.10
Luminosity	-0.08 0.09
Other Diboson + b cross-section	-0.07 0.07
Flavor tagging	0.05 0.05
t̄ cross-section	-0.05 0.05
WZ cross-section - QCD scale	-0.04 0.03
Total Systematic Uncertainty	0.28 0.32

Table 23: Summary of the most significant sources of systematic uncertainty on the measurement of WZ + b with one or two associated jets.

623 The ranking and impact of those nuisance parameters with the largest contribution to the overall  
624 uncertainty is shown in Figure 38.

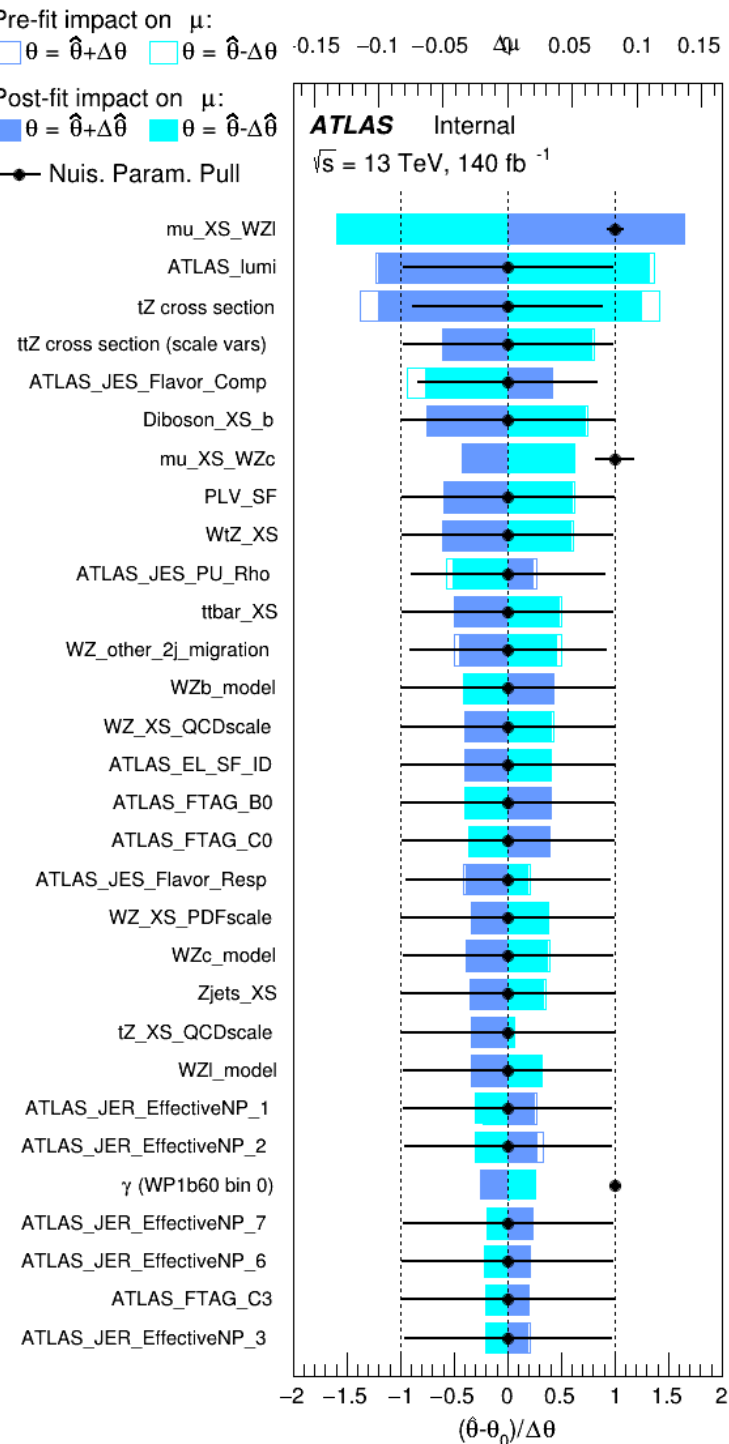


Figure 38: Impact of systematic uncertainties on the signal-strength of  $WZ + b$  for events with one or two jets

---

625 **8.4 Alternate tZ Inclusive Fit**

626 **8.4.1 tZ Inclusive Fit**

627 While tZ is often considered as a distinct process from WZ + b, this could also be considered part  
628 of the signal. Alternate studies are performed where, using the same framework as the nominal  
629 analysis, a measurement of WZ + b is performed that includes tZ as part of WZ+b.

630 Because of this change, the tZ CR is no longer necessary, and only the five pseudo-continuous  
631 b-tag regions are used in the fit. Further, systematics related to the tZ cross-section are removed  
632 from the fit, as they are now encompassed by the normalization measurement of WZ + b. All  
633 other systematic uncertainties are carried over from the nominal analysis.

634 An expected WZ + b cross-section of  $4.1^{+0.78}_{-0.74}(\text{stat})^{+0.53}_{-0.52}(\text{sys}) \text{ fb}$  is extracted from the fit, with  
635 an expected significance of  $4.0\sigma$ .

636 The impact of the predominate systematics are summarized in Table 24.

Uncertainty Source	$\Delta\mu$	
WZ + light cross-section	0.08	-0.08
Jet Energy Scale	-0.06	0.08
Luminosity	-0.05	0.06
WZ + charm cross-section	-0.04	0.05
Other Diboson + b cross-section	-0.04	0.04
WZ cross-section - QCD scale	-0.04	0.03
t̄t cross-section	-0.03	0.03
Jet Energy Resolution	-0.03	0.03
Flavor tagging	-0.03	0.03
Z+jets cross section	-0.02	0.02
Total Systematic Uncertainty	-0.15	0.16

Table 24: Summary of the most significant sources of systematic uncertainty on the measurement of WZ + b with exactly one associated jet.

637 **8.4.2 Floating tZ**

638 In order to quantify the impact of the tZ uncertainty on the fit, an alternative fit strategy is  
639 used where the tZ normalization is allowed to float. This normalization factor replaces the  
640 cross-section uncertainty on tZ, and all other parameters of the fit remain the same.

641 An uncertainty of 17% on the normalization of tZ is extracted from the fit, compared to a theory  
642 uncertainty of 15% applied to the tZ cross-section. The measured uncertainties on WZ remain  
643 the same.

## 644 9 Conclusion

645 A measurement of WZ + heavy flavor is performed using  $140 \text{ fb}^{-1}$  of  $\sqrt{s} = 13 \text{ TeV}$  proton-  
 646 proton collision data collected by the ATLAS detector at the LHC. The expected cross-section  
 647 of WZ+b with 1-jet is  $1.74^{+0.82}_{-0.75}(\text{stat})^{+0.53}_{-0.48}(\text{sys}) \text{ fb}$ , and  $14.6 \pm 2.5(\text{stat}) \pm 2.3(\text{sys}) \text{ fb}$  for WZ  
 648 + charm, with a correlation of -0.22 between them. An expected significance of 2.0 is observed  
 649 for WZ + b in this region.

650 For the 2-jet regions, an expected significance of 1.7 is observed for WZ + b, with an ex-  
 651 pected cross-section of  $2.5^{+1.3}_{-1.3}(\text{stat})^{+0.95}_{-0.83}(\text{sys}) \text{ fb}$ . For WZ + charm, a cross-section of  
 652  $12.7 \pm 3.2(\text{stat}) \pm 2.7(\text{sys}) \text{ fb}$  is expected for 2-jet events. A correlation of -0.26 is observed  
 653 for WZ+b and WZ + charm.

654 **This section will be include final results once unblinded.**

## 655 References

- 656 [1] ATLAS Collaboration. ‘Observation of electroweak  $W^\pm Z$  boson pair production in asso-  
 657 ciation with two jets in pp collisions at  $\sqrt{s} = 13 \text{ TeV}$  with the ATLAS detector’. In: *Phys.*  
 658 *Lett.* B793 (2019), pp. 469–492. doi: [10.1016/j.physletb.2019.05.012](https://doi.org/10.1016/j.physletb.2019.05.012). arXiv:  
 659 [1812.09740 \[hep-ex\]](https://arxiv.org/abs/1812.09740).
- 660 [2] ATLAS Collaboration. ‘Luminosity determination in pp collisions at  $\sqrt{s} = 7 \text{ TeV}$  using  
 661 the ATLAS detector at the LHC’. In: *Eur. Phys. J. C* 71 (2011), p. 1630. doi: [10.1140/epjc/s10052-011-1630-5](https://doi.org/10.1140/epjc/s10052-011-1630-5). arXiv: [1101.2185 \[hep-ex\]](https://arxiv.org/abs/1101.2185).
- 663 [3] ATLAS Collaboration. ‘Performance of the ATLAS detector using first collision data’.  
 664 In: *JHEP* 09 (2010), p. 056. doi: [10.1007/JHEP09\(2010\)056](https://doi.org/10.1007/JHEP09(2010)056). arXiv: [1005.5254 \[hep-ex\]](https://arxiv.org/abs/1005.5254).
- 666 [4] S. Agostinelli et al. ‘GEANT4: A Simulation toolkit’. In: *Nucl. Instrum. Meth.* A506  
 667 (2003), pp. 250–303. doi: [10.1016/S0168-9002\(03\)01368-8](https://doi.org/10.1016/S0168-9002(03)01368-8).
- 668 [5] T. Gleisberg et al. ‘Event generation with SHERPA 1.1’. In: *JHEP* 02 (2009), p. 007. doi:  
 669 [10.1088/1126-6708/2009/02/007](https://doi.org/10.1088/1126-6708/2009/02/007). arXiv: [0811.4622 \[hep-ph\]](https://arxiv.org/abs/0811.4622).
- 670 [6] H.-L. Lai et al. ‘New parton distributions for collider physics’. In: *Phys. Rev. D* 82 (2010),  
 671 p. 074024. doi: [10.1103/PhysRevD.82.074024](https://doi.org/10.1103/PhysRevD.82.074024). arXiv: [1007.2241 \[hep-ph\]](https://arxiv.org/abs/1007.2241).
- 672 [7] J. Alwall et al. ‘The automated computation of tree-level and next-to-leading order dif-  
 673 ferential cross sections, and their matching to parton shower simulations’. In: *JHEP* 07  
 674 (2014), p. 079. doi: [10.1007/JHEP07\(2014\)079](https://doi.org/10.1007/JHEP07(2014)079). arXiv: [1405.0301 \[hep-ph\]](https://arxiv.org/abs/1405.0301).
- 675 [8] R. D. Ball et al. ‘Parton distributions for the LHC Run II’. In: *JHEP* 04 (2015), p. 040.  
 676 doi: [10.1007/JHEP04\(2015\)040](https://doi.org/10.1007/JHEP04(2015)040). arXiv: [1410.8849 \[hep-ph\]](https://arxiv.org/abs/1410.8849).
- 677 [9] M. Bahr et al. ‘Herwig++ Physics and Manual’. In: *Eur. Phys. J. C* 58 (2008), p. 639. doi:  
 678 [10.1140/epjc/s10052-008-0798-9](https://doi.org/10.1140/epjc/s10052-008-0798-9). arXiv: [0803.0883 \[hep-ph\]](https://arxiv.org/abs/0803.0883).

- [679] [10] R. D. Ball et al. ‘Parton distributions with LHC data’. In: *Nucl. Phys. B* 867 (2013), p. 244.  
 [680] doi: [10.1016/j.nuclphysb.2012.10.003](https://doi.org/10.1016/j.nuclphysb.2012.10.003). arXiv: [1207.1303 \[hep-ph\]](https://arxiv.org/abs/1207.1303).
- [681] [11] S. Frixione, G. Ridolfi and P. Nason. ‘A positive-weight next-to-leading-order Monte Carlo  
 [682] for heavy flavour hadroproduction’. In: *JHEP* 09 (2007), p. 126. doi: [10.1088/1126-6708/2007/09/126](https://doi.org/10.1088/1126-6708/2007/09/126). arXiv: [0707.3088 \[hep-ph\]](https://arxiv.org/abs/0707.3088).
- [684] [12] E. Re. ‘Single-top Wt-channel production matched with parton showers using the POWHEG  
 [685] method’. In: *Eur. Phys. J. C* 71 (2011), p. 1547. doi: [10.1140/epjc/s10052-011-1547-z](https://doi.org/10.1140/epjc/s10052-011-1547-z). arXiv: [1009.2450 \[hep-ph\]](https://arxiv.org/abs/1009.2450).
- [687] [13] ATLAS Collaboration. *Electron efficiency measurements with the ATLAS detector using  
 [688] the 2015 LHC proton–proton collision data*. ATLAS-CONF-2016-024. 2016. URL: <https://cds.cern.ch/record/2157687>.
- [690] [14] ATLAS Collaboration. ‘Measurement of the muon reconstruction performance of the  
 [691] ATLAS detector using 2011 and 2012 LHC proton–proton collision data’. In: *Eur. Phys.  
 [692] J. C* 74 (2014), p. 3130. doi: [10.1140/epjc/s10052-014-3130-x](https://doi.org/10.1140/epjc/s10052-014-3130-x). arXiv: [1407.3935 \[hep-ex\]](https://arxiv.org/abs/1407.3935).
- [694] [15] R. Narayan et al. *Measurement of the total and differential cross sections of a top-quark-  
 [695] antiquark pair in association with a W boson in proton-proton collisions at a centre-of-  
 [696] mass energy of 13 TeV with ATLAS detector at the Large Hadron Collider*. Tech. rep.  
 [697] ATL-COM-PHYS-2020-217. Geneva: CERN, Mar. 2020. URL: <https://cds.cern.ch/record/2712986>.
- [699] [16] ATLAS Collaboration. *Jet Calibration and Systematic Uncertainties for Jets Reconstruc-  
 [700] ted in the ATLAS Detector at  $\sqrt{s} = 13$  TeV*. ATL-PHYS-PUB-2015-015. 2015. URL:  
<https://cds.cern.ch/record/2037613>.
- [702] [17] ATLAS Collaboration. *Selection of jets produced in 13 TeV proton–proton collisions with  
 [703] the ATLAS detector*. ATLAS-CONF-2015-029. 2015. URL: <https://cds.cern.ch/record/2037702>.
- [705] [18] ATLAS Collaboration. ‘Performance of pile-up mitigation techniques for jets in pp col-  
 [706] lisions at  $\sqrt{s} = 8$  TeV using the ATLAS detector’. In: *Eur. Phys. J. C* 76 (2016), p. 581.  
 [707] doi: [10.1140/epjc/s10052-016-4395-z](https://doi.org/10.1140/epjc/s10052-016-4395-z). arXiv: [1510.03823 \[hep-ex\]](https://arxiv.org/abs/1510.03823).
- [708] [19] ATLAS Collaboration. ‘Performance of b -jet identification in the ATLAS experiment’. In:  
*Journal of Instrumentation* 11.04 (2016), P04008. URL: <http://stacks.iop.org/1748-0221/11/i=04/a=P04008>.
- [711] [20] ATLAS Collaboration. ‘Performance of missing transverse momentum reconstruction  
 [712] with the ATLAS detector using proton–proton collisions at  $\sqrt{s} = 13$  TeV’. In: *The  
 [713] European Physical Journal C* 78.11 (Nov. 2018). ISSN: 1434-6052. doi: [10.1140/epjc/s10052-018-6288-9](https://doi.org/10.1140/epjc/s10052-018-6288-9). URL: <http://dx.doi.org/10.1140/epjc/s10052-018-6288-9>.
- [716] [21] ATLAS Collaboration. ‘Measurement of the fiducial and differential cross-section of a top  
 [717] quark pair in association with a Z boson at 13 TeV with the ATLAS detector’. In: ATL-  
 [718] COM-PHYS-2019-334 (Apr. 2019). URL: <https://cds.cern.ch/record/2672207>.

- 719 [22] T. Chen and C. Guestrin. ‘XGBoost: A Scalable Tree Boosting System’. In: *Proceedings*  
 720 *of the 22nd ACM SIGKDD International Conference on Knowledge Discovery and Data*  
 721 *Mining*. KDD ’16. San Francisco, California, USA: ACM, 2016, pp. 785–794. ISBN: 978-  
 722 1-4503-4232-2. doi: [10.1145/2939672.2939785](https://doi.org/10.1145/2939672.2939785). URL: <http://doi.acm.org/10.1145/2939672.2939785>.
- 724 [23] 2021. URL: [https://twiki.cern.ch/twiki/bin/view/AtlasProtected/BTagCalibrationRecommendationsRelease21#Tools\\_for\\_Flavor\\_Tagging\\_Calibra](https://twiki.cern.ch/twiki/bin/view/AtlasProtected/BTagCalibrationRecommendationsRelease21#Tools_for_Flavor_Tagging_Calibra).
- 727 [24] ‘Luminosity determination in pp collisions at  $\sqrt{s} = 13$  TeV using the ATLAS detector at  
 728 the LHC’. In: (June 2019).
- 729 [25] ATLAS Collaboration. ‘The new LUCID-2 detector for luminosity measurement and  
 730 monitoring in ATLAS’. In: *JINST* 13.07 (2018), P07017. doi: [10.1088/1748-0221/13/07/P07017](https://doi.org/10.1088/1748-0221/13/07/P07017).
- 732 [26] A. Collaboration. ‘Electron reconstruction and identification in the ATLAS experiment  
 733 using the 2015 and 2016 LHC proton–proton collision data at  $\sqrt{s} = 13$  TeV’. In: *The*  
 734 *European Physical Journal C* 79.8 (Aug. 2019). ISSN: 1434-6052. doi: [10.1140/epjc/s10052-019-7140-6](https://doi.org/10.1140/epjc/s10052-019-7140-6). URL: <http://dx.doi.org/10.1140/epjc/s10052-019-7140-6>.
- 737 [27] ATLAS Collaboration. ‘Jet energy scale measurements and their systematic uncertainties  
 738 in proton–proton collisions at  $\sqrt{s} = 13$  TeV with the ATLAS detector’. In: *Phys. Rev.*  
 739 *D* 96 (2017), p. 072002. doi: [10.1103/PhysRevD.96.072002](https://doi.org/10.1103/PhysRevD.96.072002). arXiv: [1703.09665](https://arxiv.org/abs/1703.09665)  
 740 [[hep-ex](#)].
- 741 [28] ATLAS Collaboration. ‘Observation of the associated production of a top quark and a  
 742 Z boson in pp collisions at  $\sqrt{s}= 13$  TeV with the ATLAS detector’. In: *Journal of High*  
 743 *Energy Physics* 2020.7 (July 2020). ISSN: 1029-8479. doi: [10.1007/jhep07\(2020\)124](https://doi.org/10.1007/jhep07(2020)124).  
 744 URL: [http://dx.doi.org/10.1007/JHEP07\(2020\)124](http://dx.doi.org/10.1007/JHEP07(2020)124).

745 **A Appendices**

746 **A.1 Non-prompt lepton MVA**

747 A lepton MVA has been developed to better reject non-prompt leptons than standard cut  
 748 based selections based upon impact parameter, isolation and PID. The name of this MVA is  
 749 `PromptLeptonIso`. The full set of studies and detailed explanation can be found in [15].

750 The decays of W and Z bosons are commonly selected by the identification of one or two electrons  
 751 or muons. The negligible lifetimes of these bosons mean that the leptons produced in the decay  
 752 originate from the interaction vertex and are thus labelled “prompt”. Analyses using these  
 753 light leptons impose strict reconstruction quality, isolation and impact parameter requirements  
 754 to remove “fake” leptons. A significant source of the fake light leptons are non-prompt leptons  
 755 produced in decays of hadrons that contain bottom (b) or charm (c) quarks. Such hadrons  
 756 typically have microscopically significant lifetimes that can be detected experimentally.

757 These non-prompt leptons can also pass the tight selection criteria. In analyses that involve top (t)  
 758 quarks, which decay almost exclusively into a W boson and a b quark, non-prompt leptons from  
 759 the semileptonic decay of bottom and charm hadrons can be a significant source of background  
 760 events. This is particularly the case in the selection of same-sign dilepton and multilepton final  
 761 states.

762 The main idea is to identify non-prompt light leptons using lifetime information associated with a  
 763 track jet that matches the selected light lepton. This lifetime information is computed using tracks  
 764 contained within the jet. Typically, lepton lifetime is determined using the impact parameter of the  
 765 track reconstructed by the inner tracking detector which is matched to the reconstructed lepton.  
 766 Using additional reconstructed charged particle tracks increases the precision of identifying the  
 767 displaced decay vertex of bottom or charm hadrons that produced a non-prompt light lepton.  
 768 The MVA also includes information related to the isolation of the lepton to reject non-prompt  
 769 leptons.

770 `PromptLeptonIso` is a gradient boosted BDT. The training of the BDT is performed on leptons  
 771 selected from the Powheg+Pythia6 non-allhad t̄t MC sample. Eight variables are used to train  
 772 the BDT in order to discriminate between prompt and non-prompt leptons. The track jets that  
 773 are matched to the non-prompt leptons correspond to jets initiated by b or c quarks, and may  
 774 contain a displaced vertex. Consequently, three of the selected variables are used to identify  
 775 b-tag jets by standard ATLAS flavour tagging algorithms. Two variables use the relationship  
 776 between the track jet and lepton: the ratio of the lepton  $p_T$  with respect to the track jet  $p_T$  and  
 777  $\Delta R$  between the lepton and the track jet axis. Finally three additional variables test whether the  
 778 reconstructed lepton is isolated: the number of tracks collected by the track jet and the lepton  
 779 track and calorimeter isolation variables. Table 25 describes the variables used to train the BDT  
 780 algorithm. The choice of input variables has been extensively discussed with Egamma, Muon,  
 781 Tracking, and Flavour Tagging CP groups.

782 The output distribution of the BDT is shown in Figure A.1.

Variable	Description
$N_{\text{track}}$ in track jet	Number of tracks collected by the track jet
$\text{IP2 log}(P_b/P_{\text{light}})$	Log-likelihood ratio between the b and light jet hypotheses with the IP2D algorithm
$\text{IP3 log}(P_b/P_{\text{light}})$	Log-likelihood ratio between the b and light jet hypotheses with the IP3D algorithm
$N_{\text{TrkAtVtx}}$ SV + JF	Number of tracks used in the secondary vertex found by the SV1 algorithm in addition to the number of tracks from secondary vertices found by the JetFitter algorithm with at least two tracks
$p_T^{\text{lepton}}/p_T^{\text{track jet}}$	The ratio of the lepton $p_T$ and the track jet $p_T$
$\Delta R(\text{lepton}, \text{track jet})$	$\Delta R$ between the lepton and the track jet axis
$p_T^{\text{VarCone30}}/p_T$	Lepton track isolation, with track collecting radius of $\Delta R < 0.3$
$E_T^{\text{TopoCone30}}/p_T$	Lepton calorimeter isolation, with topological cluster collecting radius of $\Delta R < 0.3$

Table 25: A table of the variables used in the training of `PromptLeptonIso`.

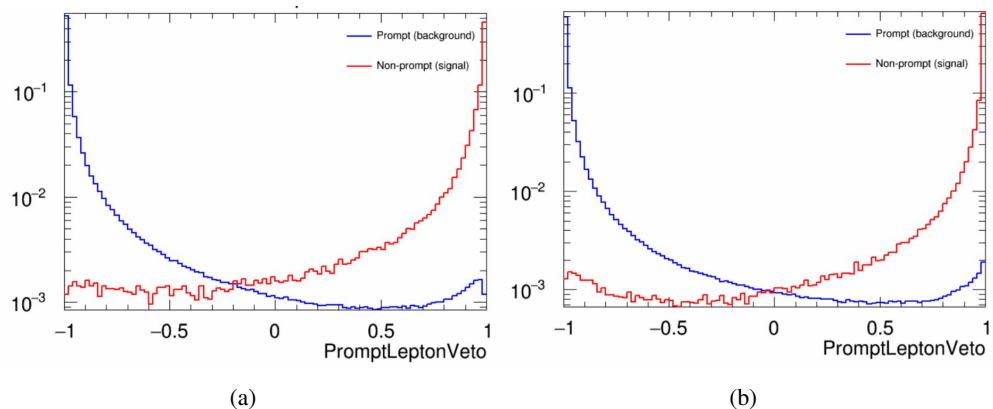


Figure 39: Distribution of the PLV BDT discriminant for (a) electrons and (b) muons

783 The ROC curve for the BDT response, compared to the standard `FixedCutTight` WP, is shown  
 784 in figure A.1, which shows a clear improvement when using this alternative training.

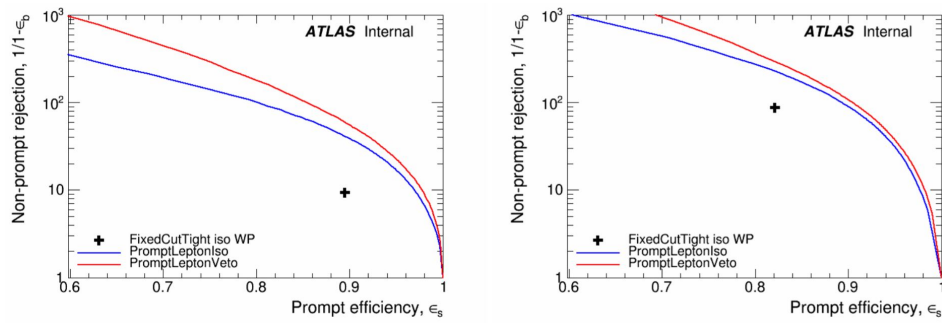


Figure 40: ROC curves for the PLV as well as the performance of the standard FixedCutTight WP for (left) electrons and (right) muons

785 A cutoff value of -0.7 for electrons and -0.5 for muons are chosen as the WPs for this MVA, based  
786 on an optimisation of  $S/\sqrt{B}$  performed in the preselection regions of the  $t\bar{t}H$  – ML analysis,  
787 which have a signature similar to that of this analysis.

788 The efficiency of the tight PromptLeptonIso working point is measured using the tag and probe  
789 method with  $Z \rightarrow \ell^+\ell^-$  events. Such calibration are performed by analysers from this analysis  
790 in communication with the Egamma and Muon combined performance groups. The scale factor  
791 are approximately 0.92 for  $10 < p_T < 15$  GeV, and averaging at 0.98 to 0.99 for higher  $p_T$   
792 leptons. An extra systematic is applied to muons within  $\Delta R < 0.6$  of a calorimeter jet, since  
793 there is a strong dependence on the scale factor due to the presence of these jets. For electrons,  
794 the dominant systematics is coming from pile-up dependence. Overall the systematics are a  
795 maximum of 3% at low  $p_T$  and decreasing at a function of  $p_T$ .

## 796 **A.2 Non-prompt CR Modelling**

797 In order to further validate the modeling in each of the non-prompt CRs, additional kinematic  
798 plots are made in the Z+jets CR and  $t\bar{t}$  CR in each of the continuous b-tag regions, after the  
799 correction factors detailed in Section 6.3 have been applied.

800 In the case of the Z+jets CR, the  $p_T$  spectrum of the lepton originating from the W candidate is  
801 shown, as this is the distribution used to extract the scale factor applied to Z+jets. These plots  
802 are shown in Figures 41 and 42.

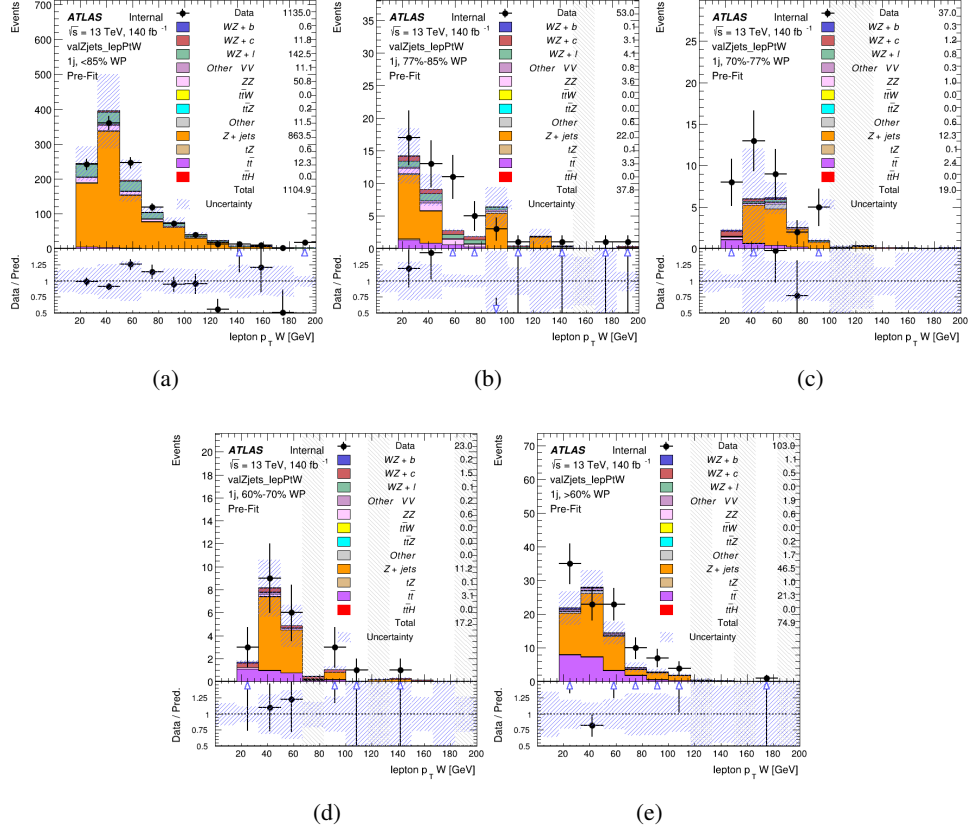


Figure 41: Comparisons between the data and MC distributions of the  $p_T$  of the lepton originating from the W-candidate in the Z+jets CR for each of the 1-jet b-tag working point regions

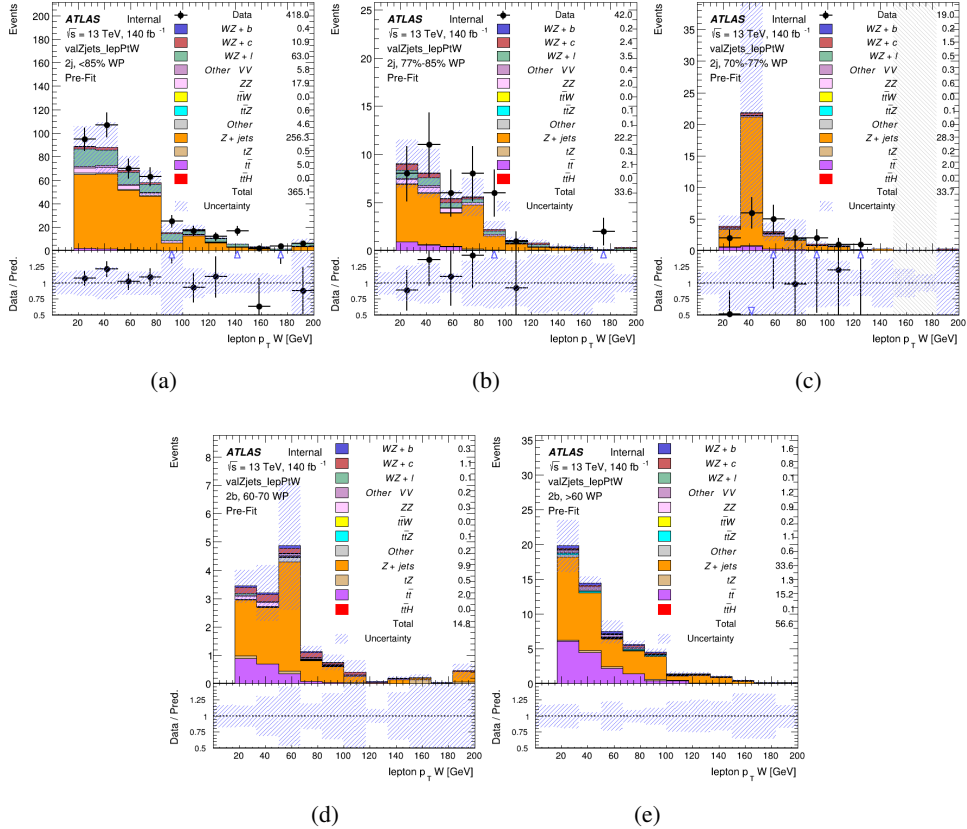


Figure 42: Comparisons between the data and MC distributions of the  $p_T$  of the lepton originating from the W-candidate in the Z+jets CR for each of the 2-jet b-tag working point regions

803 The same is shown for the  $t\bar{t}$  CR, but the  $p_T$  of the OS lepton is used instead as a representation  
 804 of the modeling, as the lepton from the W is not well defined for  $t\bar{t}$  events. These plots are shown  
 805 in Figures 43 and 44.

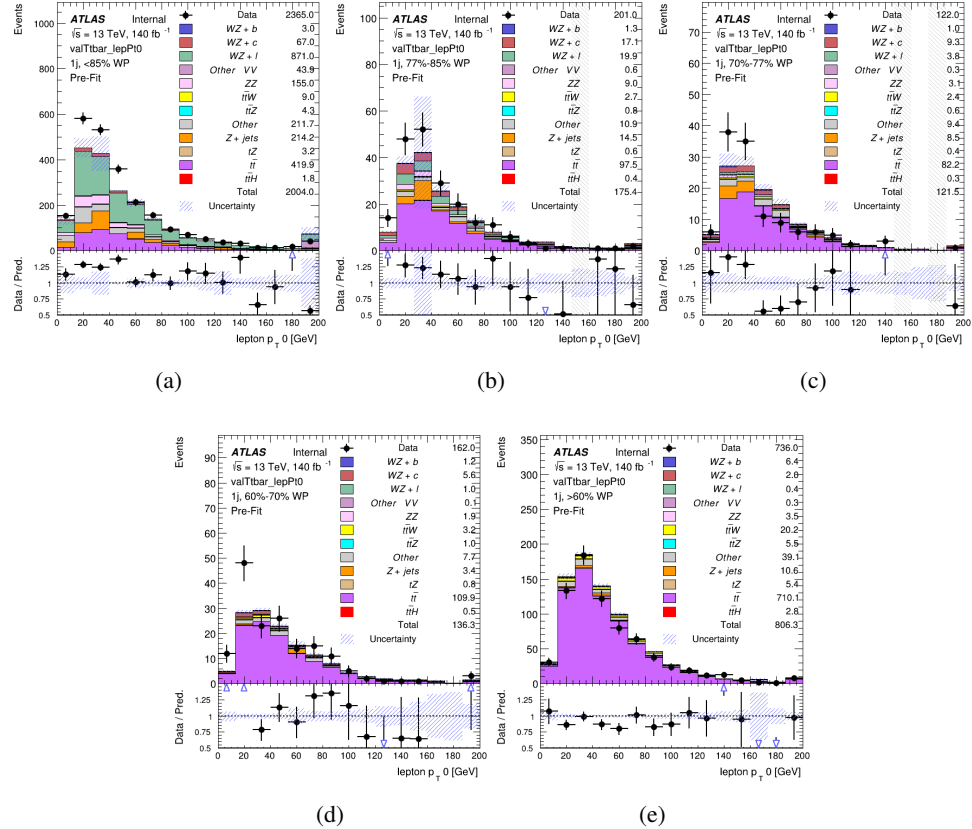


Figure 43: Comparisons between the data and MC distributions of the  $p_T$  of the OS lepton in the  $t\bar{t}$  CR for each of the 1-jet b-tag working point regions

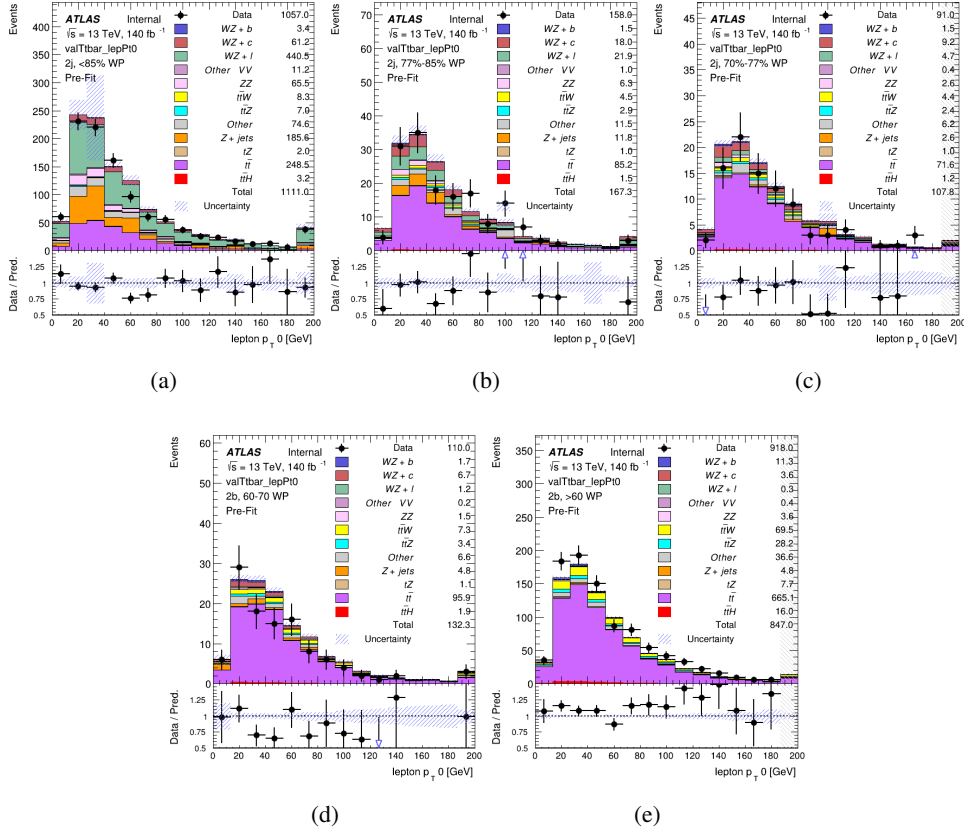


Figure 44: Comparisons between the data and MC distributions of the  $p_T$  of the OS lepton in the  $t\bar{t}$  CR for each of the 2-jet b-tag working point regions

### 806 A.3 DSID list

Data:

```
data15_13TeV.AllYear.physics_Main.PhysCont.DAOD_HIGG8D1.grp15_v01_p4134
data16_13TeV.AllYear.physics_Main.PhysCont.DAOD_HIGG8D1.grp16_v01_p4134
data17_13TeV.AllYear.physics_Main.PhysCont.DAOD_HIGG8D1.grp17_v01_p4134
data18_13TeV.AllYear.physics_Main.PhysCont.DAOD_HIGG8D1.grp18_v01_p4134
```

mc16a:

```
mc16_13TeV.361603.PowhegPy8EG_CT10nloME_AZNLOCTEQ6L1_ZZllll_mll4.deriv.DAOD_HIGG8D1.e4475_s3126_r9364_r9315_p4133
mc16_13TeV.361602.PowhegPy8EG_CT10nloME_AZNLOCTEQ6L1_WZlvvv_mll4.deriv.DAOD_HIGG8D1.e4054_s3126_r9364_r9315_p4133
mc16_13TeV.361604.PowhegPy8EG_CT10nloME_AZNLOCTEQ6L1_ZZvvll_mll4.deriv.DAOD_HIGG8D1.e4475_s3126_r9364_r9315_p4133
mc16_13TeV.361600.PowhegPy8EG_CT10nloME_AZNLOCTEQ6L1_WWlvvv.deriv.DAOD_HIGG8D1.e4616_s3126_r9364_r9315_p4133
mc16_13TeV.361605.PowhegPy8EG_CT10nloME_AZNLOCTEQ6L1_ZZvvvv_mll4.deriv.DAOD_HIGG8D1.e4054_s3126_s3136_r9364_r9315_p4133
mc16_13TeV.361601.PowhegPy8EG_CT10nloME_AZNLOCTEQ6L1_WZlvvll_mll4.deriv.DAOD_HIGG8D1.e4475_s3126_r9364_r9315_p4133
mc16_13TeV.364286.Sherpa_222_NNPDF30NNLO_llvvjj_ss_EW4.deriv.DAOD_HIGG8D1.e6055_e5984_s3126_r9364_r9315_p3983 mc16_13TeV.364285.Sherpa_222_NNPDF30NNLO_llvvjj_ss_EW4.deriv.DAOD_HIGG8D1.e7421_e5984_s3126_r9364_r9315_p4133
mc16_13TeV.364740.MGPy8EG_NNPDF30NLO_A14NNPDF23LO_llvlij_EW6_OFPlus.deriv.DAOD_HIGG8D1.e7421_e5984_s3126_r9364_r9315_p4133
mc16_13TeV.364742.MGPy8EG_NNPDF30NLO_A14NNPDF23LO_llvlij_EW6_SFPlus.deriv.DAOD_HIGG8D1.e7421_e5984_s3126_r9364_r9315_p4133
mc16_13TeV.364253.Sherpa_222_NNPDF30NNLO_llvv.deriv.DAOD_HIGG8D1.e5916_s3126_r9364_r9315_p4133
mc16_13TeV.364250.Sherpa_222_NNPDF30NNLO_llll.deriv.DAOD_HIGG8D1.e5894_s3126_r9364_r9315_p4133
mc16_13TeV.364254.Sherpa_222_NNPDF30NNLO_llvv.deriv.DAOD_HIGG8D1.e5916_s3126_r9364_r9315_p4133
```

mc16\_13TeV.364255.Sherpa\_222\_NNPDF30NNLO\_lvyy.deriv.DAOD\_HIGG8D1.e5916\_s3126\_r9364\_r9315\_p4133  
 mc16\_13TeV.410155.aMcAtNloPythia8EvtGen\_MEN30NLO\_A14N23LO\_ttW.deriv.DAOD\_HIGG8D1.e5070\_s3126\_r9364\_r9315\_p4133  
 mc16\_13TeV.410156.aMcAtNloPythia8EvtGen\_MEN30NLO\_A14N23LO\_ttZnuu.deriv.DAOD\_HIGG8D1.e5070\_s3126\_r9364\_r9315\_p4133  
 mc16\_13TeV.410157.aMcAtNloPythia8EvtGen\_MEN30NLO\_A14N23LO\_ttZqq.deriv.DAOD\_HIGG8D1.e5070\_s3126\_r9364\_r9315\_p4133  
 mc16\_13TeV.410218.aMcAtNloPythia8EvtGen\_MEN30NLO\_A14N23LO\_ttee.deriv.DAOD\_HIGG8D1.e5070\_s3126\_r9364\_r9315\_p4133  
 mc16\_13TeV.410219.aMcAtNloPythia8EvtGen\_MEN30NLO\_A14N23LO\_ttmumu.deriv.DAOD\_HIGG8D1.e5070\_s3126\_r9364\_r9315\_p4133  
 mc16\_13TeV.410220.aMcAtNloPythia8EvtGen\_MEN30NLO\_A14N23LO\_ttautau.deriv.DAOD\_HIGG8D1.e5070\_s3126\_r9364\_r9315\_p4133  
 mc16\_13TeV.412063.aMcAtNloPythia8EvtGen\_tllq\_NNPDF30\_nf4\_A4.deriv.DAOD\_TOPQ1.e7054\_e5984\_s3126\_r9364\_r9315\_p4174  
 mc16\_13TeV.410276.aMcAtNloPythia8EvtGen\_MEN30NLO\_A14N23LO\_ttee\_mll\_1\_5.deriv.DAOD\_HIGG8D1.e6087\_e5984\_s3126\_r9364\_r9315\_p4133  
 mc16\_13TeV.410277.aMcAtNloPythia8EvtGen\_MEN30NLO\_A14N23LO\_ttmumu\_mll\_1\_5.deriv.DAOD\_HIGG8D1.e6087\_e5984\_s3126\_r9364\_r9315\_p4133  
 mc16\_13TeV.410278.aMcAtNloPythia8EvtGen\_MEN30NLO\_A14N23LO\_ttautau\_mll\_1\_5.deriv.DAOD\_HIGG8D1.e6087\_e5984\_s3126\_r9364\_r9315\_p4133  
 mc16\_13TeV.410397.MadGraphPythia8EvtGen\_ttbar\_wbee\_MEN30LO\_A14N23LO.deriv.DAOD\_HIGG8D1.e6086\_e5984\_s3126\_r9364\_r9315\_p4133  
 mc16\_13TeV.410398.MadGraphPythia8EvtGen\_ttbar\_wbmumu\_MEN30LO\_A14N23LO.deriv.DAOD\_HIGG8D1.e6086\_e5984\_s3126\_r9364\_r9315\_p4133  
 mc16\_13TeV.410399.MadGraphPythia8EvtGen\_ttbar\_wbtautau\_MEN30LO\_A14N23LO.deriv.DAOD\_HIGG8D1.e6086\_e5984\_s3126\_r9364\_r9315\_p4133  
 mc16\_13TeV.410658.PhPy8EG\_A14\_tchan\_BW50\_lept\_top.deriv.DAOD\_HIGG8D1.e6671\_e5984\_s3126\_r9364\_r9315\_p4133  
 mc16\_13TeV.410659.PhPy8EG\_A14\_tchan\_BW50\_lept\_antitop.deriv.DAOD\_HIGG8D1.e6671\_e5984\_s3126\_r9364\_r9315\_p4133  
 mc16\_13TeV.410644.PowhegPythia8EvtGen\_A14\_singletop\_schan\_lept\_top.deriv.DAOD\_HIGG8D1.e6527\_e5984\_s3126\_r9364\_r9315\_p4133  
 mc16\_13TeV.410645.PowhegPythia8EvtGen\_A14\_singletop\_schan\_lept\_antitop.deriv.DAOD\_HIGG8D1.e6527\_e5984\_s3126\_r9364\_r9315\_p4133  
 mc16\_13TeV.304014.MadGraphPythia8EvtGen\_A14NNPDF23\_3top\_SM.deriv.DAOD\_HIGG8D1.e4324\_s3126\_r9364\_r9315\_p4133  
 mc16\_13TeV.410080.MadGraphPythia8EvtGen\_A14NNPDF23\_4topSM.deriv.DAOD\_HIGG8D1.e4111\_s3126\_r9364\_r9315\_p4133  
 mc16\_13TeV.410081.MadGraphPythia8EvtGen\_A14NNPDF23\_ttbarWW.deriv.DAOD\_HIGG8D1.e4111\_s3126\_r9364\_r9315\_p4133  
 mc16\_13TeV.364100.Sherpa\_221\_NNPDF30NNLO\_Zmumu\_MAXHTPTV0\_70\_CVetoBVeto.deriv.DAOD\_HIGG8D1.e5271\_s3126\_r9364\_r9315\_p4133  
 mc16\_13TeV.364101.Sherpa\_221\_NNPDF30NNLO\_Zmumu\_MAXHTPTV0\_70\_CFilterBVeto.deriv.DAOD\_HIGG8D1.e5271\_s3126\_r9364\_r9315\_p4133  
 mc16\_13TeV.364102.Sherpa\_221\_NNPDF30NNLO\_Zmumu\_MAXHTPTV0\_70\_BFilter.deriv.DAOD\_HIGG8D1.e5271\_s3126\_r9364\_r9315\_p4133  
 mc16\_13TeV.364103.Sherpa\_221\_NNPDF30NNLO\_Zmumu\_MAXHTPTV70\_140\_CVetoBVeto.deriv.DAOD\_HIGG8D1.e5271\_s3126\_r9364\_r9315\_p4133  
 mc16\_13TeV.364104.Sherpa\_221\_NNPDF30NNLO\_Zmumu\_MAXHTPTV70\_140\_CFilterBVeto.deriv.DAOD\_HIGG8D1.e5271\_s3126\_r9364\_r9315\_p4133  
 mc16\_13TeV.364106.Sherpa\_221\_NNPDF30NNLO\_Zmumu\_MAXHTPTV140\_280\_CVetoBVeto.deriv.DAOD\_HIGG8D1.e5271\_s3126\_r9364\_r9315\_p4133  
 mc16\_13TeV.364107.Sherpa\_221\_NNPDF30NNLO\_Zmumu\_MAXHTPTV140\_280\_CFilterBVeto.deriv.DAOD\_HIGG8D1.e5271\_s3126\_r9364\_r9315\_p4133  
 mc16\_13TeV.364108.Sherpa\_221\_NNPDF30NNLO\_Zmumu\_MAXHTPTV140\_280\_BFilter.deriv.DAOD\_HIGG8D1.e5271\_s3126\_r9364\_r9315\_p4133  
 mc16\_13TeV.364109.Sherpa\_221\_NNPDF30NNLO\_Zmumu\_MAXHTPTV280\_500\_CVetoBVeto.deriv.DAOD\_HIGG8D1.e5271\_s3126\_r9364\_r9315\_p4133  
 mc16\_13TeV.364110.Sherpa\_221\_NNPDF30NNLO\_Zmumu\_MAXHTPTV280\_500\_CFilterBVeto.deriv.DAOD\_HIGG8D1.e5271\_s3126\_r9364\_r9315\_p4133  
 mc16\_13TeV.364111.Sherpa\_221\_NNPDF30NNLO\_Zmumu\_MAXHTPTV280\_500\_BFilter.deriv.DAOD\_HIGG8D1.e5271\_e5984\_s3126\_r9364\_r9315\_p4133  
 mc16\_13TeV.364111.Sherpa\_221\_NNPDF30NNLO\_Zmumu\_MAXHTPTV280\_500\_BFilter.deriv.DAOD\_HIGG8D1.e5271\_s3126\_r9364\_r9315\_p4133  
 mc16\_13TeV.364112.Sherpa\_221\_NNPDF30NNLO\_Zmumu\_MAXHTPTV500\_1000.deriv.DAOD\_HIGG8D1.e5271\_s3126\_r9364\_r9315\_p4133  
 mc16\_13TeV.364113.Sherpa\_221\_NNPDF30NNLO\_Zmumu\_MAXHTPTV1000\_E\_CMS.deriv.DAOD\_HIGG8D1.e5271\_s3126\_r9364\_r9315\_p4133  
 mc16\_13TeV.364114.Sherpa\_221\_NNPDF30NNLO\_Zee\_MAXHTPTV0\_70\_CVetoBVeto.deriv.DAOD\_HIGG8D1.e5299\_s3126\_r9364\_r9315\_p4133  
 mc16\_13TeV.364115.Sherpa\_221\_NNPDF30NNLO\_Zee\_MAXHTPTV0\_70\_CFilterBVeto.deriv.DAOD\_HIGG8D1.e5299\_s3126\_r9364\_r9315\_p4133  
 mc16\_13TeV.364116.Sherpa\_221\_NNPDF30NNLO\_Zee\_MAXHTPTV0\_70\_BFilter.deriv.DAOD\_HIGG8D1.e5299\_s3126\_r9364\_r9315\_p4133  
 mc16\_13TeV.364117.Sherpa\_221\_NNPDF30NNLO\_Zee\_MAXHTPTV70\_140\_CVetoBVeto.deriv.DAOD\_HIGG8D1.e5299\_s3126\_r9364\_r9315\_p4133  
 mc16\_13TeV.364118.Sherpa\_221\_NNPDF30NNLO\_Zee\_MAXHTPTV70\_140\_CFilterBVeto.deriv.DAOD\_HIGG8D1.e5299\_s3126\_r9364\_r9315\_p4133  
 mc16\_13TeV.364119.Sherpa\_221\_NNPDF30NNLO\_Zee\_MAXHTPTV70\_140\_BFilter.deriv.DAOD\_HIGG8D1.e5299\_s3126\_r9364\_r9315\_p4133  
 mc16\_13TeV.364120.Sherpa\_221\_NNPDF30NNLO\_Zee\_MAXHTPTV140\_280\_CVetoBVeto.deriv.DAOD\_HIGG8D1.e5299\_s3126\_r9364\_r9315\_p4133  
 mc16\_13TeV.364121.Sherpa\_221\_NNPDF30NNLO\_Zee\_MAXHTPTV140\_280\_CFilterBVeto.deriv.DAOD\_HIGG8D1.e5299\_s3126\_r9364\_r9315\_p4133  
 mc16\_13TeV.364122.Sherpa\_221\_NNPDF30NNLO\_Zee\_MAXHTPTV140\_280\_BFilter.deriv.DAOD\_HIGG8D1.e5299\_s3126\_r9364\_r9315\_p4133  
 mc16\_13TeV.364123.Sherpa\_221\_NNPDF30NNLO\_Zee\_MAXHTPTV280\_500\_CVetoBVeto.deriv.DAOD\_HIGG8D1.e5299\_s3126\_r9364\_r9315\_p4133  
 mc16\_13TeV.364124.Sherpa\_221\_NNPDF30NNLO\_Zee\_MAXHTPTV280\_500\_CFilterBVeto.deriv.DAOD\_HIGG8D1.e5299\_s3126\_r9364\_r9315\_p4133  
 mc16\_13TeV.364125.Sherpa\_221\_NNPDF30NNLO\_Zee\_MAXHTPTV280\_500\_BFilter.deriv.DAOD\_HIGG8D1.e5299\_s3126\_r9364\_r9315\_p4133  
 mc16\_13TeV.364126.Sherpa\_221\_NNPDF30NNLO\_Zee\_MAXHTPTV280\_500\_BFilter.deriv.DAOD\_HIGG8D1.e5299\_s3126\_r9364\_r9315\_p4133  
 mc16\_13TeV.364127.Sherpa\_221\_NNPDF30NNLO\_Zee\_MAXHTPTV1000\_E\_CMS.deriv.DAOD\_HIGG8D1.e5299\_s3126\_r9364\_r9315\_p4133  
 mc16\_13TeV.364128.Sherpa\_221\_NNPDF30NNLO\_Ztautau\_MAXHTPTV0\_70\_CVetoBVeto.deriv.DAOD\_HIGG8D1.e5307\_s3126\_r9364\_r9315\_p4133  
 mc16\_13TeV.364129.Sherpa\_221\_NNPDF30NNLO\_Ztautau\_MAXHTPTV0\_70\_CFilterBVeto.deriv.DAOD\_HIGG8D1.e5307\_s3126\_r9364\_r9315\_p4133  
 mc16\_13TeV.364130.Sherpa\_221\_NNPDF30NNLO\_Ztautau\_MAXHTPTV0\_70\_BFilter.deriv.DAOD\_HIGG8D1.e5307\_s3126\_r9364\_r9315\_p4133  
 mc16\_13TeV.364131.Sherpa\_221\_NNPDF30NNLO\_Ztautau\_MAXHTPTV70\_140\_CVetoBVeto.deriv.DAOD\_HIGG8D1.e5307\_s3126\_r9364\_r9315\_p4133  
 mc16\_13TeV.364132.Sherpa\_221\_NNPDF30NNLO\_Ztautau\_MAXHTPTV70\_140\_CFilterBVeto.deriv.DAOD\_HIGG8D1.e5307\_s3126\_r9364\_r9315\_p4133  
 mc16\_13TeV.364133.Sherpa\_221\_NNPDF30NNLO\_Ztautau\_MAXHTPTV70\_140\_BFilter.deriv.DAOD\_HIGG8D1.e5307\_s3126\_r9364\_r9315\_p4133  
 mc16\_13TeV.364134.Sherpa\_221\_NNPDF30NNLO\_Ztautau\_MAXHTPTV140\_280\_CVetoBVeto.deriv.DAOD\_HIGG8D1.e5307\_s3126\_r9364\_r9315\_p4133  
 mc16\_13TeV.364135.Sherpa\_221\_NNPDF30NNLO\_Ztautau\_MAXHTPTV140\_280\_CFilterBVeto.deriv.DAOD\_HIGG8D1.e5307\_s3126\_r9364\_r9315\_p4133  
 mc16\_13TeV.364136.Sherpa\_221\_NNPDF30NNLO\_Ztautau\_MAXHTPTV140\_280\_BFilter.deriv.DAOD\_HIGG8D1.e5307\_s3126\_r9364\_r9315\_p4133  
 mc16\_13TeV.364137.Sherpa\_221\_NNPDF30NNLO\_Ztautau\_MAXHTPTV280\_500\_CVetoBVeto.deriv.DAOD\_HIGG8D1.e5307\_e5984\_s3126\_r9364\_r9315\_p4133  
 mc16\_13TeV.364138.Sherpa\_221\_NNPDF30NNLO\_Ztautau\_MAXHTPTV280\_500\_CFilterBVeto.deriv.DAOD\_HIGG8D1.e5313\_s3126\_r9364\_r9315\_p4133



mc16\_13TeV.364189.Sherpa\_221\_NNPDF30NNLO\_Wtaunu\_MAXHTPTV70\_140\_BFilter.deriv.DAOD\_HIGG8D1.e5340\_s3126\_r9364\_r9315\_p4133  
 mc16\_13TeV.364190.Sherpa\_221\_NNPDF30NNLO\_Wtaunu\_MAXHTPTV140\_280\_CVetoBVeto.deriv.DAOD\_HIGG8D1.e5340\_e5984\_s3126\_r9364\_r9315\_p4133  
 mc16\_13TeV.364190.Sherpa\_221\_NNPDF30NNLO\_Wtaunu\_MAXHTPTV140\_280\_CVetoBVeto.deriv.DAOD\_HIGG8D1.e5340\_s3126\_r9364\_r9315\_p4133  
 mc16\_13TeV.364191.Sherpa\_221\_NNPDF30NNLO\_Wtaunu\_MAXHTPTV140\_280\_CFilterBVeto.deriv.DAOD\_HIGG8D1.e5340\_s3126\_r9364\_r9315\_p4133  
 mc16\_13TeV.364191.Sherpa\_221\_NNPDF30NNLO\_Wtaunu\_MAXHTPTV140\_280\_CFilterBVeto.deriv.DAOD\_HIGG8D1.e5340\_e5984\_s3126\_s3136\_r9364\_r9315\_p4133  
 mc16\_13TeV.364192.Sherpa\_221\_NNPDF30NNLO\_Wtaunu\_MAXHTPTV140\_280\_BFilter.deriv.DAOD\_HIGG8D1.e5340\_s3126\_r9364\_r9315\_p4133  
 mc16\_13TeV.364193.Sherpa\_221\_NNPDF30NNLO\_Wtaunu\_MAXHTPTV280\_500\_CVetoBVeto.deriv.DAOD\_HIGG8D1.e5340\_s3126\_r9364\_r9315\_p4133  
 mc16\_13TeV.364193.Sherpa\_221\_NNPDF30NNLO\_Wtaunu\_MAXHTPTV280\_500\_CVetoBVeto.deriv.DAOD\_HIGG8D1.e5340\_e5984\_s3126\_s3136\_r9364\_r9315\_p4133  
 mc16\_13TeV.364194.Sherpa\_221\_NNPDF30NNLO\_Wtaunu\_MAXHTPTV280\_500\_CFilterBVeto.deriv.DAOD\_HIGG8D1.e5340\_s3126\_r9364\_r9315\_p4133  
 mc16\_13TeV.364194.Sherpa\_221\_NNPDF30NNLO\_Wtaunu\_MAXHTPTV280\_500\_CFilterBVeto.deriv.DAOD\_HIGG8D1.e5340\_e5984\_s3126\_s3136\_r9364\_r9315\_p4133  
 mc16\_13TeV.364195.Sherpa\_221\_NNPDF30NNLO\_Wtaunu\_MAXHTPTV280\_500\_BFilter.deriv.DAOD\_HIGG8D1.e5340\_s3126\_r9364\_r9315\_p4133  
 mc16\_13TeV.364196.Sherpa\_221\_NNPDF30NNLO\_Wtaunu\_MAXHTPTV500\_1000.deriv.DAOD\_HIGG8D1.e5340\_s3126\_r9364\_r9315\_p4133  
 mc16\_13TeV.364197.Sherpa\_221\_NNPDF30NNLO\_Wtaunu\_MAXHTPTV1000\_E\_CMS.deriv.DAOD\_HIGG8D1.e5340\_s3126\_r9364\_r9315\_p4133  
 mc16\_13TeV.364500.Sherpa\_222\_NNPDF30NNLO\_eegamma\_pty\_7\_15.deriv.DAOD\_HIGG8D1.e5928\_e5984\_s3126\_r9364\_r9315\_p4133  
 mc16\_13TeV.364501.Sherpa\_222\_NNPDF30NNLO\_eegamma\_pty\_15\_35.deriv.DAOD\_HIGG8D1.e5928\_e5984\_s3126\_r9364\_r9315\_p4133  
 mc16\_13TeV.364502.Sherpa\_222\_NNPDF30NNLO\_eegamma\_pty\_35\_70.deriv.DAOD\_HIGG8D1.e5928\_e5984\_s3126\_r9364\_r9315\_p4133  
 mc16\_13TeV.364503.Sherpa\_222\_NNPDF30NNLO\_eegamma\_pty\_70\_140.deriv.DAOD\_HIGG8D1.e5928\_e5984\_s3126\_r9364\_r9315\_p4133  
 mc16\_13TeV.364504.Sherpa\_222\_NNPDF30NNLO\_eegamma\_pty\_140\_E\_CMS.deriv.DAOD\_HIGG8D1.e5928\_e5984\_s3126\_r9364\_r9315\_p4133  
 mc16\_13TeV.364505.Sherpa\_222\_NNPDF30NNLO\_mumugamma\_pty\_7\_15.deriv.DAOD\_HIGG8D1.e5928\_e5984\_s3126\_r9364\_r9315\_p4133  
 mc16\_13TeV.364506.Sherpa\_222\_NNPDF30NNLO\_mumugamma\_pty\_15\_35.deriv.DAOD\_HIGG8D1.e5988\_e5984\_s3126\_r9364\_r9315\_p4133  
 mc16\_13TeV.364507.Sherpa\_222\_NNPDF30NNLO\_mumugamma\_pty\_35\_70.deriv.DAOD\_HIGG8D1.e5928\_e5984\_s3126\_r9364\_r9315\_p4133  
 mc16\_13TeV.364508.Sherpa\_222\_NNPDF30NNLO\_mumugamma\_pty\_70\_140.deriv.DAOD\_HIGG8D1.e5928\_e5984\_s3126\_r9364\_r9315\_p4133  
 mc16\_13TeV.364509.Sherpa\_222\_NNPDF30NNLO\_mumugamma\_pty\_140\_E\_CMS.deriv.DAOD\_HIGG8D1.e5928\_e5984\_s3126\_r9364\_r9315\_p4133  
 mc16\_13TeV.364510.Sherpa\_222\_NNPDF30NNLO\_tautaugamma\_pty\_7\_15.deriv.DAOD\_HIGG8D1.e5928\_s3126\_r9364\_r9315\_p4133  
 mc16\_13TeV.364511.Sherpa\_222\_NNPDF30NNLO\_tautaugamma\_pty\_15\_35.deriv.DAOD\_HIGG8D1.e5928\_s3126\_r9364\_r9315\_p4133  
 mc16\_13TeV.364512.Sherpa\_222\_NNPDF30NNLO\_tautaugamma\_pty\_35\_70.deriv.DAOD\_HIGG8D1.e5928\_s3126\_r9364\_r9315\_p4133  
 mc16\_13TeV.364513.Sherpa\_222\_NNPDF30NNLO\_tautaugamma\_pty\_70\_140.deriv.DAOD\_HIGG8D1.e5982\_s3126\_r9364\_r9315\_p4133  
 mc16\_13TeV.364514.Sherpa\_222\_NNPDF30NNLO\_tautaugamma\_pty\_140\_E\_CMS.deriv.DAOD\_HIGG8D1.e5928\_s3126\_r9364\_r9315\_p4133  
 mc16\_13TeV.364521.Sherpa\_222\_NNPDF30NNLO\_enugamma\_pty\_7\_15.deriv.DAOD\_HIGG8D1.e5928\_s3126\_r9364\_r9315\_p4133  
 mc16\_13TeV.364522.Sherpa\_222\_NNPDF30NNLO\_enugamma\_pty\_15\_35.deriv.DAOD\_HIGG8D1.e5928\_s3126\_r9364\_r9315\_p4133  
 mc16\_13TeV.364523.Sherpa\_222\_NNPDF30NNLO\_enugamma\_pty\_35\_70.deriv.DAOD\_HIGG8D1.e5928\_s3126\_r9364\_r9315\_p4133  
 mc16\_13TeV.364524.Sherpa\_222\_NNPDF30NNLO\_enugamma\_pty\_70\_140.deriv.DAOD\_HIGG8D1.e5928\_s3126\_r9364\_r9315\_p4133  
 mc16\_13TeV.364525.Sherpa\_222\_NNPDF30NNLO\_enugamma\_pty\_140\_E\_CMS.deriv.DAOD\_HIGG8D1.e5928\_s3126\_r9364\_r9315\_p4133  
 mc16\_13TeV.364525.Sherpa\_222\_NNPDF30NNLO\_enugamma\_pty\_140\_E\_CMS.deriv.DAOD\_HIGG8D1.e5928\_e5984\_s3126\_r9364\_r9315\_p4133  
 mc16\_13TeV.364526.Sherpa\_222\_NNPDF30NNLO\_munugamma\_pty\_7\_15.deriv.DAOD\_HIGG8D1.e5928\_s3126\_r9364\_r9315\_p4133  
 mc16\_13TeV.364527.Sherpa\_222\_NNPDF30NNLO\_munugamma\_pty\_15\_35.deriv.DAOD\_HIGG8D1.e5928\_s3126\_r9364\_r9315\_p4133  
 mc16\_13TeV.364528.Sherpa\_222\_NNPDF30NNLO\_munugamma\_pty\_35\_70.deriv.DAOD\_HIGG8D1.e5928\_s3126\_r9364\_r9315\_p4133  
 mc16\_13TeV.364529.Sherpa\_222\_NNPDF30NNLO\_munugamma\_pty\_70\_140.deriv.DAOD\_HIGG8D1.e5928\_s3126\_r9364\_r9315\_p4133  
 mc16\_13TeV.364530.Sherpa\_222\_NNPDF30NNLO\_munugamma\_pty\_140\_E\_CMS.deriv.DAOD\_HIGG8D1.e5928\_s3126\_r9364\_r9315\_p4133  
 mc16\_13TeV.364530.Sherpa\_222\_NNPDF30NNLO\_munugamma\_pty\_140\_E\_CMS.deriv.DAOD\_HIGG8D1.e5928\_e5984\_s3126\_r9364\_r9315\_p4133  
 mc16\_13TeV.364531.Sherpa\_222\_NNPDF30NNLO\_taunugamma\_pty\_7\_15.deriv.DAOD\_HIGG8D1.e5928\_s3126\_r9364\_r9315\_p4133  
 mc16\_13TeV.364532.Sherpa\_222\_NNPDF30NNLO\_taunugamma\_pty\_15\_35.deriv.DAOD\_HIGG8D1.e5928\_s3126\_r9364\_r9315\_p4133  
 mc16\_13TeV.364533.Sherpa\_222\_NNPDF30NNLO\_taunugamma\_pty\_35\_70.deriv.DAOD\_HIGG8D1.e5928\_s3126\_r9364\_r9315\_p4133  
 mc16\_13TeV.364534.Sherpa\_222\_NNPDF30NNLO\_taunugamma\_pty\_70\_140.deriv.DAOD\_HIGG8D1.e5928\_s3126\_r9364\_r9315\_p4133  
 mc16\_13TeV.364535.Sherpa\_222\_NNPDF30NNLO\_taunugamma\_pty\_140\_E\_CMS.deriv.DAOD\_HIGG8D1.e5928\_s3126\_r9364\_r9315\_p4133  
 mc16\_13TeV.364535.Sherpa\_222\_NNPDF30NNLO\_taunugamma\_pty\_140\_E\_CMS.deriv.DAOD\_HIGG8D1.e5928\_e5984\_s3126\_r9364\_r9315\_p4133  
 mc16\_13TeV.410560.MadGraphPythia8EvtGen\_A14\_Z\_4fl\_tchan\_noAllHad.deriv.DAOD\_HIGG8D1.e5803\_s3126\_r9364\_r9315\_p4133  
 mc16\_13TeV.410013.PowhegPythiaEvtGen\_P2012\_Wt\_inclusive\_top.deriv.DAOD\_HIGG8D1.e3753\_s3126\_r9364\_r9315\_p4133  
 mc16\_13TeV.410014.PowhegPythiaEvtGen\_P2012\_Wt\_inclusive\_antitop.deriv.DAOD\_HIGG8D1.e3753\_s3126\_r9364\_r9315\_p4133  
 mc16\_13TeV.410408.aMcAtNloPythia8EvtGen\_tWZ\_Ztoll\_minDR1.deriv.DAOD\_HIGG8D1.e6423\_e5984\_s3126\_r9364\_r9315\_p4133  
 mc16\_13TeV.364242.Sherpa\_222\_NNPDF30NNLO\_WWW\_31v\_EW6.deriv.DAOD\_HIGG8D1.e5887\_s3126\_r9364\_r9315\_p4133  
 mc16\_13TeV.364243.Sherpa\_222\_NNPDF30NNLO\_WWW\_412v\_EW6.deriv.DAOD\_HIGG8D1.e5887\_s3126\_r9364\_r9315\_p4133  
 mc16\_13TeV.364244.Sherpa\_222\_NNPDF30NNLO\_WWW\_214v\_EW6.deriv.DAOD\_HIGG8D1.e5887\_s3126\_r9364\_r9315\_p4133  
 mc16\_13TeV.364245.Sherpa\_222\_NNPDF30NNLO\_WZZ\_51v\_EW6.deriv.DAOD\_HIGG8D1.e5887\_s3126\_r9364\_r9315\_p4133  
 mc16\_13TeV.364246.Sherpa\_222\_NNPDF30NNLO\_WZZ\_31v\_EW6.deriv.DAOD\_HIGG8D1.e5887\_s3126\_r9364\_r9315\_p4133  
 mc16\_13TeV.364247.Sherpa\_222\_NNPDF30NNLO\_ZZZ\_610v\_EW6.deriv.DAOD\_HIGG8D1.e5887\_s3126\_r9364\_r9315\_p4133  
 mc16\_13TeV.364248.Sherpa\_222\_NNPDF30NNLO\_ZZZ\_412v\_EW6.deriv.DAOD\_HIGG8D1.e5887\_s3126\_r9364\_r9315\_p4133  
 mc16\_13TeV.364249.Sherpa\_222\_NNPDF30NNLO\_ZZZ\_214v\_EW6.deriv.DAOD\_HIGG8D1.e5887\_s3126\_r9364\_r9315\_p4133  
 mc16\_13TeV.342284.Pythia8EvtGen\_A14NNPDF23LO\_WH125\_inc.deriv.DAOD\_HIGG8D1.e4246\_s3126\_r9364\_r9315\_p4133  
 mc16\_13TeV.342285.Pythia8EvtGen\_A14NNPDF23LO\_ZH125\_inc.deriv.DAOD\_HIGG8D1.e4246\_s3126\_r9364\_r9315\_p4133  
 mc16\_13TeV.341998.aMcAtNloHppEG\_UEEE5\_CTEQ6L1\_CT10ME\_tWH125\_gamgam\_yt\_plus1.deriv.DAOD\_HIGG8D1.e4394\_e5984\_s3126\_r9364\_r9315\_p4133  
 mc16\_13TeV.410389.MadGraphPythia8EvtGen\_A14NNPDF23\_ttgamma\_nonallhadronic.deriv.DAOD\_HIGG8D1.e6155\_e5984\_s3126\_r9364\_r9315\_p4133

mc16\_13TeV.410470.PhPy8EG\_A14\_ttbar\_hdamp258p75\_nonallhad.deriv.DAOD\_HIGG8D1.e6337\_e5984\_s3126\_r9364\_r9315\_p4133  
 mc16\_13TeV.410472.PhPy8EG\_A14\_ttbar\_hdamp258p75\_dil.deriv.DAOD\_HIGG8D1.e6348\_e5984\_s3126\_r9364\_r9315\_p4133  
 mc16\_13TeV.346343.PhPy8EG\_A14NNPDF23\_NNPDF30ME\_ttH125\_allhad.deriv.DAOD\_HIGG8D1.e7148\_e5984\_s3126\_r9364\_r9315\_p4133  
 mc16\_13TeV.346344.PhPy8EG\_A14NNPDF23\_NNPDF30ME\_ttH125\_semilep.deriv.DAOD\_HIGG8D1.e7148\_e5984\_s3126\_r9364\_r9315\_p4133  
 mc16\_13TeV.346345.PhPy8EG\_A14NNPDF23\_NNPDF30ME\_ttH125\_dilep.deriv.DAOD\_HIGG8D1.e7148\_e5984\_s3126\_r9364\_r9315\_p4133  
  
 mc16d:  
 mc16\_13TeV.364253.Sherpa\_222\_NNPDF30NNLO\_lllv.deriv.DAOD\_HIGG8D1.e5916\_e5984\_s3126\_r10201\_r10210\_p4133  
 mc16\_13TeV.364250.Sherpa\_222\_NNPDF30NNLO\_llll.deriv.DAOD\_HIGG8D1.e5984\_e5984\_s3126\_r10201\_r10210\_p4133  
 mc16\_13TeV.364254.Sherpa\_222\_NNPDF30NNLO\_llvv.deriv.DAOD\_HIGG8D1.e5916\_e5984\_s3126\_r10201\_r10210\_p4133  
 mc16\_13TeV.364255.Sherpa\_222\_NNPDF30NNLO\_lvvv.deriv.DAOD\_HIGG8D1.e5916\_e5984\_s3126\_r10201\_r10210\_p4133  
 mc16\_13TeV.410155.aMcAtNloPythia8EvtGen\_MEN30NLO\_A14N23LO\_ttW.deriv.DAOD\_HIGG8D1.e5070\_e5984\_s3126\_r10201\_r10210\_p4133  
 mc16\_13TeV.410156.aMcAtNloPythia8EvtGen\_MEN30NLO\_A14N23LO\_ttZnunu.deriv.DAOD\_HIGG8D1.e5070\_e5984\_s3126\_r10201\_r10210\_p4133  
 mc16\_13TeV.410157.aMcAtNloPythia8EvtGen\_MEN30NLO\_A14N23LO\_ttZqq.deriv.DAOD\_HIGG8D1.e5070\_e5984\_s3126\_r10201\_r10210\_p4133  
 mc16\_13TeV.410218.aMcAtNloPythia8EvtGen\_MEN30NLO\_A14N23LO\_ttee.deriv.DAOD\_HIGG8D1.e5070\_e5984\_s3126\_r10201\_r10210\_p4133  
 mc16\_13TeV.410219.aMcAtNloPythia8EvtGen\_MEN30NLO\_A14N23LO\_ttmumu.deriv.DAOD\_HIGG8D1.e5070\_e5984\_s3126\_r10201\_r10210\_p4133  
 mc16\_13TeV.410220.aMcAtNloPythia8EvtGen\_MEN30NLO\_A14N23LO\_ttautau.deriv.DAOD\_HIGG8D1.e5070\_e5984\_s3126\_r10201\_r10210\_p4133  
 mc16\_13TeV.410276.aMcAtNloPythia8EvtGen\_MEN30NLO\_A14N23LO\_ttautau\_mll\_1\_5.deriv.DAOD\_HIGG8D1.e6087\_e5984\_s3126\_r10201\_r10210\_p4133  
 mc16\_13TeV.410277.aMcAtNloPythia8EvtGen\_MEN30NLO\_A14N23LO\_ttautau\_mll\_1\_5.deriv.DAOD\_HIGG8D1.e6087\_e5984\_s3126\_r10201\_r10210\_p4133  
 mc16\_13TeV.410278.aMcAtNloPythia8EvtGen\_MEN30NLO\_A14N23LO\_ttautau\_mll\_1\_5.deriv.DAOD\_HIGG8D1.e6087\_e5984\_s3126\_r10201\_r10210\_p4133  
 mc16\_13TeV.410397.MadGraphPythia8EvtGen\_ttbar\_wbee\_MEN30LO\_A14N23LO.deriv.DAOD\_HIGG8D1.e6086\_e5984\_s3126\_r10201\_r10210\_p4133  
 mc16\_13TeV.410398.MadGraphPythia8EvtGen\_ttbar\_wbmumu\_MEN30LO\_A14N23LO.deriv.DAOD\_HIGG8D1.e6086\_e5984\_s3126\_r10201\_r10210\_p4133  
 mc16\_13TeV.410399.MadGraphPythia8EvtGen\_ttbar\_wbtautau\_MEN30LO\_A14N23LO.deriv.DAOD\_HIGG8D1.e6086\_e5984\_s3126\_r10201\_r10210\_p4133  
 mc16\_13TeV.410658.PhPy8EG\_A14\_tchan\_BW50\_lept\_top.deriv.DAOD\_HIGG8D1.e6671\_e5984\_s3126\_r10201\_r10210\_p4133  
 mc16\_13TeV.410659.PhPy8EG\_A14\_tchan\_BW50\_lept\_antitop.deriv.DAOD\_HIGG8D1.e6671\_e5984\_s3126\_r10201\_r10210\_p4133  
 mc16\_13TeV.410644.PowhegPythia8EvtGen\_A14\_singleton\_schan\_lept\_top.deriv.DAOD\_HIGG8D1.e6527\_e5984\_s3126\_r10201\_r10210\_p4133  
 mc16\_13TeV.410645.PowhegPythia8EvtGen\_A14\_singleton\_schan\_lept\_antitop.deriv.DAOD\_HIGG8D1.e6527\_s3126\_r10201\_r10210\_p4133  
 mc16\_13TeV.412063.aMcAtNloPythia8EvtGen\_tllq\_NNPDF30\_nf4\_A14.deriv.DAOD\_TOPQ1.e7054\_e5984\_s3126\_r10201\_r10210\_p4174  
 mc16\_13TeV.304014.MadGraphPythia8EvtGen\_A14NNPDF23\_3top\_SM.deriv.DAOD\_HIGG8D1.e4324\_e5984\_s3126\_r10201\_r10210\_p4133  
 mc16\_13TeV.410080.MadGraphPythia8EvtGen\_A14NNPDF23\_4topSM.deriv.DAOD\_HIGG8D1.e4111\_e5984\_s3126\_r10201\_r10210\_p4133  
 mc16\_13TeV.410081.MadGraphPythia8EvtGen\_A14NNPDF23\_ttbarWW.deriv.DAOD\_HIGG8D1.e4111\_e5984\_s3126\_r10201\_r10210\_p4133  
 mc16\_13TeV.364100.Sherpa\_221\_NNPDF30NNLO\_Zmumu\_MAXHTPTV0\_70\_CVetoBVeto.deriv.DAOD\_HIGG8D1.e5271\_s3126\_r10201\_r10210\_p4133  
 mc16\_13TeV.364101.Sherpa\_221\_NNPDF30NNLO\_Zmumu\_MAXHTPTV0\_70\_CFilterBVeto.deriv.DAOD\_HIGG8D1.e5271\_s3126\_r10201\_r10210\_p4133  
 mc16\_13TeV.364101.Sherpa\_221\_NNPDF30NNLO\_Zmumu\_MAXHTPTV0\_70\_CFilterBVeto.deriv.DAOD\_HIGG8D1.e5271\_s3126\_r10201\_r10210\_p4133  
 mc16\_13TeV.364102.Sherpa\_221\_NNPDF30NNLO\_Zmumu\_MAXHTPTV0\_70\_BFilter.deriv.DAOD\_HIGG8D1.e5271\_s3126\_r10201\_r10210\_p4133  
 mc16\_13TeV.364103.Sherpa\_221\_NNPDF30NNLO\_Zmumu\_MAXHTPTV70\_140\_CVetoBVeto.deriv.DAOD\_HIGG8D1.e5271\_s3126\_r10201\_r10210\_p4133  
 mc16\_13TeV.364104.Sherpa\_221\_NNPDF30NNLO\_Zmumu\_MAXHTPTV70\_140\_CFilterBVeto.deriv.DAOD\_HIGG8D1.e5271\_s3126\_r10201\_r10210\_p4133  
 mc16\_13TeV.364106.Sherpa\_221\_NNPDF30NNLO\_Zmumu\_MAXHTPTV140\_280\_CVetoBVeto.deriv.DAOD\_HIGG8D1.e5271\_s3126\_r10201\_r10210\_p4133  
 mc16\_13TeV.364107.Sherpa\_221\_NNPDF30NNLO\_Zmumu\_MAXHTPTV140\_280\_CFilterBVeto.deriv.DAOD\_HIGG8D1.e5271\_s3126\_r10201\_r10210\_p4133  
 mc16\_13TeV.364108.Sherpa\_221\_NNPDF30NNLO\_Zmumu\_MAXHTPTV140\_280\_BFilter.deriv.DAOD\_HIGG8D1.e5271\_s3126\_r10201\_r10210\_p4133  
 mc16\_13TeV.364108.Sherpa\_221\_NNPDF30NNLO\_Zmumu\_MAXHTPTV140\_280\_BFilter.deriv.DAOD\_HIGG8D1.e5271\_s3126\_r10201\_r10210\_p4133  
 mc16\_13TeV.364109.Sherpa\_221\_NNPDF30NNLO\_Zmumu\_MAXHTPTV280\_500\_CVetoBVeto.deriv.DAOD\_HIGG8D1.e5271\_s3126\_r10201\_r10210\_p4133  
 mc16\_13TeV.364109.Sherpa\_221\_NNPDF30NNLO\_Zmumu\_MAXHTPTV280\_500\_CVetoBVeto.deriv.DAOD\_HIGG8D1.e5271\_s3126\_r10201\_r10210\_p4133  
 mc16\_13TeV.364110.Sherpa\_221\_NNPDF30NNLO\_Zmumu\_MAXHTPTV280\_500\_CFilterBVeto.deriv.DAOD\_HIGG8D1.e5271\_s3126\_r10201\_r10210\_p4133  
 mc16\_13TeV.364111.Sherpa\_221\_NNPDF30NNLO\_Zmumu\_MAXHTPTV280\_500\_BFilter.deriv.DAOD\_HIGG8D1.e5271\_s3126\_r10201\_r10210\_p4133  
 mc16\_13TeV.364112.Sherpa\_221\_NNPDF30NNLO\_Zmumu\_MAXHTPTV280\_500\_BFilter.deriv.DAOD\_HIGG8D1.e5271\_s3126\_r10201\_r10210\_p4133  
 mc16\_13TeV.364112.Sherpa\_221\_NNPDF30NNLO\_Zmumu\_MAXHTPTV500\_1000.deriv.DAOD\_HIGG8D1.e5271\_s3126\_r10201\_r10210\_p4133  
 mc16\_13TeV.364113.Sherpa\_221\_NNPDF30NNLO\_Zmumu\_MAXHTPTV1000\_E\_CMS.deriv.DAOD\_HIGG8D1.e5271\_s3126\_r10201\_r10210\_p4133  
 mc16\_13TeV.364114.Sherpa\_221\_NNPDF30NNLO\_Zee\_MAXHTPTV0\_70\_CVetoBVeto.deriv.DAOD\_HIGG8D1.e5299\_s3126\_r10201\_r10210\_p4133  
 mc16\_13TeV.364115.Sherpa\_221\_NNPDF30NNLO\_Zee\_MAXHTPTV0\_70\_CFilterBVeto.deriv.DAOD\_HIGG8D1.e5299\_e5984\_s3126\_r10201\_r10210\_p4133  
 mc16\_13TeV.364116.Sherpa\_221\_NNPDF30NNLO\_Zee\_MAXHTPTV0\_70\_BFilter.deriv.DAOD\_HIGG8D1.e5299\_e5984\_s3126\_r10201\_r10210\_p4133  
 mc16\_13TeV.364117.Sherpa\_221\_NNPDF30NNLO\_Zee\_MAXHTPTV70\_140\_CVetoBVeto.deriv.DAOD\_HIGG8D1.e5299\_e5984\_s3126\_r10201\_r10210\_p4133  
 mc16\_13TeV.364118.Sherpa\_221\_NNPDF30NNLO\_Zee\_MAXHTPTV70\_140\_CFilterBVeto.deriv.DAOD\_HIGG8D1.e5299\_e5984\_s3126\_r10201\_r10210\_p4133  
 mc16\_13TeV.364119.Sherpa\_221\_NNPDF30NNLO\_Zee\_MAXHTPTV70\_140\_BFilter.deriv.DAOD\_HIGG8D1.e5299\_e5984\_s3126\_r10201\_r10210\_p4133  
 mc16\_13TeV.364120.Sherpa\_221\_NNPDF30NNLO\_Zee\_MAXHTPTV140\_280\_CVetoBVeto.deriv.DAOD\_HIGG8D1.e5299\_e5984\_s3126\_r10201\_r10210\_p4133  
 mc16\_13TeV.364121.Sherpa\_221\_NNPDF30NNLO\_Zee\_MAXHTPTV140\_280\_CFilterBVeto.deriv.DAOD\_HIGG8D1.e5299\_e5984\_s3126\_r10201\_r10210\_p4133  
 mc16\_13TeV.364122.Sherpa\_221\_NNPDF30NNLO\_Zee\_MAXHTPTV140\_280\_BFilter.deriv.DAOD\_HIGG8D1.e5299\_e5984\_s3126\_r10201\_r10210\_p4133  
 mc16\_13TeV.364123.Sherpa\_221\_NNPDF30NNLO\_Zee\_MAXHTPTV280\_500\_CVetoBVeto.deriv.DAOD\_HIGG8D1.e5299\_e5984\_s3126\_r10201\_r10210\_p4133  
 mc16\_13TeV.364124.Sherpa\_221\_NNPDF30NNLO\_Zee\_MAXHTPTV280\_500\_CFilterBVeto.deriv.DAOD\_HIGG8D1.e5299\_e5984\_s3126\_r10201\_r10210\_p4133  
 mc16\_13TeV.364125.Sherpa\_221\_NNPDF30NNLO\_Zee\_MAXHTPTV280\_500\_BFilter.deriv.DAOD\_HIGG8D1.e5299\_e5984\_s3126\_r10201\_r10210\_p4133  
 mc16\_13TeV.364126.Sherpa\_221\_NNPDF30NNLO\_Zee\_MAXHTPTV500\_1000.deriv.DAOD\_HIGG8D1.e5299\_e5984\_s3126\_r10201\_r10210\_p4133





mc16\_13TeV.364506.Sherpa\_222\_NNPDF30NNLO\_mumugamma\_pty\_15\_35.deriv.DAOD\_HIGG8D1.e5928\_e5984\_s3126\_r10201\_r10210\_p4133  
mc16\_13TeV.364507.Sherpa\_222\_NNPDF30NNLO\_mumugamma\_pty\_35\_70.deriv.DAOD\_HIGG8D1.e5928\_e5984\_s3126\_r10201\_r10210\_p4133  
mc16\_13TeV.364508.Sherpa\_222\_NNPDF30NNLO\_mumugamma\_pty\_70\_140.deriv.DAOD\_HIGG8D1.e5928\_e5984\_s3126\_r10201\_r10210\_p4133  
mc16\_13TeV.364509.Sherpa\_222\_NNPDF30NNLO\_mumugamma\_pty\_140\_E\_CMS.deriv.DAOD\_HIGG8D1.e5928\_e5984\_s3126\_r10201\_r10210\_p4133  
mc16\_13TeV.364510.Sherpa\_222\_NNPDF30NNLO\_tautaugamma\_pty\_7\_15.deriv.DAOD\_HIGG8D1.e5928\_e5984\_s3126\_r10201\_r10210\_p4133  
mc16\_13TeV.364511.Sherpa\_222\_NNPDF30NNLO\_tautaugamma\_pty\_15\_35.deriv.DAOD\_HIGG8D1.e5928\_e5984\_s3126\_r10201\_r10210\_p4133  
mc16\_13TeV.364512.Sherpa\_222\_NNPDF30NNLO\_tautaugamma\_pty\_35\_70.deriv.DAOD\_HIGG8D1.e5928\_e5984\_s3126\_r10201\_r10210\_p4133  
mc16\_13TeV.364513.Sherpa\_222\_NNPDF30NNLO\_tautaugamma\_pty\_70\_140.deriv.DAOD\_HIGG8D1.e5928\_e5984\_s3126\_r10201\_r10210\_p4133  
mc16\_13TeV.364513.Sherpa\_222\_NNPDF30NNLO\_tautaugamma\_pty\_70\_140.deriv.DAOD\_HIGG8D1.e5928\_e5984\_s3126\_r10201\_r10210\_p4133  
mc16\_13TeV.364514.Sherpa\_222\_NNPDF30NNLO\_tautaugamma\_pty\_140\_E\_CMS.deriv.DAOD\_HIGG8D1.e5928\_e5984\_s3126\_r10201\_r10210\_p4133  
mc16\_13TeV.364521.Sherpa\_222\_NNPDF30NNLO\_enugamma\_pty\_7\_15.deriv.DAOD\_HIGG8D1.e5928\_e5984\_s3126\_r10201\_r10210\_p4133  
mc16\_13TeV.364522.Sherpa\_222\_NNPDF30NNLO\_enugamma\_pty\_15\_35.deriv.DAOD\_HIGG8D1.e5928\_e5984\_s3126\_r10201\_r10210\_p4133  
mc16\_13TeV.364523.Sherpa\_222\_NNPDF30NNLO\_enugamma\_pty\_35\_70.deriv.DAOD\_HIGG8D1.e5928\_e5984\_s3126\_r10201\_r10210\_p4133  
mc16\_13TeV.364524.Sherpa\_222\_NNPDF30NNLO\_enugamma\_pty\_70\_140.deriv.DAOD\_HIGG8D1.e5928\_e5984\_s3126\_r10201\_r10210\_p4133  
mc16\_13TeV.364525.Sherpa\_222\_NNPDF30NNLO\_enugamma\_pty\_140\_E\_CMS.deriv.DAOD\_HIGG8D1.e5928\_e5984\_s3126\_r10201\_r10210\_p4133  
mc16\_13TeV.364526.Sherpa\_222\_NNPDF30NNLO\_munugamma\_pty\_7\_15.deriv.DAOD\_HIGG8D1.e5928\_e5984\_s3126\_r10201\_r10210\_p4133  
mc16\_13TeV.364527.Sherpa\_222\_NNPDF30NNLO\_munugamma\_pty\_15\_35.deriv.DAOD\_HIGG8D1.e5928\_e5984\_s3126\_r10201\_r10210\_p4133  
mc16\_13TeV.364528.Sherpa\_222\_NNPDF30NNLO\_munugamma\_pty\_35\_70.deriv.DAOD\_HIGG8D1.e5928\_e5984\_s3126\_r10201\_r10210\_p4133  
mc16\_13TeV.364529.Sherpa\_222\_NNPDF30NNLO\_munugamma\_pty\_70\_140.deriv.DAOD\_HIGG8D1.e5928\_e5984\_s3126\_r10201\_r10210\_p4133  
mc16\_13TeV.364530.Sherpa\_222\_NNPDF30NNLO\_munugamma\_pty\_140\_E\_CMS.deriv.DAOD\_HIGG8D1.e5928\_e5984\_s3126\_r10201\_r10210\_p4133  
mc16\_13TeV.364531.Sherpa\_222\_NNPDF30NNLO\_taunugamma\_pty\_7\_15.deriv.DAOD\_HIGG8D1.e5928\_e5984\_s3126\_r10201\_r10210\_p4133  
mc16\_13TeV.364532.Sherpa\_222\_NNPDF30NNLO\_taunugamma\_pty\_15\_35.deriv.DAOD\_HIGG8D1.e5928\_e5984\_s3126\_r10201\_r10210\_p4133  
mc16\_13TeV.364533.Sherpa\_222\_NNPDF30NNLO\_taunugamma\_pty\_35\_70.deriv.DAOD\_HIGG8D1.e5928\_e5984\_s3126\_r10201\_r10210\_p4133  
mc16\_13TeV.364534.Sherpa\_222\_NNPDF30NNLO\_taunugamma\_pty\_70\_140.deriv.DAOD\_HIGG8D1.e5928\_e5984\_s3126\_r10201\_r10210\_p4133  
mc16\_13TeV.364535.Sherpa\_222\_NNPDF30NNLO\_taunugamma\_pty\_140\_E\_CMS.deriv.DAOD\_HIGG8D1.e5928\_e5984\_s3126\_r10201\_r10210\_p4133  
mc16\_13TeV.410056.MadGraphPythiaEvtGen\_A14\_iZ\_4fl\_tchan\_noAllHad.deriv.DAOD\_HIGG8D1.e5803\_e5984\_s3126\_r10201\_r10210\_p4133  
mc16\_13TeV.410013.PowhegPythiaEvtGen\_P2012\_Wt\_inclusive\_top.deriv.DAOD\_HIGG8D1.e3753\_s3126\_r10201\_r10210\_p4133  
mc16\_13TeV.410014.PowhegPythiaEvtGen\_P2012\_Wt\_inclusive\_antitop.deriv.DAOD\_HIGG8D1.e3753\_s3126\_r10201\_r10210\_p4133  
mc16\_13TeV.410408.aMcAtNloPythia8EvtGen\_tWZ\_Ztoll\_minDR1.deriv.DAOD\_HIGG8D1.e6423\_e5984\_s3126\_r10201\_r10210\_p4133  
mc16\_13TeV.364242.Sherpa\_222\_NNPDF30NNLO\_WWW\_313v\_EW6.deriv.DAOD\_HIGG8D1.e5887\_e5984\_s3126\_r10201\_r10210\_p4133  
mc16\_13TeV.364243.Sherpa\_222\_NNPDF30NNLO\_WWW\_421v\_EW6.deriv.DAOD\_HIGG8D1.e5887\_e5984\_s3126\_r10201\_r10210\_p4133  
mc16\_13TeV.364244.Sherpa\_222\_NNPDF30NNLO\_WWW\_214v\_EW6.deriv.DAOD\_HIGG8D1.e5887\_e5984\_s3126\_r10201\_r10210\_p4133  
mc16\_13TeV.364245.Sherpa\_222\_NNPDF30NNLO\_WZZ\_511v\_EW6.deriv.DAOD\_HIGG8D1.e5887\_e5984\_s3126\_r10201\_r10210\_p4133  
mc16\_13TeV.364246.Sherpa\_222\_NNPDF30NNLO\_WZZ\_313v\_EW6.deriv.DAOD\_HIGG8D1.e5887\_e5984\_s3126\_r10201\_r10210\_p4133  
mc16\_13TeV.364247.Sherpa\_222\_NNPDF30NNLO\_ZZZ\_610v\_EW6.deriv.DAOD\_HIGG8D1.e5887\_e5984\_s3126\_r10201\_r10210\_p4133  
mc16\_13TeV.364248.Sherpa\_222\_NNPDF30NNLO\_ZZZ\_421v\_EW6.deriv.DAOD\_HIGG8D1.e5887\_e5984\_s3126\_r10201\_r10210\_p4133  
mc16\_13TeV.364249.Sherpa\_222\_NNPDF30NNLO\_ZZZ\_214v\_EW6.deriv.DAOD\_HIGG8D1.e5887\_e5984\_s3126\_r10201\_r10210\_p4133  
mc16\_13TeV.342284.Pythia8EvtGen\_A14NNPDF23LO\_WH125\_inc.deriv.DAOD\_HIGG8D1.e4246\_e5984\_s3126\_r10201\_r10210\_p4133  
mc16\_13TeV.342285.Pythia8EvtGen\_A14NNPDF23LO\_ZH125\_inc.deriv.DAOD\_HIGG8D1.e4246\_e5984\_s3126\_r10201\_r10210\_p4133  
mc16\_13TeV.341998.aMcAtNloHppEG\_UEEE5\_CTEQ6L1\_CT10ME\_tWH125\_gamgam\_yt\_plus1.deriv.DAOD\_HIGG8D1.e4394\_e5984\_s3126\_r10201\_r10210\_p4133  
mc16\_13TeV.410470.PhPy8EG\_A14\_ttbar\_hdamp258p75\_nonallhad.deriv.DAOD\_HIGG8D1.e6337\_e5984\_s3126\_r10201\_r10210\_p4133  
mc16\_13TeV.410472.PhPy8EG\_A14\_ttbar\_hdamp258p75\_dil.deriv.DAOD\_HIGG8D1.e6348\_e5984\_s3126\_r10201\_r10210\_p4133  
mc16\_13TeV.346343.PhPy8EG\_A14NNPDF23\_NNPDF30ME\_ttH125\_allhad.deriv.DAOD\_HIGG8D1.e7148\_e5984\_s3126\_r10201\_r10210\_p4133  
mc16\_13TeV.346344.PhPy8EG\_A14NNPDF23\_NNPDF30ME\_ttH125\_semilep.deriv.DAOD\_HIGG8D1.e7148\_e5984\_a875\_r10201\_r10210\_p4133  
mc16\_13TeV.346345.PhPy8EG\_A14NNPDF23\_NNPDF30ME\_ttH125\_dilep.deriv.DAOD\_HIGG8D1.e7148\_e5984\_a875\_r10201\_r10210\_p4133

mc16e:

mc16\_13TeV.361605.PowhegPy8EG\_CT10nloME\_AZNLOCTEQ6L1\_ZZvvvv\_mll4.deriv.DAOD\_HIGG8D1.e4054\_e5984\_s3126\_r10724\_r10726\_p4133  
mc16\_13TeV.361602.PowhegPy8EG\_CT10nloME\_AZNLOCTEQ6L1\_WZlvvv\_mll4.deriv.DAOD\_HIGG8D1.e4054\_e5984\_s3126\_r10724\_r10726\_p4133  
mc16\_13TeV.361601.PowhegPy8EG\_CT10nloME\_AZNLOCTEQ6L1\_WZlavl\_mll4.deriv.DAOD\_HIGG8D1.e4475\_e5984\_s3126\_r10724\_r10726\_p4133  
mc16\_13TeV.361600.PowhegPy8EG\_CT10nloME\_AZNLOCTEQ6L1\_WWlvlv.deriv.DAOD\_HIGG8D1.e4616\_e5984\_s3126\_r10724\_r10726\_p4133  
mc16\_13TeV.361603.PowhegPy8EG\_CT10nloME\_AZNLOCTEQ6L1\_ZZllll\_mll4.deriv.DAOD\_HIGG8D1.e4475\_e5984\_s3126\_r10724\_r10726\_p4133  
mc16\_13TeV.361604.PowhegPy8EG\_CT10nloME\_AZNLOCTEQ6L1\_ZZvvll\_mll4.deriv.DAOD\_HIGG8D1.e4475\_e5984\_s3126\_r10724\_r10726\_p4133  
mc16\_13TeV.364288.Sherpa\_222\_NNPDF30NNLO\_llll\_lowMllPtComplement.deriv.DAOD\_HIGG8D1.e6096\_s3126\_r10724\_p3983 mc16\_13TeV.364287.Sherpa\_222\_NNPDF30NNLO\_llll\_lowMllPtComplement.deriv.DAOD\_HIGG8D1.e6096\_s3126\_r10724\_p3983  
mc16\_13TeV.364285.Sherpa\_222\_NNPDF30NNLO\_llvjj\_EW6.deriv.DAOD\_HIGG8D1.e6055\_s3126\_r10724\_p3983  
mc16\_13TeV.364284.Sherpa\_222\_NNPDF30NNLO\_llvjj\_EW6.deriv.DAOD\_HIGG8D1.e6055\_s3126\_r10724\_p3983  
mc16\_13TeV.364283.Sherpa\_222\_NNPDF30NNLO\_lllijj\_EW6.deriv.DAOD\_HIGG8D1.e6055\_s3126\_r10724\_p3983  
mc16\_13TeV.364739.MGPy8EG\_NNPDF30NLO\_A14NNPDF23LO\_lvjlljjEW6\_OFMinus.deriv.DAOD\_HIGG8D1.e7421\_e5984\_s3126\_r10724\_r10726\_p4133  
mc16\_13TeV.364742.MGPy8EG\_NNPDF30NLO\_A14NNPDF23LO\_lvjlljjEW6\_SFPlus.deriv.DAOD\_HIGG8D1.e7421\_e5984\_s3126\_r10724\_r10726\_p4133  
mc16\_13TeV.364740.MGPy8EG\_NNPDF30NLO\_A14NNPDF23LO\_lvjlljjEW6\_OFPlus.deriv.DAOD\_HIGG8D1.e7421\_e5984\_s3126\_r10724\_r10726\_p4133  
mc16\_13TeV.364741.MGPy8EG\_NNPDF30NLO\_A14NNPDF23LO\_lvjlljjEW6\_SFMinus.deriv.DAOD\_HIGG8D1.e7421\_e5984\_s3126\_r10724\_r10726\_p4133  
mc16\_13TeV.364253.Sherpa\_222\_NNPDF30NNLO\_llv.deriv.DAOD\_HIGG8D1.e5916\_e5984\_s3126\_r10724\_r10726\_p4133

mc16\_13TeV.364250.Sherpa\_222\_NNPDF30NNLO\_llll.deriv.DAOD\_HIGG8D1.e5894\_e5984\_s3126\_r10724\_r10726\_p4133  
 mc16\_13TeV.364254.Sherpa\_222\_NNPDF30NNLO\_llvv.deriv.DAOD\_HIGG8D1.e5916\_e5984\_s3126\_r10724\_r10726\_p4133  
 mc16\_13TeV.364255.Sherpa\_222\_NNPDF30NNLO\_lvvv.deriv.DAOD\_HIGG8D1.e5916\_e5984\_s3126\_r10724\_r10726\_p4133  
 mc16\_13TeV.410155.aMcAtNloPythia8EvtGen\_MEN30NLO\_A14N23LO\_ttW.deriv.DAOD\_HIGG8D1.e5070\_e5984\_s3126\_r10724\_r10726\_p4133  
 mc16\_13TeV.410156.aMcAtNloPythia8EvtGen\_MEN30NLO\_A14N23LO\_ttZnunu.deriv.DAOD\_HIGG8D1.e5070\_e5984\_s3126\_r10724\_r10726\_p4133  
 mc16\_13TeV.410157.aMcAtNloPythia8EvtGen\_MEN30NLO\_A14N23LO\_ttZqq.deriv.DAOD\_HIGG8D1.e5070\_e5984\_s3126\_r10724\_r10726\_p4133  
 mc16\_13TeV.410218.aMcAtNloPythia8EvtGen\_MEN30NLO\_A14N23LO\_ttee.deriv.DAOD\_HIGG8D1.e5070\_e5984\_s3126\_r10724\_r10726\_p4133  
 mc16\_13TeV.410219.aMcAtNloPythia8EvtGen\_MEN30NLO\_A14N23LO\_ttmumu.deriv.DAOD\_HIGG8D1.e5070\_e5984\_s3126\_r10724\_r10726\_p4133  
 mc16\_13TeV.410220.aMcAtNloPythia8EvtGen\_MEN30NLO\_A14N23LO\_ttautau.deriv.DAOD\_HIGG8D1.e5070\_e5984\_s3126\_r10724\_r10726\_p4133  
 mc16\_13TeV.410276.aMcAtNloPythia8EvtGen\_MEN30NLO\_A14N23LO\_ttee\_mll\_1\_5.deriv.DAOD\_HIGG8D1.e6087\_e5984\_s3126\_r10724\_r10726\_p4133  
 mc16\_13TeV.410277.aMcAtNloPythia8EvtGen\_MEN30NLO\_A14N23LO\_ttmumu\_mll\_1\_5.deriv.DAOD\_HIGG8D1.e6087\_e5984\_s3126\_r10724\_r10726\_p4133  
 mc16\_13TeV.410278.aMcAtNloPythia8EvtGen\_MEN30NLO\_A14N23LO\_ttautau\_mll\_1\_5.deriv.DAOD\_HIGG8D1.e6087\_e5984\_s3126\_r10724\_r10726\_p4133  
 mc16\_13TeV.410397.MadGraphPythia8EvtGen\_ttbar\_wbee\_MEN30NLO\_A14N23LO.deriv.DAOD\_HIGG8D1.e6086\_e5984\_s3126\_r10724\_r10726\_p4133  
 mc16\_13TeV.410398.MadGraphPythia8EvtGen\_ttbar\_wbmumu\_MEN30NLO\_A14N23LO.deriv.DAOD\_HIGG8D1.e6086\_e5984\_s3126\_r10724\_r10726\_p4133  
 mc16\_13TeV.410399.MadGraphPythia8EvtGen\_ttbar\_wbtautau\_MEN30NLO\_A14N23LO.deriv.DAOD\_HIGG8D1.e6086\_e5984\_s3126\_r10724\_r10726\_p4133  
 mc16\_13TeV.410658.PhPy8EG\_A14\_tchan\_BW50\_lept\_top.deriv.DAOD\_HIGG8D1.e6671\_e5984\_s3126\_s3136\_r10724\_r10726\_p4133  
 mc16\_13TeV.410659.PhPy8EG\_A14\_tchan\_BW50\_lept\_antitop.deriv.DAOD\_HIGG8D1.e6671\_e5984\_s3126\_s3136\_r10724\_r10726\_p4133  
 mc16\_13TeV.410644.PowhegPythia8EvtGen\_A14\_singletop\_schan\_lept\_top.deriv.DAOD\_HIGG8D1.e6527\_e5984\_s3126\_r10724\_r10726\_p4133  
 mc16\_13TeV.410645.PowhegPythia8EvtGen\_A14\_singletop\_schan\_lept\_antitop.deriv.DAOD\_HIGG8D1.e6527\_e5984\_s3126\_r10724\_r10726\_p4133  
 mc16\_13TeV.412063.aMcAtNloPythia8EvtGen\_tllq\_NNPDF30\_nf4\_A14.deriv.DAOD\_TOPQ1.e7054\_e5984\_s3126\_r10724\_r10726\_p4174  
 mc16\_13TeV.304014.MadGraphPythia8EvtGen\_A14NNPDF23\_3top\_SM.deriv.DAOD\_HIGG8D1.e4324\_e5984\_s3126\_r10724\_r10726\_p4133  
 mc16\_13TeV.410080.MadGraphPythia8EvtGen\_A14NNPDF23\_4topSM.deriv.DAOD\_HIGG8D1.e4111\_e5984\_s3126\_r10724\_r10726\_p4133  
 mc16\_13TeV.410081.MadGraphPythia8EvtGen\_A14NNPDF23\_ttbarWW.deriv.DAOD\_HIGG8D1.e4111\_e5984\_s3126\_r10724\_r10726\_p4133  
 mc16\_13TeV.364100.Sherpa\_221\_NNPDF30NNLO\_Zmumu\_MAXHPTV0\_70\_CVetoBVeto.deriv.DAOD\_HIGG8D1.e5271\_e5984\_s3126\_s3136\_r10724\_r10726\_p4133  
 mc16\_13TeV.364100.Sherpa\_221\_NNPDF30NNLO\_Zmumu\_MAXHPTV0\_70\_CVetoBVeto.deriv.DAOD\_HIGG8D1.e5271\_e5984\_s3126\_r10724\_r10726\_p4133  
 mc16\_13TeV.364101.Sherpa\_221\_NNPDF30NNLO\_Zmumu\_MAXHPTV0\_70\_CFilterBVeto.deriv.DAOD\_HIGG8D1.e5271\_e5984\_s3126\_r10724\_r10726\_p4133  
 mc16\_13TeV.364102.Sherpa\_221\_NNPDF30NNLO\_Zmumu\_MAXHPTV0\_70\_BFilter.deriv.DAOD\_HIGG8D1.e5271\_e5984\_s3126\_s3136\_r10724\_r10726\_p4133  
 mc16\_13TeV.364102.Sherpa\_221\_NNPDF30NNLO\_Zmumu\_MAXHPTV0\_70\_BFilter.deriv.DAOD\_HIGG8D1.e5271\_e5984\_s3126\_r10724\_r10726\_p4133  
 mc16\_13TeV.364103.Sherpa\_221\_NNPDF30NNLO\_Zmumu\_MAXHPTV70\_140\_CVetoBVeto.deriv.DAOD\_HIGG8D1.e5271\_e5984\_s3126\_r10724\_r10726\_p4133  
 mc16\_13TeV.364103.Sherpa\_221\_NNPDF30NNLO\_Zmumu\_MAXHPTV70\_140\_CVetoBVeto.deriv.DAOD\_HIGG8D1.e5271\_e5984\_s3126\_s3136\_r10724\_r10726\_p4133  
 mc16\_13TeV.364104.Sherpa\_221\_NNPDF30NNLO\_Zmumu\_MAXHPTV70\_140\_CFilterBVeto.deriv.DAOD\_HIGG8D1.e5271\_e5984\_s3126\_r10724\_r10726\_p4133  
 mc16\_13TeV.364104.Sherpa\_221\_NNPDF30NNLO\_Zmumu\_MAXHPTV70\_140\_CFilterBVeto.deriv.DAOD\_HIGG8D1.e5271\_e5984\_s3126\_s3136\_r10724\_r10726\_p4133  
 mc16\_13TeV.364106.Sherpa\_221\_NNPDF30NNLO\_Zmumu\_MAXHPTV140\_280\_CVetoBVeto.deriv.DAOD\_HIGG8D1.e5271\_e5984\_s3126\_s3136\_r10724\_r10726\_p4133  
 mc16\_13TeV.364106.Sherpa\_221\_NNPDF30NNLO\_Zmumu\_MAXHPTV140\_280\_CVetoBVeto.deriv.DAOD\_HIGG8D1.e5271\_e5984\_s3126\_r10724\_r10726\_p4133  
 mc16\_13TeV.364107.Sherpa\_221\_NNPDF30NNLO\_Zmumu\_MAXHPTV140\_280\_CFilterBVeto.deriv.DAOD\_HIGG8D1.e5271\_e5984\_s3126\_r10724\_r10726\_p4133  
 mc16\_13TeV.364107.Sherpa\_221\_NNPDF30NNLO\_Zmumu\_MAXHPTV140\_280\_CFilterBVeto.deriv.DAOD\_HIGG8D1.e5271\_e5984\_s3126\_s3136\_r10724\_r10726\_p4133  
 mc16\_13TeV.364108.Sherpa\_221\_NNPDF30NNLO\_Zmumu\_MAXHPTV140\_280\_BFilter.deriv.DAOD\_HIGG8D1.e5271\_e5984\_s3126\_r10724\_r10726\_p4133  
 mc16\_13TeV.364109.Sherpa\_221\_NNPDF30NNLO\_Zmumu\_MAXHPTV280\_500\_CVetoBVeto.deriv.DAOD\_HIGG8D1.e5271\_e5984\_s3126\_r10724\_r10726\_p4133  
 mc16\_13TeV.364110.Sherpa\_221\_NNPDF30NNLO\_Zmumu\_MAXHPTV280\_500\_CFilterBVeto.deriv.DAOD\_HIGG8D1.e5271\_e5984\_s3126\_r10724\_r10726\_p4133  
 mc16\_13TeV.364110.Sherpa\_221\_NNPDF30NNLO\_Zmumu\_MAXHPTV280\_500\_CFilterBVeto.deriv.DAOD\_HIGG8D1.e5271\_e5984\_s3126\_s3136\_r10724\_r10726\_p4133  
 mc16\_13TeV.364111.Sherpa\_221\_NNPDF30NNLO\_Zmumu\_MAXHPTV280\_500\_BFilter.deriv.DAOD\_HIGG8D1.e5271\_e5984\_s3126\_s3136\_r10724\_r10726\_p4133  
 mc16\_13TeV.364111.Sherpa\_221\_NNPDF30NNLO\_Zmumu\_MAXHPTV280\_500\_BFilter.deriv.DAOD\_HIGG8D1.e5271\_e5984\_s3126\_r10724\_r10726\_p4133  
 mc16\_13TeV.364112.Sherpa\_221\_NNPDF30NNLO\_Zmumu\_MAXHPTV500\_1000.deriv.DAOD\_HIGG8D1.e5271\_e5984\_s3126\_r10724\_r10726\_p4133  
 mc16\_13TeV.364113.Sherpa\_221\_NNPDF30NNLO\_Zmumu\_MAXHPTV1000\_E\_CMS.deriv.DAOD\_HIGG8D1.e5271\_e5984\_s3126\_r10724\_r10726\_p4133  
 mc16\_13TeV.364113.Sherpa\_221\_NNPDF30NNLO\_Zmumu\_MAXHPTV1000\_E\_CMS.deriv.DAOD\_HIGG8D1.e5271\_e5984\_s3126\_s3136\_r10724\_r10726\_p4133  
 mc16\_13TeV.364114.Sherpa\_221\_NNPDF30NNLO\_Zee\_MAXHPTV0\_70\_CVetoBVeto.deriv.DAOD\_HIGG8D1.e5299\_e5984\_s3126\_s3136\_r10724\_r10726\_p4133  
 mc16\_13TeV.364114.Sherpa\_221\_NNPDF30NNLO\_Zee\_MAXHPTV0\_70\_CVetoBVeto.deriv.DAOD\_HIGG8D1.e5299\_e5984\_s3126\_r10724\_r10726\_p4133  
 mc16\_13TeV.364115.Sherpa\_221\_NNPDF30NNLO\_Zee\_MAXHPTV0\_70\_CFilterBVeto.deriv.DAOD\_HIGG8D1.e5299\_e5984\_s3126\_s3136\_r10724\_r10726\_p4133  
 mc16\_13TeV.364115.Sherpa\_221\_NNPDF30NNLO\_Zee\_MAXHPTV0\_70\_CFilterBVeto.deriv.DAOD\_HIGG8D1.e5299\_e5984\_s3126\_r10724\_r10726\_p4133  
 mc16\_13TeV.364116.Sherpa\_221\_NNPDF30NNLO\_Zee\_MAXHPTV0\_70\_BFilter.deriv.DAOD\_HIGG8D1.e5299\_e5984\_s3126\_r10724\_r10726\_p4133  
 mc16\_13TeV.364117.Sherpa\_221\_NNPDF30NNLO\_Zee\_MAXHPTV70\_140\_CVetoBVeto.deriv.DAOD\_HIGG8D1.e5299\_e5984\_s3126\_s3136\_r10724\_r10726\_p4133  
 mc16\_13TeV.364117.Sherpa\_221\_NNPDF30NNLO\_Zee\_MAXHPTV70\_140\_CVetoBVeto.deriv.DAOD\_HIGG8D1.e5299\_e5984\_s3126\_r10724\_r10726\_p4133  
 mc16\_13TeV.364118.Sherpa\_221\_NNPDF30NNLO\_Zee\_MAXHPTV70\_140\_CFilterBVeto.deriv.DAOD\_HIGG8D1.e5299\_e5984\_s3126\_s3136\_r10724\_r10726\_p4133  
 mc16\_13TeV.364118.Sherpa\_221\_NNPDF30NNLO\_Zee\_MAXHPTV70\_140\_CFilterBVeto.deriv.DAOD\_HIGG8D1.e5299\_e5984\_s3126\_r10724\_r10726\_p4133  
 mc16\_13TeV.364119.Sherpa\_221\_NNPDF30NNLO\_Zee\_MAXHPTV70\_140\_BFilter.deriv.DAOD\_HIGG8D1.e5299\_e5984\_s3126\_r10724\_r10726\_p4133  
 mc16\_13TeV.364120.Sherpa\_221\_NNPDF30NNLO\_Zee\_MAXHPTV140\_280\_CVetoBVeto.deriv.DAOD\_HIGG8D1.e5299\_e5984\_s3126\_r10724\_r10726\_p4133  
 mc16\_13TeV.364121.Sherpa\_221\_NNPDF30NNLO\_Zee\_MAXHPTV140\_280\_CFilterBVeto.deriv.DAOD\_HIGG8D1.e5299\_e5984\_s3126\_r10724\_r10726\_p4133  
 mc16\_13TeV.364122.Sherpa\_221\_NNPDF30NNLO\_Zee\_MAXHPTV140\_280\_BFilter.deriv.DAOD\_HIGG8D1.e5299\_e5984\_s3126\_s3136\_r10724\_r10726\_p4133  
 mc16\_13TeV.364122.Sherpa\_221\_NNPDF30NNLO\_Zee\_MAXHPTV140\_280\_BFilter.deriv.DAOD\_HIGG8D1.e5299\_e5984\_s3126\_r10724\_r10726\_p4133  
 mc16\_13TeV.364123.Sherpa\_221\_NNPDF30NNLO\_Zee\_MAXHPTV280\_500\_CVetoBVeto.deriv.DAOD\_HIGG8D1.e5299\_e5984\_s3126\_r10724\_r10726\_p4133  
 mc16\_13TeV.364124.Sherpa\_221\_NNPDF30NNLO\_Zee\_MAXHPTV280\_500\_CFilterBVeto.deriv.DAOD\_HIGG8D1.e5299\_e5984\_s3126\_r10724\_r10726\_p4133  
 mc16\_13TeV.364125.Sherpa\_221\_NNPDF30NNLO\_Zee\_MAXHPTV280\_500\_BFilter.deriv.DAOD\_HIGG8D1.e5299\_e5984\_s3126\_s3136\_r10724\_r10726\_p4133





mc16\_13TeV.364513.Sherpa\_222\_NNPDF30NNLO\_tautaugamma\_pty\_70\_140.deriv.DAOD\_HIGG8D1.e5982\_e5984\_s3126\_r10724\_r10726\_p4133  
 mc16\_13TeV.364514.Sherpa\_222\_NNPDF30NNLO\_tautaugamma\_pty\_140\_E\_CMS.deriv.DAOD\_HIGG8D1.e5928\_e5984\_s3126\_r10724\_r10726\_p4133  
 mc16\_13TeV.364522.Sherpa\_222\_NNPDF30NNLO\_enugamma\_pty\_15\_35.deriv.DAOD\_HIGG8D1.e5928\_e5984\_s3126\_r10724\_r10726\_p4133  
 mc16\_13TeV.364523.Sherpa\_222\_NNPDF30NNLO\_enugamma\_pty\_35\_70.deriv.DAOD\_HIGG8D1.e5928\_e5984\_s3126\_r10724\_r10726\_p4133  
 mc16\_13TeV.364524.Sherpa\_222\_NNPDF30NNLO\_enugamma\_pty\_70\_140.deriv.DAOD\_HIGG8D1.e5928\_e5984\_s3126\_r10724\_r10726\_p4133  
 mc16\_13TeV.364525.Sherpa\_222\_NNPDF30NNLO\_enugamma\_pty\_140\_E\_CMS.deriv.DAOD\_HIGG8D1.e5928\_e5984\_s3126\_r10724\_r10726\_p4133  
 mc16\_13TeV.364527.Sherpa\_222\_NNPDF30NNLO\_munugamma\_pty\_15\_35.deriv.DAOD\_HIGG8D1.e5928\_e5984\_s3126\_r10724\_r10726\_p4133  
 mc16\_13TeV.364528.Sherpa\_222\_NNPDF30NNLO\_munugamma\_pty\_35\_70.deriv.DAOD\_HIGG8D1.e5928\_e5984\_s3126\_r10724\_r10726\_p4133  
 mc16\_13TeV.364529.Sherpa\_222\_NNPDF30NNLO\_munugamma\_pty\_70\_140.deriv.DAOD\_HIGG8D1.e5928\_e5984\_s3126\_r10724\_r10726\_p4133  
 mc16\_13TeV.364530.Sherpa\_222\_NNPDF30NNLO\_munugamma\_pty\_140\_E\_CMS.deriv.DAOD\_HIGG8D1.e5928\_e5984\_s3126\_r10724\_r10726\_p4133  
 mc16\_13TeV.364532.Sherpa\_222\_NNPDF30NNLO\_taunugamma\_pty\_15\_35.deriv.DAOD\_HIGG8D1.e5928\_e5984\_s3126\_r10724\_r10726\_p4133  
 mc16\_13TeV.364533.Sherpa\_222\_NNPDF30NNLO\_taunugamma\_pty\_35\_70.deriv.DAOD\_HIGG8D1.e5928\_e5984\_s3126\_r10724\_r10726\_p4133  
 mc16\_13TeV.364534.Sherpa\_222\_NNPDF30NNLO\_taunugamma\_pty\_70\_140.deriv.DAOD\_HIGG8D1.e5928\_e5984\_s3126\_r10724\_r10726\_p4133  
 mc16\_13TeV.364535.Sherpa\_222\_NNPDF30NNLO\_taunugamma\_pty\_140\_E\_CMS.deriv.DAOD\_HIGG8D1.e5928\_e5984\_s3126\_r10724\_r10726\_p4133  
 mc16\_13TeV.410560.MadGraphPythia8EvtGen\_A14\_tZ\_4fl\_tchan\_noAllHad.deriv.DAOD\_HIGG8D1.e5803\_e5984\_s3126\_r10724\_r10726\_p4133  
 mc16\_13TeV.410408.aMcAtNloPythia8EvtGen\_tWZ\_Ztoll\_minDR1.deriv.DAOD\_HIGG8D1.e6423\_e5984\_s3126\_r10724\_r10726\_p4133  
 mc16\_13TeV.364242.Sherpa\_222\_NNPDF30NNLO\_WWW\_3l3v\_EW6.deriv.DAOD\_HIGG8D1.e5887\_e5984\_s3126\_r10724\_r10726\_p4133  
 mc16\_13TeV.364243.Sherpa\_222\_NNPDF30NNLO\_WWZ\_4l2v\_EW6.deriv.DAOD\_HIGG8D1.e5887\_e5984\_s3126\_r10724\_r10726\_p4133  
 mc16\_13TeV.364244.Sherpa\_222\_NNPDF30NNLO\_WWZ\_2l4v\_EW6.deriv.DAOD\_HIGG8D1.e5887\_e5984\_s3126\_r10724\_r10726\_p4133  
 mc16\_13TeV.364245.Sherpa\_222\_NNPDF30NNLO\_WZZ\_5l1v\_EW6.deriv.DAOD\_HIGG8D1.e5887\_e5984\_s3126\_r10724\_r10726\_p4133  
 mc16\_13TeV.364246.Sherpa\_222\_NNPDF30NNLO\_WZZ\_3l3v\_EW6.deriv.DAOD\_HIGG8D1.e5887\_e5984\_s3126\_r10724\_r10726\_p4133  
 mc16\_13TeV.364247.Sherpa\_222\_NNPDF30NNLO\_ZZZ\_6l0v\_EW6.deriv.DAOD\_HIGG8D1.e5887\_e5984\_s3126\_r10724\_r10726\_p4133  
 mc16\_13TeV.364248.Sherpa\_222\_NNPDF30NNLO\_ZZZ\_4l2v\_EW6.deriv.DAOD\_HIGG8D1.e5887\_e5984\_s3126\_r10724\_r10726\_p4133  
 mc16\_13TeV.364249.Sherpa\_222\_NNPDF30NNLO\_ZZZ\_2l4v\_EW6.deriv.DAOD\_HIGG8D1.e5887\_e5984\_s3126\_r10724\_r10726\_p4133  
 mc16\_13TeV.342284.Pythia8EvtGen\_A14NNPDF23LO\_WH125\_inc.deriv.DAOD\_HIGG8D1.e4246\_e5984\_s3126\_r10724\_r10726\_p4133  
 mc16\_13TeV.342285.Pythia8EvtGen\_A14NNPDF23LO\_ZH125\_inc.deriv.DAOD\_HIGG8D1.e4246\_e5984\_s3126\_r10724\_r10726\_p4133  
 mc16\_13TeV.341998.aMcAtNloHppEG\_UEEE5\_CTEQ6L1\_CT10ME\_tWH125\_gamgam\_yt\_plus1.deriv.DAOD\_HIGG8D1.e4394\_e5984\_s3126\_r10724\_r10726\_p4133  
 mc16\_13TeV.410389.MadGraphPythia8EvtGen\_A14NNPDF23\_ttgamma\_nonallhadronic.deriv.DAOD\_HIGG8D1.e6155\_e5984\_s3126\_r10724\_r10726\_p4133  
 mc16\_13TeV.410470.PhPy8EG\_A14\_ttbar\_hdamp258p75\_nonallhad.deriv.DAOD\_HIGG8D1.e6337\_e5984\_s3126\_r10724\_r10726\_p4133  
 mc16\_13TeV.410472.PhPy8EG\_A14\_ttbar\_hdamp258p75\_dil.deriv.DAOD\_HIGG8D1.e6348\_e5984\_s3126\_r10724\_r10726\_p4133  
 mc16\_13TeV.346343.PhPy8EG\_A14NNPDF23\_NNPDF30ME\_ttH125\_allhad.deriv.DAOD\_HIGG8D1.e7148\_e5984\_s3126\_r10724\_r10726\_p4133  
 mc16\_13TeV.346343.PhPy8EG\_A14NNPDF23\_NNPDF30ME\_ttH125\_allhad.deriv.DAOD\_HIGG8D1.e7148\_e5984\_a875\_r10724\_r10726\_p4133  
 mc16\_13TeV.346344.PhPy8EG\_A14NNPDF23\_NNPDF30ME\_ttH125\_semilep.deriv.DAOD\_HIGG8D1.e7148\_e5984\_a875\_r10724\_r10726\_p4133  
 mc16\_13TeV.346344.PhPy8EG\_A14NNPDF23\_NNPDF30ME\_ttH125\_semilep.deriv.DAOD\_HIGG8D1.e7148\_e5984\_s3126\_r10724\_r10726\_p4133  
 mc16\_13TeV.346345.PhPy8EG\_A14NNPDF23\_NNPDF30ME\_ttH125\_dilep.deriv.DAOD\_HIGG8D1.e7148\_e5984\_a875\_r10724\_r10726\_p4133  
 mc16\_13TeV.346345.PhPy8EG\_A14NNPDF23\_NNPDF30ME\_ttH125\_dilep.deriv.DAOD\_HIGG8D1.e7148\_e5984\_s3126\_r10724\_r10726\_p4133